Title

Utilizing Sum Frequency Generation Vibrational Spectroscopy to Study Platinum-Catalyzed Alcohol Oxidation at the Solid-Liquid and Solid-Gas Interfaces

Author

Keller, Lindsay Carl

Publication Date

2017

Peer reviewed|Thesis/dissertation

Utilizing Sum Frequency Generation Vibrational Spectroscopy to Study Platinum-Catalyzed Alcohol Oxidation at the Solid-Liquid and Solid-Gas Interfaces

By

Lindsay Carl Keller

A dissertation submitted in partial satisfaction of the

requirements for the degree of

Doctor of Philosophy

in

Chemistry

in the

Graduate Division

of the

University of California, Berkeley

Committee in charge:

Professor Gabor A. Somorjai, Chair
Professor Peidong Yang
Professor Holger Müller

Fall 2017

Abstract

Utilizing Sum Frequency Generation Spectroscopy to Study Platinum-Catalyzed Alcohol Oxidation at the Solid-Liquid and Solid-Gas Interfaces

By

Lindsay Carl Keller

Doctor of Philosophy in Chemistry

University of California, Berkeley

Professor Gabor A. Somorjai, Chair

Sum frequency generation (SFG) vibrational spectroscopy is utilized in this work to study the oxidation of alcohols on platinum catalysts. A brief overview of SFG spectroscopy is provided, including a short theoretical summary of the information pertinent to understand the technique. Background information on the oxidation of alcohols is also provided. A description of techniques and experimental setups is discussed, including detailed information on the preparation of catalysts and SFG laser setups.

The oxidation of 1-propanol to propanal by molecular oxygen at 60^{o}C was studied at the solid-liquid and solid-gas interfaces using a range of nanoparticle sizes from 2-7 nm. The reaction rate at the solid-liquid interface was found to be two orders of magnitude greater than that at the solid-gas interface after normalizing to the concentration. In addition, catalytic activity increases with the size of platinum nanoparticles for both reactions. Moreover, water substantially promotes 1-propanol oxidation in the liquid phase, decreasing the activation energy by 21 kJ/mol. However, water inhibits the reaction in the gas phase, increasing the activation energy by 31 kJ/mol. The liquid-phase and gas-phase reactions appear to undergo different mechanisms due to differing kinetic results. This correlates well with different orientations of the 1-propanol species at the solid-liquid interface versus the solid-gas interface as probed by SFG spectroscopy under reaction conditions and simulated by computational calculations.

The oxidation of 2-butanol was carried out in both the liquid and the gas phase. Size-controlled platinum nanoparticles loaded into mesoporous silica MCF-17 were synthesized and studied in the oxidation reaction of 2-butanol with molecular oxygen in the gas and liquid phases. The turnover frequency values increased as the nanoparticle size became larger in both phases, with a consistently high selectivity toward 2-butanone. The activation energy in the gas phase was twice as much as that in the liquid phase. Water did not interrupt the reaction progress in the gas phase, while it poisoned the Pt surface fully to decrease the turnover rate significantly in the liquid phase. SFG spectra were taken of the gas-phase 2-butanol reaction on Pt in both reactive and inert conditions. Water was determined to have no significant effect on the 2-butanol spectra, supporting the reaction data. Combined with the DFT calculations, it was determined that the

molecule tends to lay down in the low surface concentration but tends to stand up in the high surface concentration.

SFG studies were carried out to study the oxidation of 1-butanol on a platinum thin film. These studies examined the effects of oxygen and water on the gas-phase reaction. Spectra of 1-butanol were taken in both nitrogen and oxygen environments, providing information about both the reactive and inert conditions. Spectra were also taken of 1-butanol in the presence of oxygen and water in order to study the effect of water on the surface.

1,3-butadiene hydrogenation was performed on 4 nm Pt, Pd, and Rh nanoparticles encapsulated in SiO_2 shells at 20, 60, and 100°C. The core-shells were grown around PVP-coated nanoparticles prepared by colloidal synthesis. SFG spectroscopy was performed to correlate surface intermediates observed under reaction conditions with reaction selectivity. Using SFG, it was possible to compare the surface vibrational spectra of Pt@ SiO_2, Pd@ SiO_2, and Rh@ SiO_2. These studies that the calcination is effective at removing PVP, and that the SFG signal can be generated from the metal surface through the outer SiO_2 shell. This work was then used to investigate Pt@SiO_2 nanoparticles as potential catalysts for the liquid-phase oxidation of isopropanol. It was found that these nanoparticles were successful in the gas and liquid phases for reaction studies. However, despite several attempts, a clear SFG spectrum was not able to be obtained on a Langmuir-Blodgett film of these nanoparticles.

Table of Contents

Acknowledgements

I would like to start by expressing my gratitude to Professor Gabor Somorjai for providing me with this great opportunity and guidance throughout my graduate studies. I am very grateful that I have been able to work in his research group, and I deeply appreciate his mentorship and support.

I have been lucky enough to have a support system of amazing researchers to work with in the Somorjai group throughout the past several years. I give special thanks to Jim Krier and Chris Thompson, who taught me SFG spectroscopy. I am also grateful to Hui-Ling Han, Yonatan Horowitz, and Griffin Kennedy, all of whom have helped me in my research as well. In addition, I would like to thank Walter Ralston for his assistance and advice, especially in these past few months of writing.

My deepest thanks also goes out to Dr. Anderson Marsh, my undergraduate research advisor at Lebanon Valley College. He encouraged me to apply for a summer research position in his group my freshman year, and he encouraged me to apply to UC Berkeley my senior year. I truly would not be where I am without his guidance.

I would also like to thank my parents, Dale and Brenda Carl. They have always encouraged me to do my best and have helped me become the person I am today. No matter how old I am or how far away from home I move, they continue to cheer on all my accomplishments and support me when I need it, and I am very grateful for them both.

Finally, I would like to thank my husband, Brandon Keller. I am so grateful for his continued love and support throughout the entirety of graduate school. He has shown me so much patience and understanding these past five years, and I look forward to starting this next chapter of my life with him by my side.

This work is funded by the Director, Office of Science, Office of Basic Energy Sciences, Division of Materials Sciences and Engineering, of the U.S. Department of Energy under Contract No. DE-AC02-05CH11231

Chapter 1

Introduction

Chemistry is a dynamic science, rooted in the change of molecules from reactants to products. These changes – known as reactions – can be sped up or altered course by the presence of a catalyst. It is therefore appropriate to say that catalysts are one of the most fundamental parts of chemistry, and that the study of catalysis is an integral part of understanding how molecules react. Catalysis also plays an integral role in biology, as enzyme catalysis allows life to exist as we know it.

Catalysis has been a part of chemistry dating back to the early 1800s. It was discovered by Thénard in 1813 that ammonia decomposed when passed through a hot porcelain tube only if certain metals – such as iron, copper, silver, or platinum – were present in the tube. However, it was not until 1835 that Berzelius realized that this experiment, as well as a number of others, could be explained as what he referred to as "catalytic power".[1] The field of catalysis grew throughout the next century, with a large number of reactions and catalysts being studied. However, it was only possible at this time to study these catalysts at the macroscopic level.

In the 1950s, technologies were developed that allowed chemists to examine surfaces, including those of catalysts, under ultrahigh vacuum (UHV) systems. These systems – capable of pumping down to 10^{-7} Torr or lower – allowed researchers to study a surface without contamination from other gases. Techniques such as Auger electron spectroscopy and x-ray photoelectron spectroscopy (XPS) offered a previously unavailable insight into these surfaces at the molecular level. These processes work through measuring the energies of emitted electrons from a surface, providing information about its chemical composition. Collisions with gas molecules can potentially lower the energy of these electrons, skewing the data. Therefore, it is important for these methods (and many others that were developed) to have as few gas particles in the UHV chamber as possible.[2] Due to these low pressure restrictions, it was only possible to examine the catalyst either before the reaction began or after it ended – technologies were not available that would allow the catalyst to be probed during the reaction itself. It was not until techniques such as sum frequency generation (SFG) vibrational spectroscopy were developed that it became possible to study the surface of the catalyst as the reaction was taking place. SFG spectroscopy can be used in ambient pressure environments under reaction conditions, because it is a surface-specific process, meaning that a signal will only be generated at a surface. This removes any interference from the bulk materials and allows a look into the way the molecules are arranged at an interface between two different substances.[3]

In the field of surface science, SFG spectroscopy is a fairly new technique. Bloembergen and Pershan first laid out the theoretical basis for non-linear spectroscopy in 1962, but the first SFG spectra were not recorded until the late 1980s by Shen and Harris.[4–7] And it was not until 1995

that SFG was used as a tool for studying the catalytic surface of platinum during ethylene hydrogenation.[8,9] In the past 20 years since these initial studies, SFG has been used to study numerous interfaces and investigate a wide variety of reactions and conditions.[10–15]

This work outlines studies carried out employing SFG spectroscopy to study the solid-gas and solid-liquid interfaces under reaction conditions. Platinum is used as the primary catalyst, in both thin film and nanoparticle form. Thin films of platinum are easy to create and use, and they have previously been utilized in several other SFG studies.[16,17] Platinum nanoparticles pose several difficulties for use in SFG studies, but they also offer several advantages over thin films. One of the main advantages of nanoparticles (especially from a catalytic standpoint) is the ability to control their size and shape, which studies have found can change the selectivity of products.[18]

Studying both gas and liquid phase reactions on Pt is important as well due to the differences between the phases. The liquid phase is much denser than the gas phase, and as a result, it may pose diffusion limitations not found in the gas phase. However, there are many molecules – especially larger ones – that have very low vapor pressure, making them unable to be studied in the gas phase. This work seeks to provide an insight into the possibilities of reactions in both phases, and to study the differences between them. The oxidation of primary and secondary alcohols is the main reaction studied, but other reactions (including the hydrogenation reactions of ethylene and 1,3 butadiene) are carried out as well.

Chapter 2 provides a brief introduction to SFG spectroscopy, outlining important theoretical information needed to understand the technique. A short background on alcohol oxidation is also included.

Chapter 3 provides information on the notable experimental setups used in this work, including descriptions of the catalyst preparation and SFG setups.

Chapter 4 examines the 1-propanol oxidation reaction on platinum. SFG spectroscopy is utilized to examine the catalyst in both the liquid and the gas phase, and reaction data notes several significant differences between the gas phase and liquid phase reactions. Notably, there was a large difference found between the way that water affects the liquid and gas phase reactions.

Chapter 5 discusses 1,3 butadiene hydrogenation on core-shell nanoparticles. An understanding of these core-shell catalysts is important, as they are later employed in this work to study the liquid-phase oxidation of isopropanol.

Chapter 6 provides insight into the effects of nanoparticle size and water on the platinum-catalyzed 2-butanol oxidation reaction in both the gas and liquid phases.

Chapter 7 examines the oxidation of 1-butanol on platinum in the gas phase. SFG spectroscopy is used to examine the platinum-gas interface under reaction conditions.

Chapter 8 discusses work carried out investigating platinum nanoparticles as potential liquid-phase catalysts for the isopropanol oxidation reaction. Ethylene hydrogenation is also used to determine catalyst viability.

References

(1) Roberts, M. W. Birth of the Catalytic Concept (1800-1900). *Catal. Letters* **2000**, *67*, 1–4.

(2) Somorjai, G. A.; Li, Y. *Introduction to Surface Chemistry and Catalysis*, 2nd Ed.; Wiley, 2010.

(3) Lambert, A. G.; Davies, P. B.; Neivandt, D. J. Implementing the Theory of Sum Frequency Generation Vibrational Spectroscopy: A Tutorial Review. *Appl. Spectrosc. Rev.* **2005**, *40* (2), 103–145.

(4) Bloembergen, N.; Pershan, P. S. Light Waves at the Boundary of Nonlinear Media. *Phys. Rev.* **1962**, *128* (2), 606–622.

(5) Zhu, X. D.; Suhr, H.; Shen, Y. R. Surface Vibrational Spectroscopy by Infrared-Visible Sum Frequency Generation. *Phys. Rev. B* **1987**, *35* (6), 3047–3050.

(6) Harris, A. L.; Chidsey, C. E. D.; Levinos, N. J.; Loiacono, D. N. Monolayer Vibrational Spectroscopy By Infrared-Visible Sum Frequency Generation at Metal and Semiconductor Surfaces. *Chem. Phys. Lett.* **1987**, *14* (4), 350–356.

(7) Shen, Y. R. Surface Properties Probed by Second-Harmonic and Sum-Frequency Generation. *Nature* **1989**, *337*, 519–525.

(8) Cremer, P. S.; Su, X.; Shen, Y. R.; Somorjai, G. A.; August, R. V. Ethylene Hydrogenation on Pt (111) Monitored in Situ at High Pressures Using Sum Frequency Generation. *J. Am. Chem. Soc.* **1996**, *118*, 2942–2949.

(9) Cremer, P.; Stanners, C.; Niemantsverdriet, J. W.; Shen, Y. R. The Conversion of Di-O-Bonded Ethylene to Ethylidyne on Pt(111) Monitored with Sum Frequency Generation : Evidence for an Ethylidene (or Ethyl) Intermediate. *Surf. Sci.* **1995**, *328*, 111–118.

(10) Su, X.; Kung, K. Y.; Lahtinen, J.; Shen, Y. R.; Somorjai, G. A. 1,3- and 1,4-Cyclohexene Hydrogenation and Dehydrogenation on Pt(111) Crystal Surface: A Combined Reaction Kinetics and Surface Vibrational Spectroscopy Study Using Sum Frequency Generation. *J. Mol. Catal. A* **1999**, *141*, 9–19.

(11) Schnaidt, J.; Heinen, M.; Jusys, Z.; Behm, R. J. Oxidation of 1-Propanol on a Pt Film Electrode Studied by Combined Electrochemical, in Situ IR Spectroscopy and Online Mass Spectrometry Measurements. *Electrochim. Acta* **2013**, *104*, 505–517.

(12) Morin, C.; Simon, D.; Sautet, P. Intermediates in the Hydrogenation of Benzene to Cyclohexene on Pt (1 1 1) and Pd (1 1 1): A Comparison from DFT Calculations. *Surf. Sci.* **2006**, *600*, 1339–1350.

(13) Bratlie, K. M.; Komvopoulos, K.; Somorjai, G. A. Sum Frequency Generation Vibrational Spectroscopy of Pyridine Hydrogenation on Platinum Nanoparticles. *J. Phys. Chem. C* **2008**, *112*, 11865–11868.

(14) Gomes, J. F.; Bergamaski, K.; Pinto, M. F. S.; Miranda, P. B. Reaction Intermediates of Ethanol Electro-Oxidation on Platinum Investigated by SFG Spectroscopy. *J. Catal.* **2013**, *302*, 67–82.

(15) Richmond, G. L. Molecular Bonding and Interactions at Aqueous Surfaces as Probed by Vibrational Sum Frequency Spectroscopy. *Chem. Rev.* **2002**, *102*, 2693–2724.

(16) Thompson, C. M.; Carl, L. M.; Somorjai, G. A. Sum Frequency Generation Study of the Interfacial Layer in Liquid-Phase Heterogeneously Catalyzed Oxidation of 2-Propanol on Platinum: Effect of the Concentrations of Water and 2-Propanol at the Interface. *J. Phys. Chem. C* **2013**, *117* (49).

(17) Wang, H.; Sapi, A.; Thompson, C. M.; Liu, F.; Zherebetskyy, D.; Krier, J. M.; Carl, L. M.; Cai, X.; Wang, L.-W.; Somorjai, G. A. Dramatically Different Kinetics and Mechanism at Solid/liquid and Solid/gas Interfaces for Catalytic Isopropanol Oxidation over Size-Controlled Platinum Nanoparticles. *J. Am. Chem. Soc.* **2014**, *136* (29).

(18) An, K.; Somorjai, G. A. Size and Shape Control of Metal Nanoparticles for Reaction Selectivity in Catalysis. *ChemCatChem* **2012**, *4* (10), 1512–1524.

Chapter 2

Background Information on Sum Frequency Generation and the Alcohol Oxidation Reaction

Introduction

The experiments presented in this work utilize sum frequency generation (SFG) vibrational spectroscopy to study platinum catalysts at the solid-gas and solid-liquid interfaces. SFG spectroscopy is a useful tool for studying catalytic reactions, as it is a surface-specific technique that allows for the interfacial molecular vibrations to be examined while removing interferences from the bulk materials.[1] As such, SFG is one of a limited number of techniques that is able to obtain molecular information from a reaction interface which can be related directly to that catalyst's behavior.[2,3] In this chapter, a brief overview of SFG theory is presented, as well as information on alcohol oxidation reactions studied throughout this work.

Theory of Sum Frequency Generation

Sum frequency generation (SFG) vibrational spectroscopy is a non-linear, surface-specific technique involving two laser beams – a fixed visible frequency beam and a tunable IR frequency beam. In order to achieve an SFG signal, it is necessary to have both spatial and temporal overlap of these two beams on the surface. Light is then emitted at the sum of the two frequencies.[1,4]

$$\omega_{SFG} = \omega_{IR} + \omega_{VIS}$$

The intensity of the light is resonantly enhanced when the IR beam frequency coincides with a vibrational mode of the molecules at the measured interface. The SFG light is then detected as a function of IR frequency, and a vibrational spectrum is obtained.

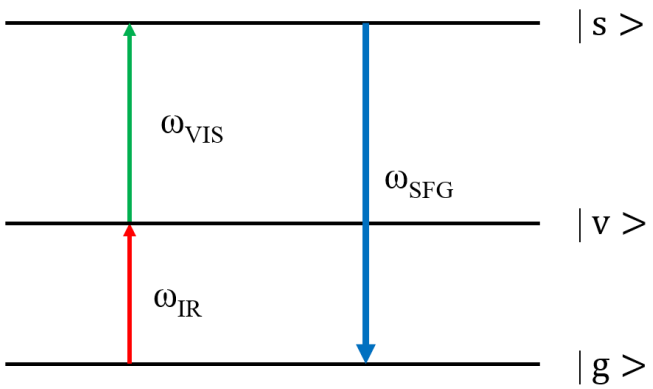

Figure 1 – A schematic showing an on-resonance SFG transition – the energy of the infrared radiation matches a molecular vibration, and the SFG is resonantly enhanced.

In looking at Figure 1, it is easy to see how SFG is essentially a combination of IR absorption and anti-Stokes Raman scattering. However, unlike IR absorption or Raman scattering, SFG is a coherent process – light generated at the surface has a direction, magnitude, and phase directly related to the incident laser beams. Therefore, analyzing spectra recorded with different incident beam polarizations provides information on the average tilt angle of the interfacial molecules with respect to the surface. In addition, as the following equation shows, both momentum and energy are conserved in the SFG process.[1]

$$n_{SF}\,\omega_{SF}\sin\theta_{SF} = n_{vis}\omega_{vis}\sin\theta_{vis} \pm n_{IR}\omega_{IR}\sin\theta_{IR}$$

In order for a vibrational mode to be active, it must be in an asymmetric environment – both on a macroscopic and microscopic scale. On the macroscopic level, the isotropic orientation of bulk molecules is centrosymmetric, making the material SFG inactive. This isotropic symmetry can be broken by the addition of an interface, allowing for SFG measurements of the interfacial molecules. Additionally, for molecules at an interface to be SFG active, they must have a net polar orientation – no signal will arise from a completely disordered surface or from molecules arranged equally in opposite orientations.[1]

This surface specificity can also be understood by examining the nonlinear susceptibility, $\chi^{(2)}_{ijk}$. In a centrosymmetric environment, all directions are equal and therefore $\chi^{(2)}_{ijk}$ must be identical for any two opposing directions, meaning that:

$$\chi^{(2)}_{ijk} = \chi^{(2)}_{-i-j-k}.$$

In order to satisfy this and other centrosymmetric requirements, $\chi^{(2)}$ must be zero. However, an interface between two materials is not centrosymmetric and $\chi^{(2)} \neq 0$, which allows SFG to occur. $\chi^{(2)}$ is comprised of two parts – a resonant (R) and a nonresonant (NR) susceptibility.

$$\chi^{(2)} = \chi_R^{(2)} + \chi_{NR}^{(2)}$$

For dielectric materials, $\chi_{NR}^{(2)}$ is generally very small. However, for metal surfaces $\chi_{NR}^{(2)}$ can be significant due to plasmon resonance, but is generally independent of frequency.

The SFG intensity is proportional to the square of the nonlinear polarization at the surface, which is generated from the two incident beams (in this case, visible and IR beams).[5] The SFG polarization, $\mathbf{P_{SFG}}$, is dependent on the previously established nonlinear susceptibility, $\chi^{(2)}_{SFG}$, as well as the electric field components, such that:

$$\mathbf{P}^{(2)}=\varepsilon_0\chi^{(2)}\mathbf{E}_1\mathbf{E}_2$$

$\chi^{(2)}$ is the second-order non-linear susceptibility, and it describes the relationship between the two applied electric field vectors – $\mathbf{E}_1$ and $\mathbf{E}_2$ – and the second-order non-linear polarization. It is also the macroscopic average of the hyperpolarizability of the molecules adsorbed at the surface (β). As the frequency of the IR beam is tuned through a molecular resonance, β – and therefore $\chi^{(2)}$ – increases, resulting in a change in the SFG intensity.[1]

In further examining the SFG surface, it can be assumed that the interface is isotropic around the surface normal, creating a C_∞ surface where $z \neq -z$ but $x = -x$ and $y = -y$. The x and y axes are considered equivalent for an isotropic surface, meaning that only four $\chi^{(2)}_{ijk}$ components can generate an SFG signal: $\chi^{(2)}_{zxx} \equiv \chi^{(2)}_{zyy}$, $\chi^{(2)}_{xzx} \equiv \chi^{(2)}_{yzy}$, $\chi^{(2)}_{xxz} \equiv \chi^{(2)}_{yyz}$, and $\chi^{(2)}_{zzz}$. [1]

It is then possible to resolve each of the electric fields into components that are polarized parallel and perpendicular to the surface. For metallic substrates (such as the platinum utilized in this work), the reflectivity in the IR region is high, resulting in a large electric field in the z direction but negligible electric fields in the x and y directions. Therefore, only resonant susceptibilities with a z infrared component generate a signal.[1] These are listed below with their corresponding polarizations – an electric field polarized parallel to the surface is denoted s polarized, and an electric field polarized perpendicular to the surface is considered p polarized.

Polarization	**$\chi^{(2)}_{ijk}$ elements**
pss	$\chi^{(2)}_{zyy}$
sps	$\chi^{(2)}_{yzy}$
ssp	$\chi^{(2)}_{yyz}$
ppp	$\chi^{(2)}_{zzz}$, $\chi^{(2)}_{zxx}$, $\chi^{(2)}_{xzx}$, $\chi^{(2)}_{xxz}$

Table 1 – A chart of SFG polarization combinations and the elements of $\chi^{(2)}_{ijk}$ that contribute to each polarization. The polarizations are listed as SFG, visible, and infrared.

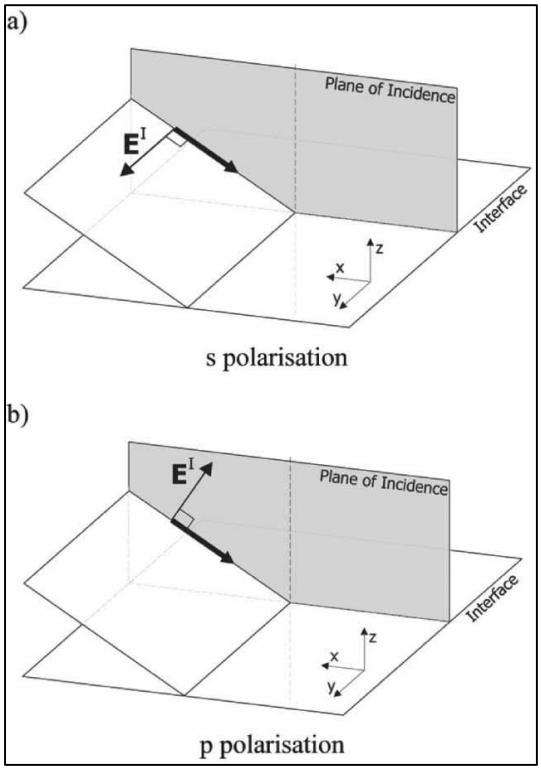

Figure 2 – A schematic showing light polarized (a) parallel to the surface, known as s polarization, and (b) perpendicular to the surface, known as p polarization.[1]

Previous Alcohol Oxidation Studies

The aqueous phase platinum-catalyzed oxidation of alcohols was discovered in 1845 by Döbereiner. Since this finding, the process has been significantly improved with the development of heterogeneous catalysis. While platinum has been found to be an excellent catalyst, palladium has also been successfully used.[6]

The oxidation of alcohols into aldehydes, ketones, and/or carboxylic acids is an extremely useful and important reaction in the chemical, pharmaceutical, and agrochemical fields.[7–9] Primary alcohols are easily oxidized to carboxylic acids, especially in basic solutions. In acidic solutions or in organic solvents, they may oxidize to form aldehydes. Secondary alcohols are oxidized to their corresponding ketone.[10]

Alcohols can also function as a model catalyst – the relatively short hydrocarbon chains of the alcohols studied in this work allow for easily identifiable peaks, but the fundamental discoveries have the potential to translate to larger molecules necessary for pharmaceutical and industrial molecules.[6,11] The alcohol oxidation reaction is also a valuable reaction to study, as it can be run under mild conditions (20-90°C) and does not require a special reactor.[6]

In these reactions, the oxidant is usually air or oxygen (as is the case with all work presented here), and the rate of the reaction has been found to increase with increasing the partial pressure of oxygen. The alcohol oxidation reaction has been extensively studied under a variety of conditions and with a variety of alcohols, but little work has been done utilizing SFG to study it under reaction conditions.[6,11–13]

References

(1) Lambert, A. G.; Davies, P. B.; Neivandt, D. J. Implementing the Theory of Sum Frequency Generation Vibrational Spectroscopy: A Tutorial Review. *Appl. Spectrosc. Rev.* **2005**, *40* (2), 103–145.

(2) Miranda, P. B.; Shen, Y. R. Liquid Interfaces : A Study by Sum-Frequency Vibrational Spectroscopy. *J. Phys. Chem. B* **1999**, *103*, 3292–3307.

(3) Baldelli, S.; Markovic, N.; Ross, P.; Shen, Y.; Somorjai, G. Sum Frequency Generation of CO on (111) and Polycrystalline Platinum Electrode Surfaces: Evidence for SFG Invisible Surface CO. *J. Phys. Chem. B* **1999**, *103*, 8920–8925.

(4) Shen, Y. R. *The Principles of Nonlinear Optics*; Wiley, 1984.

(5) Richmond, G. L. Molecular Bonding and Interactions at Aqueous Surfaces as Probed by Vibrational Sum Frequency Spectroscopy. *Chem. Rev.* **2002**, *102*, 2693–2724.

(6) Mallat, T.; Baiker, A. Oxidation of Alcohols with Molecular Oxygen on Platinum Metal Catalysts in Aqueous Solutions. *Catal. Today* **1994**, *19* (93), 247–284.

(7) Chibani, S.; Michel, C.; Delbecq, F.; Pinel, C.; Besson, M. On the Key Role of Hydroxyl Groups in Platinum-Catalysed Alcohol Oxidation in Aqueous Medium. *Catal. Sci. Technol.* **2013**, *3* (2), 339–350.

(8) Gomes, J. F.; Bergamaski, K.; Pinto, M. F. S.; Miranda, P. B. Reaction Intermediates of Ethanol Electro-Oxidation on Platinum Investigated by SFG Spectroscopy. *J. Catal.* **2013**, *302*, 67–82.

(9) Gauthier, E.; Benzinger, J. B. Gas Management and Multiphase Flow in Direct Alcohol Fuel Cells. *Electrochim. Acta* **2014**, *13*, 238–247.

(10) Dicosimo, R.; Whitesides, G. M. 2-Propanol to Acetone by Dioxygen on a Platinized Electrode under Open-Circuit Conditions'. *J. Phys. Chem.* **1989**, *93*, 768–775.

(11) Mallat, T.; Baiker, A. Oxidation of Alcohols with Molecular Oxygen on Solid Catalysts. *Chem. Rev.* **2004**, *104* (6), 3037–3058.

(12) Jelemensky, L.; Kuster, B. F. M.; Marin, G. B. Multiple Steady-States for the Oxidation of Aqueous Ethanol with Oxygen on a Carbon Supported Platinum Catalyst. *Catal. Letters* **1995**, *30*, 269–277.

(13) Besson, M.; Gallezot, P. Selective Oxidation of Alcohols and Aldehydes on Metal Catalysts. *Catal. Today* **2000**, *57* (1–2), 127–141.

Chapter 3

Preparation of Platinum Catalysts and Experimental SFG Setups

Introduction

Sum frequency generation (SFG) spectroscopy is a useful tool for studying catalysis under a variety of settings in both the gas and liquid phases.[1–7] This chapter describes the experimental designs that were fundamental to this research. The notable similarities and differences between the gas and liquid phase SFG setups are discussed. In addition, both thin film and nanoparticle catalysts were synthesized and studied using the following methods.

Catalyst Preparation

Nanoparticle Synthesis

Platinum nanoparticles were synthesized under argon atmosphere using a previously established method.[8] Polyvinylpyrrolidone (molecular weight = 29,000) was utilized as a capping agent. 4.0 ± 0.3 nm Pt-PVP nanoparticles were prepared by combining 20 mL of EG, 100 mg of $H_2PtCl_6 \cdot 6H_2O$ (1.9×10^{-4} mol, Sigma-Aldrich), and 440 mg of PVP (4×10^{-3} mol) in a 50 mL three-neck round bottom flask. The flask was sealed and residual air was evacuated by three cycles of vacuum pumping followed by an Ar purge. The synthesis was carried out at 165°C with vigorous stirring in Ar flow for 25 min.

When the solution returned to room temperature after synthesis, 100 mL of acetone was added to the solution and the nanoparticles were precipitated by centrifugation for approximately 10 min. The nanoparticles (black precipitate) were then redispersed in ethanol (10-20 mL) and precipitated with hexane (40-80 mL) three times to wash away excess PVP.

Core-shell nanoparticles were synthesized by dissolving 100-300 μL Pt-PVP and 5-10 μL tetraethyl orthosilicate (TEOS) with 15 mL ethanol in a 20 mL glass scintillation vial.[9] 2.25 mL of ammonium hydroxide was then added dropwise while the mixture was stirred. After all the ammonium hydroxide was added, the mixture was left in the sonicator for 2 hours. To separate the $Pt@SiO_2$ nanoparticles from the synthesis mixture, 6 mL acetone and 22 mL hexane were added and centrifuged at 4000 rpm for 10 min. Pt-PVP@SiO_2 were then washed two additional times by dissolving in 2 mL ethanol and precipitating in 12 mL hexane, followed by centrifugation and redissolution in ethanol.

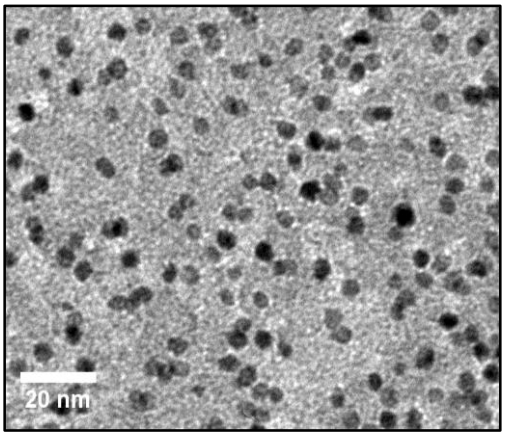

Figure 1 – TEM image of synthesized Pt-PVP nanoparticles determined to be 4 nm in diameter.

Langmuir-Blodgett Deposition

Langmuir-Blodgett (LB) monolayer film deposition was utilized for all SFG experiments on nanoparticles. PVP capped Pt nanoparticles were dissolved in a 50/50 ethanol/chloroform solution, then added dropwise to the surface of a water-filled trough. The solvent was then left to evaporate for 30 minutes, creating a layer of nanoparticles on the surface of the water. A probe was used to monitor the surface tension. The film was then compressed at a rate of 5 mm/min using Teflon barriers while monitoring the surface tension. Once the surface tension leveled off, indicating a monolayer of nanoparticles, the two-dimensional quartz substrate was raised from the water, allowing the nanoparticle film to be deposited on the quartz surface.

Transmission Electron Microscopy

Transmission electron microscopy (TEM) was used throughout this work to characterize nanoparticles. All images were collected using a JEOL 2100-F 200 kV Field-Emission TEM and analyzed using ImageJ software.

Electron Beam Deposition

In these studies, thin films of platinum nanoparticles were created using electron beam deposition. A 2 nm layer of titanium was deposited to aid in adhesion of the platinum to the silicon dioxide surface. 6 nm of platinum was then deposited on top of the titanium adhesion layer. The electron beam chamber was kept at a pressure below 10^{-5} Torr throughout the deposition. A quartz crystal microbalance was used to measure the deposition rate and film thickness.

Liquid Phase Setup

Liquid Reactor

In order to study liquid phase reactions with SFG spectroscopy, a specific flow cell and setup were utilized. A Teflon cell with a volume of 770 µL was used for the reaction flow cell. Teflon was chosen for the cell material, as its chemical inertness prevents it from interfering with any possible alcohol oxidation reactions. However, Teflon is a fairly soft material and has low thermal conductivity, which prevents it from being used above 80°C. In order to help support the cell, it was placed inside of an aluminum housing block with heating tape wrapped around the outside of the block. This allows for support of the Teflon cell and even heating. The flow of the cell was controlled by a peristaltic pump (Watson-Marlow 120U) which was run at 40-80 µL/min. The tubing utilized was silicone tubing with an inner diameter of 0.060 inches. Prior to passing through the Teflon cell, the reactant liquid was bubbled with a mixture of nitrogen and air controlled by mass flow controllers. The mixture was then transported to the reaction cell using stainless steel tubing so as to ensure constant concentration of the gases. After passing through the reactor, the liquid was pumped to a liquid-vapor exchange column in which the vapors from the product were mixed with nitrogen gas which was then able to be sampled by a gas chomatograph.

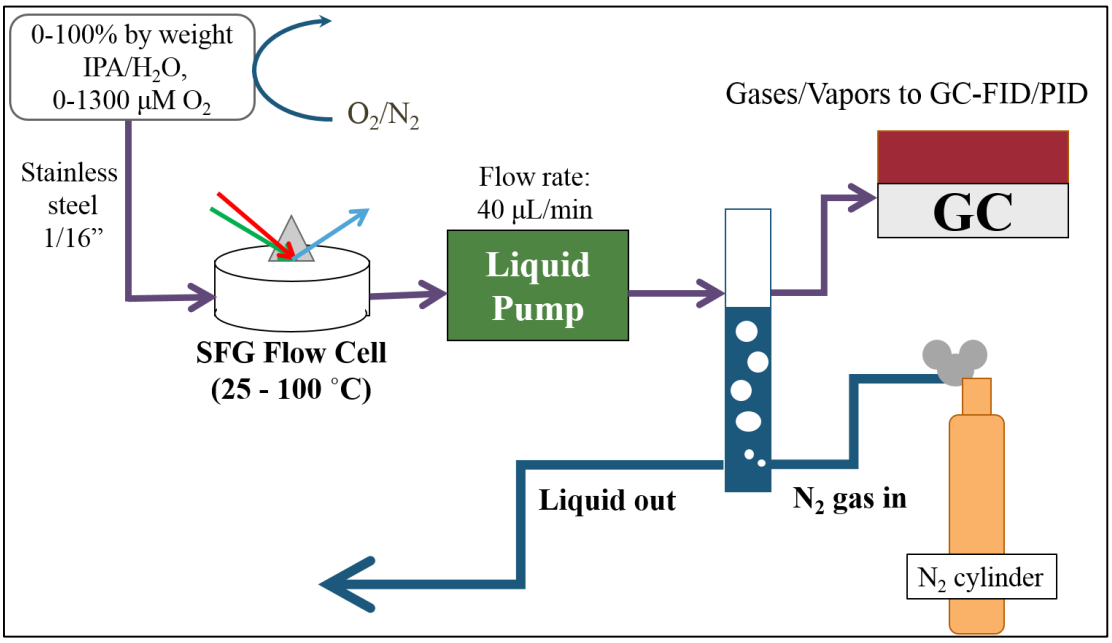

Figure 2 – Schematic of the setup for studying alcohol oxidation in the liquid phase with SFG spectroscopy.

Liquid Phase SFG

For all liquid phase SFG experiments outlined in this work, a picosecond neodymium:yttrium aluminum garnet (Nd:YAG) laser was used. This laser produces a 1064 nm beam with 20 ps

pulses of 15-20 mJ. This 1064 nm beam then is split into a 532 nm visible beam and a tunable infrared beam capable of scanning 2700-3500 cm^{-1}. The 532 nm beam is produced by passing the part of the 1064 nm beam through a frequency-doubling crystal of beta barium oxide (BBO). The 532 nm beam is then split, with part of the beam traveling to the sample and part of the beam pumping two potassium titanyl phosphate (KTP) crystals for optical parametric generation (OPG). This beam then passes through two potassium titanyl arsenate (KTA) crystals. Rotating these KTP and KTA crystals results in a changing IR beam that can scan from approximately 2700 cm^{-1} to 3500 cm^{-1}.

The visible and IR beams then pass through a polarizer and waveplate to achieve the desired polarization and are directed to the sample surface. The visible beam strikes the surface at an incident angle of 62° and the IR beam at an angle of 45°. These beams pass through a CaF_2 prism and the catalyst sample deposited on a quartz window. CaF_2 is utilized due to its high IR wavelength transmission, but the sample itself is deposited on quartz for greater ease in sample preparation and to allow use in aqueous phase reactions.

In order to maximize the light transmission between the CaF_2 prism and the quartz window, an IR-transparent index matching gel was created in the Somorjai group consisting of a mixture of d_8-polystyrene and d_{18}-decahydronapthalene. As this gel is made of deuterated materials and has an index of refraction close to quartz and CaF_2, it minimizes both refraction between the materials and possible IR interference.

The SFG signal generated from the surface is then detected by a photomultiplier tube (PMT) detector. A gated integrator system with a 100 ns gate time was used to improve the signal-to-noise ratio.

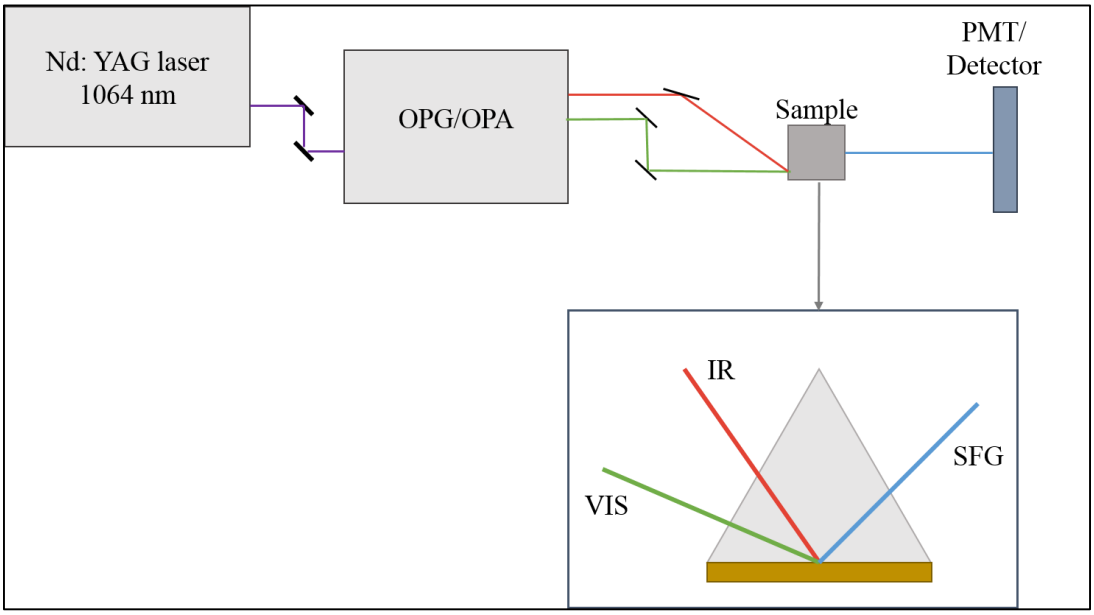

Figure 3 – A schematic of the liquid-phase SFG setup, including the Nd:YAG laser, OPG/OPA, sample stage, and PMT.

Gas Phase Setup

The gas phase SFG setup utilized was similar to the liquid phase setup. An Nd:YAG laser was also used for the gas phase reactions, and the 1064 nm beam from the laser passed through an OPG/OPA to achieve a 532 nm beam and a tunable IR beam of 2700-3500 cm^{-1}. The SFG signal from the solid-gas interface was also collected with a PMT detector and integrated using a gated integrator system.

However, there were several key differences between the liquid phase and gas phase systems. Primarily, the positions of the IR and visible beams approaching the sample were reversed, with the visible beam incident on the surface at a 40° angle and the IR beam incident at a 50° angle relative to the surface normal. The angle adjustments were made to account for the differences in indexes of refraction between gas and liquid phases.

The reactor setup was significantly different as well. Instead of using a Teflon cell nested inside of an aluminum block, the gas-phase reactor was made entirely of aluminum. This allows for higher temperatures than with the Teflon cell (up to approximately 120°C). The quartz window is pressed against the aluminum with a small hollow in the aluminum underneath to allow reaction gases to come into contact with the catalyst surface. A Kalrez o-ring is used to provide a seal. The cell is connected through stainless steel tubing to a gas reservoir and recirculation pump, as well as a gas manifold to allow various reaction gases to be introduced to the system. A mechanical pump and turbomolecular pump are connected to the SFG reactor, allowing the system to be pumped down to 10^{-5} Torr. This allows the reactor to be essentially completely cleared of gas in between each SFG scan.

Gas Chromatography

Throughout these experiments, catalytic reaction studies were carried out, and a gas chromatograph (GC) was utilized to detect the composition of the product mixtures. The reactor setup for the gas phase reactions employed a batch reactor setup. A mechanical pump and turbomolecular pump were connected to the reactor for gas evacuation, much like the SFG gas phase system. The catalyst was placed into the reactor on the sample heater. A recirculation pump was used for gas mixing, and a manifold allowed gases to be introduced in a controlled manner. The products were sampled into the GC over a time span of several hours and identified using a flame ionization detector (FID).

Conclusion

Sum frequency generation studies were carried out at both the solid-liquid and solid-gas interfaces, with setups designed specifically for each interface. The liquid phase SFG system utilized a flow cell reactor, whereas the gas phase system was a batch reactor. The methods for creating both the thin films and nanoparticles which were used in this work have been described as well.

References

(1) Richmond, G. L. Molecular Bonding and Interactions at Aqueous Surfaces as Probed by

Vibrational Sum Frequency Spectroscopy. *Chem. Rev.* **2002**, *102*, 2693–2724.

(2) Miranda, P. B.; Shen, Y. R. Liquid Interfaces : A Study by Sum-Frequency Vibrational Spectroscopy. *J. Phys. Chem. B* **1999**, *103*, 3292–3307.

(3) Cremer, P. S.; Su, X.; Shen, Y. R.; Somorjai, G. A.; August, R. V. Ethylene Hydrogenation on Pt (111) Monitored in Situ at High Pressures Using Sum Frequency Generation. *J. Am. Chem. Soc.* **1996**, *118*, 2942–2949.

(4) Thompson, C. M.; Carl, L. M.; Somorjai, G. A. Sum Frequency Generation Study of the Interfacial Layer in Liquid-Phase Heterogeneously Catalyzed Oxidation of 2-Propanol on Platinum: Effect of the Concentrations of Water and 2-Propanol at the Interface. *J. Phys. Chem. C* **2013**, *117* (49).

(5) Gomes, J. F.; Bergamaski, K.; Pinto, M. F. S.; Miranda, P. B. Reaction Intermediates of Ethanol Electro-Oxidation on Platinum Investigated by SFG Spectroscopy. *J. Catal.* **2013**, *302*, 67–82.

(6) Marsh, A. L.; Becraft, K. A.; Somorjai, G. A. Methane Dissociative Adsorption on the Pt(111) Surface over the 300-500 K Temperature and 1-10 Torr Pressure Ranges. *J. Phys. Chem. B* **2005**, *109*, 13619–13622.

(7) Harris, A. L.; Chidsey, C. E. D.; Levinos, N. J.; Loiacono, D. N. Monolayer Vibrational Spectroscopy By Infrared-Visible Sum Frequency Generation at Metal and Semiconductor Surfaces. *Chem. Phys. Lett.* **1987**, *14* (4), 350–356.

(8) Tsung, C.; Kuhn, J. N.; Huang, W.; Aliaga, C.; Hung, L.; Somorjai, G. A.; Yang, P. Sub-10 Nm Platinum Nanocrystals with Size and Shape Control : Catalytic Study for Ethylene and Pyrrole. *J. Am. Chem. Soc.* **2009**, *131*, 5816–5822.

(9) Michalak, W. D.; Krier, J. M.; Alayoglu, S.; Shin, J.; An, K.; Komvopoulos, K.; Liu, Z.; Somorjai, G. A. CO Oxidation on PtSn Nanoparticle Catalysts Occurs at the Interface of Pt and Sn Oxide Domains Formed under Reaction Conditions. *J. Catal.* **2014**, *312*, 17–25.

Chapter 4

Significant Differences in Kinetics and Mechanisms of Catalytic 1-Propanol Oxidation on Size-controlled Platinum Nanoparticles at Solid-Gas and Solid-Liquid Interfaces

Introduction

Heterogeneous catalysis - including solid-gas, solid-liquid, and liquid-gas reactions - contributes largely to the production of chemical feedstock and energy sources. For example, the total or partial oxidation of alcohols is very important for fuel cells and fine chemical synthesis.[1–6] In addition, many industrial catalytic alcohol oxidation reactions are carried out in the liquid phase, but their reaction kinetics and mechanisms are not as well understood as those in the gas phase.[7]

Previously, we found that Pt nanoparticles were good catalysts for the oxidation of methanol, ethanol, and isopropanol to different products in both the gas and liquid phases.[8–10] We observed several variances between the two phases such as the reaction rates, product selectivity, apparent activation energies, (E_a) and H_2O effects. We attributed these differences to the molecular orientation at the surface of the catalyst in each phase.[9,10] Herein, the catalytic oxidation of 1-propanol by oxygen on size-controlled Pt nanoparticles has been chosen to be studied as it offers a unique insight into the general kinetics and mechanisms of alcohol oxidation as a longer chain, primary alcohol. In this study, 1-propanol was systematically studied with kinetic measurements and SFG to investigate the interfacial environment – which may be significantly different from the bulk liquid in terms of local component concentrations – and correlate this with the catalytic activity measured simultaneously.

Experimental

Synthesis of Pt Nanoparticles

The Pt nanoparticles with various controlled sizes (2, 4.5, 6 and 7 nm) were synthesized through colloidal methods using ethylene glycol as the solvent and reducing agent and polyvinylpyrrolidone (PVP) as the capping agent (details are described in Supporting Material). The average sizes for as-synthesized Pt nanoparticles are 1.6 ± 0.2, 4.6 ± 0.7, 6.2 ± 0.7, and 6.9 ± 0.9 nm, which were determined from the transmission electron microscopy (TEM) images shown in Figure S1 with narrow size distributions (Figure S2 in Supporting Material). From the inserted high resolution TEM images, all Pt nanoparticles have clear lattice fringes and the measured interplanar distances are about 0.227 nm, indicating the exposure of Pt (111). All the as-

synthesized Pt nanoparticles are mainly in the metallic phase (Pt0), as confirmed by the X-ray absorption near edge structure (XANES) spectra (Figure S3). Before performing the reactions, the Pt nanoparticles were immobilized into the inert mesoporous silica support (MCF-17) using an ultrasonication method (TEM images shown in Figure S4), and the elemental analysis was carried out using inductively coupled plasma atomic emission spectroscopy (ICP-AES) to determine the Pt contents in Pt/MCF-17 samples for the calculation of turnover frequency (TOF).

Sum Frequency Generation Vibrational Spectroscopy

Sum Frequency Generation Vibrational Spectroscopy (SFG-VS) is a nonlinear spectroscopic technique that allows for vibrational spectra to be collected specifically from surfaces and interfaces. Rather than probing the molecular dipole (Infrared absorption) or polarizability (Raman spectroscopy) SFG probes the molecular hyperpolarizability. The hyperpolarizability (β) can be represented as the product of the molecular dipole (μ) and polarizability (α).

$$\beta_{abc} = \mu_c \cdot \alpha_{ab}$$

Under the assumption of electro-diploe approximation, centrosymmetry cannot have a vibrational mode with both a nonzero dipole moment and a nonzero polarizability, thus SFG can only occur when centrosymmetry is broken – most importantly, at interfaces between phases. This property makes SFG exceedingly useful for selectively obtaining vibrational spectra from molecules adsorbed at a gas-solid or liquid-solid interface. The SFG signal is generated when two beams – a visible beam with a fixed wavelength and an infrared beam with a tunable wavelength – are overlapped at the interface both spatially and temporally. The signal intensity increases when the wavelength of the infrared beam is resonant with a vibrational mode of a molecule at that interface, thus giving an SFG spectrum.

In this study, this was accomplished using an active/passive mode-locked Nd:YAG laser (Continuum Leopard D-20) which produces 20 ps pulses of 1064 nm light at a repetition rate of 20 Hz. The fundamental 1064 nm output was passed through an optical parametric generator/amplifier (LaserVision) to give a second harmonic visible beam (VIS) of 532 nm and a mid-infrared beam (IR) tunable from 2700 – 3600 cm^{-1}. The IR and VIS beams each have a power of 200 μJ per pulse. Details have been described in the previous work.[10] The SFG signal was collected using a PMT accompanied by a gated integrator to improve the signal quality. Using a home-built cell, the surface was heated and a recirculating mixture of the reaction gases/liquid is passed onto the platinum film.

Results and Discussion

1-Propanol Oxidation in the Gas and Liquid Phases

The Pt nanoparticles with various controlled sizes (2, 4.5, 6 and 7 nm) were synthesized and characterized (see details in Supporting Information). The gas phase 1-propanol oxidation reactions were carried out in a gold-coated batch reactor, while the liquid phase reactions were performed using a high-pressure, Teflon-lined autoclave (Parr reactor) (see details in Supporting Information). The main products in both the gas and liquid phase reactions were detected by gas chromatography. Figure S4 shows selectivity for 1-propanol oxidation at 60°C on Pt/MCF-17

with different Pt NP sizes in gas phase and liquid phase. It is interesting to note a significant difference in the product yield for 1-propanol oxidation reactions at the solid-gas and solid-liquid interfaces. For gas phase reaction, the selectivity to propanal was 76-83% and the selectivity to CO_2 was 17-24% (Figure S4A). However, for the liquid phase reaction on the same samples, the selectivity to propanal was above 99.7% and the selectivity to CO_2 was less than 0.3% over various size of Pt nanoparticles (Figure S4B). More of the complete oxidation product CO_2 was formed at the solid-gas interface than at the solid-liquid interface, presumably due to the different reaction mechanisms. However, no obvious correlation between Pt nanoparticle size and product selectivity was observed for either the gas or liquid phase reactions. This result is similar to a previous ethanol oxidation study, in which acetaldehyde selectivity was found to be constant regardless of nanoparticle size.[9]

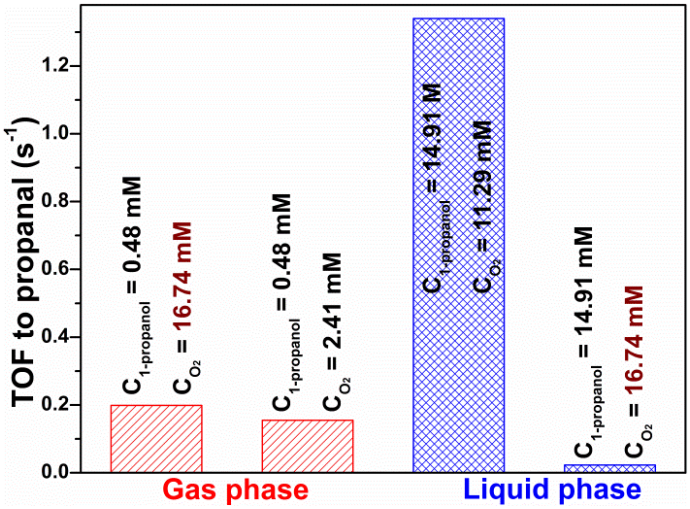

Figure 1 – TOF value comparison of 1-propanol to propanal in gas phase and liquid phase reactions under different reactant concentrations at 60°C on 4.5 nm Pt/MCF-17.

In regards to the turnover rate of 1-propanol to propanal as shown in Figure 1, for 4.5 nm Pt nanoparticles/MCF-17, the TOF value in the gas phase reaction was 0.199 s^{-1} at 60°C when using 10 Torr of 1-propanol and 347 Torr of O_2 as reactants, and He as balance (corresponding to [1-propanol] = 0.48 mM and [O_2] = 16.74 mM). By reducing the oxygen concentration to 2.41 mM, the TOF value slightly decreased to 0.155 s^{-1}, showing the near saturation concentration for molecular oxygen on the Pt. For the liquid phase reaction on the same sample using pure 1-propanol and dissolved oxygen at atmospheric pressure as reactants at 60°C (corresponding to [1-propanol] = 14.91 M and [O_2] = 11.29 mM), the TOF value was as high as 1.335 s^{-1}. This value is 6.7 times the activity of the gas phase reaction with the O_2 concentration on the same order of magnitude. However, this is presumably due to the much higher surface density of pure 1-propanol, as the 1-propanol concentration in the liquid phase reaction was nearly 31,000 times higher than that in the gas phase reaction. In order to lessen the contrast of TOF values between the gas phase and the liquid phase reactions, the liquid 1-propanol was diluted to 1:1000 ratio with heptane, which is a neutral solvent and showed only a negligible effect on the reaction kinetics of alcohol oxidation under similar reaction conditions.[11] After heptane dilution ([1-

propanol] = 14.91 mM and [O_2] = 16.74 mM), the TOF value of the liquid phase reaction was dramatically decreased to 0.023 s^{-1}. Therefore, after normalizing to the concentration, the gas-phase 1-propanol oxidation catalyzed by Pt nanoparticles is 2 orders of magnitude faster than in the liquid phase. This result shows a significant effect of 1-propanol concentration on the turnover frequency and also suggests different reaction kinetics in the solid/liquid phase.

The catalytic activities on size dependence in both the gas phase and liquid phase were also evaluated, as shown in Figure 2, and 1-propanol oxidations show highly size-dependent. Higher TOF value was observed for larger Pt nanoparticles. In the gas phase reaction at 60ºC, the TOF of 1-propanol was only 0.028 s^{-1} on 2 nm Pt, and this value increased to 0.162 s^{-1} on 4.5 nm Pt, 0.221 s^{-1} on 6 nm Pt and 0.255 s^{-1} on 7 nm Pt (increased ca. 9 times). For the pure liquid 1-propanol at 60ºC, the TOF of 1-propanol showed an obvious increase with the growth of Pt nanoparticle size (increased ca. 8 times), i.e. 0.752, 1.338, 2.939 and 6.064 s^{-1} on 2, 4.5, 6 and 7 nm Pt, respectively. The activation energies (E_a) of 1-propanol on Pt nanoparticles, calculated from the measurement of the temperature dependence of 1-propanol oxidation reactions (Figure S5), show size dependence in both the gas and liquid phases as shown in Figure 2B.

However, the liquid phase reaction also showed a much stronger dependence on particle size than the gas phase, especially at larger sizes. At the solid-gas interface, the Ea for 1-propanol oxidation was found to be as high as 179 kJ/mol on 2 nm Pt nanoparticles. Ea values decreased to 123, 118, and 113 kJ/mol on 4.5, 6, and 7 nm Pt, respectively. At the solid-liquid interface, the Ea was ~5 times lower (32 kJ/mol) on 2 nm Pt, and this value further decreased to 29, 20, 15 kJ/mol on 4.5, 6, and 7 nm Pt, respectively. Furthermore, in the gas phase, the propanal production on all Pt nanoparticles in the range of 2-7 nm all show a higher yield at higher temperatures (Figure S6A); however, in the liquid phase, the temperature effect is negligible on selectivity towards propanal (Figure S6B). These results all suggest different reaction mechanisms were present under different surface concentration of 1-propanol at the solid-liquid and the solid-gas interfaces.

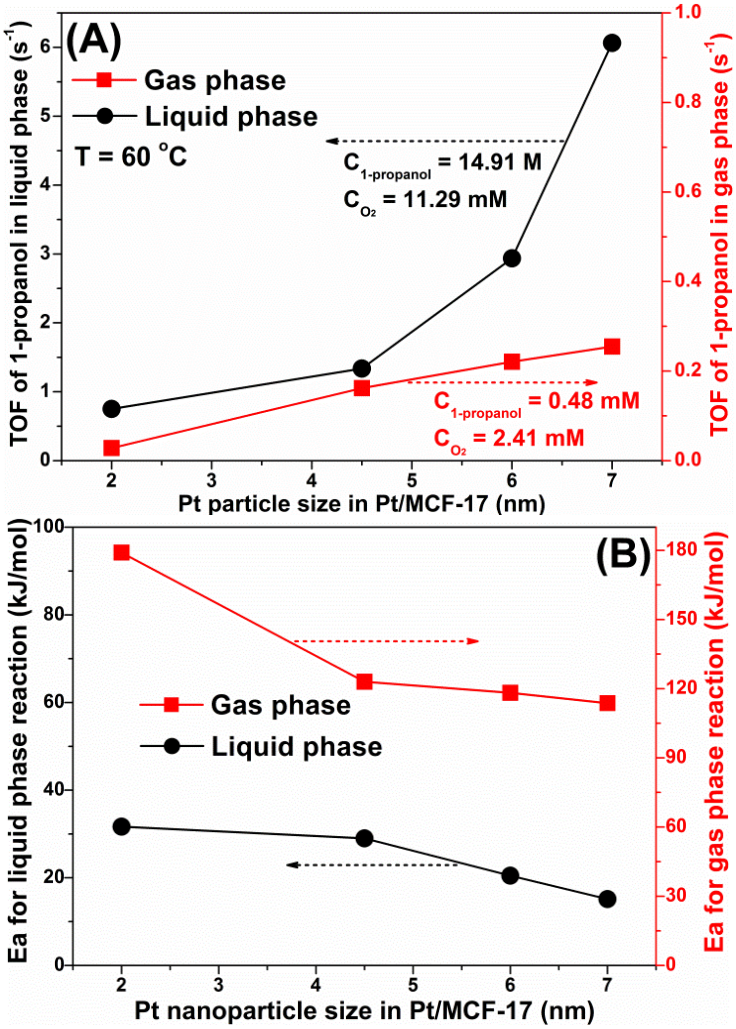

Figure 2 – Size effect of Pt nanoparticles on (A) Turnover frequency (TOF) of 1-propanol at 60°C and (B) apparent activation energy (E_a) of 1-propanol oxidation in gas and liquid phases.

Water Effects

We further examined the effect of coordinated water on oxidation of 1-propanol in gas and liquid phases on 4.5 nm Pt/MCF-17 – the results are shown in Figure 3.

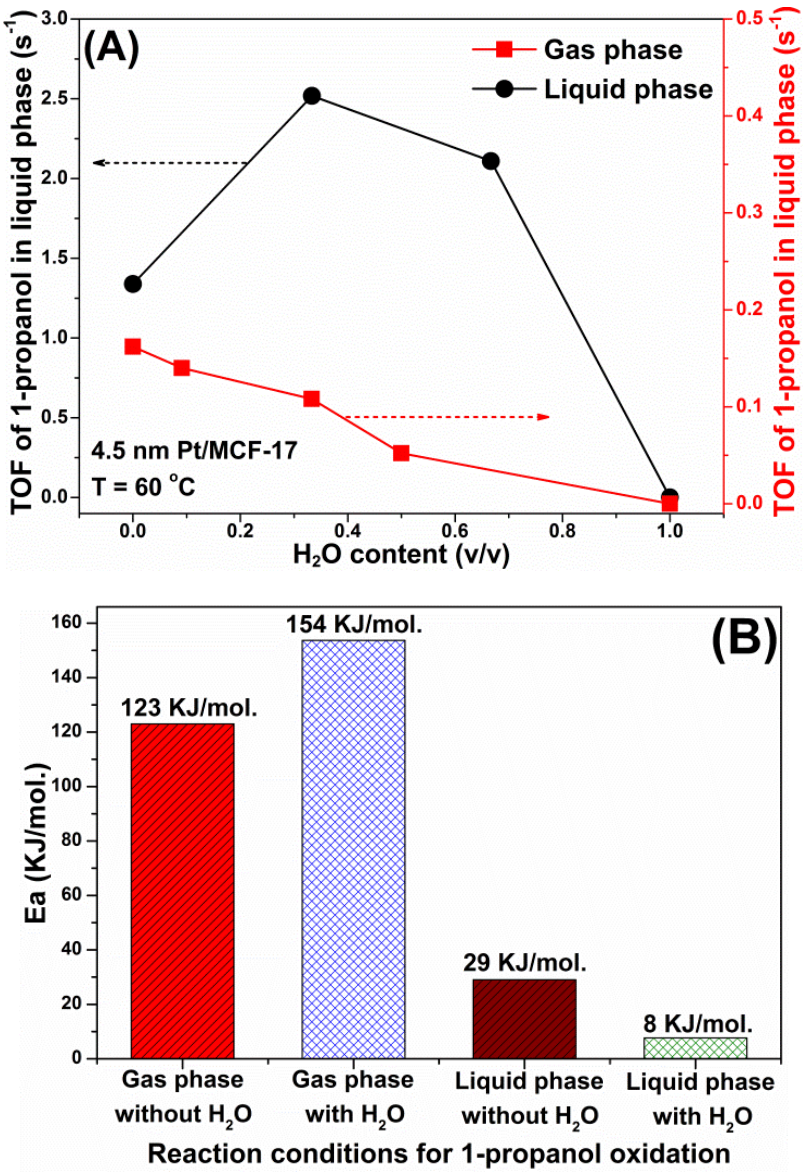

Figure 3 – (A) Effect of H_2O addition on TOF of 1-propanol over 4.5 nm Pt-MCF-17 at 60ºC in gas and liquid phases; (B) Apparent activation energy for 1-propanol oxidation on 4.5 nm Pt/MCF-17 in gas and liquid phases with/without H_2O.

Distinct responses to water were observed for the gas phase reaction. The TOF of 1-propanol in the H_2O-free reaction condition at 60ºC (10 Torr of 1-propanol and 50 of Torr O_2) was 0.162 s^{-1},

with a significant decrease to 0.140, 0.108 and 0.052 s^{-1} in the presence of 1, 5, and 10 Torr of water vapor, respectively (Figure 3A). The water vapor showed a strong inhibiting effect on the 1-propanol oxidation in the gas phase, likely due to the blocking of active sites on the Pt surface by water vapor, resulting in the insufficient adsorption of alcohols and a drastic decline in activity. However, in a striking contrast, water showed a significant promoting effect on the 1-propanol oxidation in the liquid phase. For example, under the water-free reaction condition with pure 1-propanol and dissolved oxygen at 60^{o}C, the TOF of 1-propanol was 1.338 s^{-1}, while this value remarkably increased to 2.518 s^{-1} when the 1-propanol to water ratio was at 2:1. Further increasing the water content with the 1-propanol to water ratio to 1:2 led to the slight decrease of the TOF value to 2.109 s^{-1}. The activity was still 57% higher than that in the water-free condition. These findings correlate with the previous studies carried out on ethanol oxidation, in which water was also found to have a promoting effect in the liquid phase and an inhibiting effect in the gas phase.[9]

A noteworthy interesting result is that the presence of water vapor or liquid water slightly decreased the propanal selectivity and improved the CO_2 selectivity to a certain extent for 1-propanol oxidation in the gas phase and liquid phase, respectively (Figure S7). This result indicates that the surface hydroxyls resulting from H_2O adsorption on Pt nanoparticles might be a common reactive species participating in the 1-propanol oxidation processes at both the solid-gas and solid-liquid interfaces. The important role of surface hydroxyls resulting from H_2O on Pt and Au catalysts for alcohol oxidation reactions were also emphasized by other researchers.[11,12]

In these studies, the presence of water itself was not found to enhance the rate, but rather the rate was enhanced by the reaction of water with dissociated oxygen to form hydroxyl species. The reactive alcohol was found to then preferentially interact with these pre-adsorbed hydroxyl species over chemisorbing to the Pt surface. This is believed to be due to thermodynamic effects, in which an alcohol bonding to a pre-adsorbed hydroxyl species was found to be 0.32 eV more stable than the co-chemisorption of the two molecules each on top of a Pt atom.[13] Furthermore, the temperature dependence of 1-propanol oxidation reactions with and without H_2O in the range of 50-80^{o}C on 4.5 nm Pt/MCF-17 was investigated in detail (Figure S8).

The apparent activation energy of 1-propanol oxidation in the presence of H_2O in the gas phase and liquid phase (Figure 3B) showed dramatic change compared with the activation energy in the absence of H_2O. In the case of the gas phase 1-propanol oxidation, the presence of water vapor led to the obvious increase of Ea by ca. 25%. In contrast, for the liquid phase 1-propanol oxidation, the presence of liquid water significantly decreased the Ea value by ca. 72% from 29 to 8 kJ/mol, evidence that liquid water is an efficient promoter for this reaction, with less sensitivity to the reaction temperature. All these results point to a conclusion that the 1-propanol oxidation on Pt nanoparticles undergo kinetics and mechanisms at the solid-gas and solid-liquid interfaces. It is therefore essential to examine the reaction at the molecular level with an in situ surface sensitive technique, such as sum frequency generation (SFG) vibrational spectroscopy along with cooperate mechanistic studies using DFT to elucidate the reaction mechanisms.[14–18]

Sum Frequency Generation Vibrational Studies and DFT Calculations

Sum Frequency Generation Vibrational Spectroscopy, an *in-situ* surface specific technique, is utilized here to understand how the reactant molecules interact with the catalyst surface under

working catalytic conditions and correlate these interactions with the reaction results. Spectroscopic studies were done on electron beam deposited platinum thin films at 60 °C. First, to examine the effect of surface density on the surface species and molecular structure under reaction, the gas phase spectrum was taken under 1-propanol vapor pressures of 14 and 68 Torr with 760 Torr of O_2 as shown in Figure 4 a and b. We assign observed peaks in the SFG spectra, including a symmetric CH_2 stretch at ~2840 cm^{-1}, a symmetric CH_3 stretch at ~2870 cm^{-1}, an asymmetric CH_2 stretch at ~2910 cm^{-1}, a CH_3 Fermi resonance at ~2935 cm^{-1}, and an asymmetric CH_3 stretch at ~2970 cm^{-1}. These spectra also exhibit an appreciable difference in both the strength of the CH_2 peaks and the ratios between the asymmetric and symmetric methyl stretches, which is direct evidence that surface orientation is dependent on reactant density. To further verify the surface species, we flowed propanal purged with N_2 in place of 1-propanol. The SFG spectrum of propanal on Pt as shown in Figure 4c shows peaks at ~2750 cm^{-1}, ~2890 cm^{-1}, and ~2950 cm^{-1}, which does not match the 1-propanol spectrum on Pt under reaction conditions. This result suggests a lack of reaction product, propanal, on the surface during the reaction, and indicates that the surface is instead populated with reactant intermediates.

Given the SFG measurement was taken only under the ppp polarization, the absolute orientation of the surface molecules cannot be determined straightforwardly under these conditions. However, SFG theory predicts that a change in the orientation of a functional group relative to the surface can lead to a change in the intensity ratio of the vibrational modes for the same functional group.[10] In this experiment, the Pt surface is considered to have C_∞ symmetry, and it is assumed that the 1-propanol molecules orient isotropically with respect to the azimuthal angle to the z-axis. This allows the average tilt angle from the surface, θ, of the CH_3 group to be described by the measurement. A change in the symmetric/asymmetric mode ratio between spectra is indicative of a change in θ. With lower partial pressure of 1-propanol, the ratio between the symmetric and asymmetric stretches is roughly 0.5:1. With higher partial pressure of 1-propanol, however, the ratio changes to approximately 2:1. This fourfold increase in the ratio suggests a significant difference in θ and therefore a different orientation under the differing surface density conditions. These results also support the DFT data (details are described in Supporting Information), which indicate a change from a “lying down” to a “standing up” orientation as the surface concentration increases.

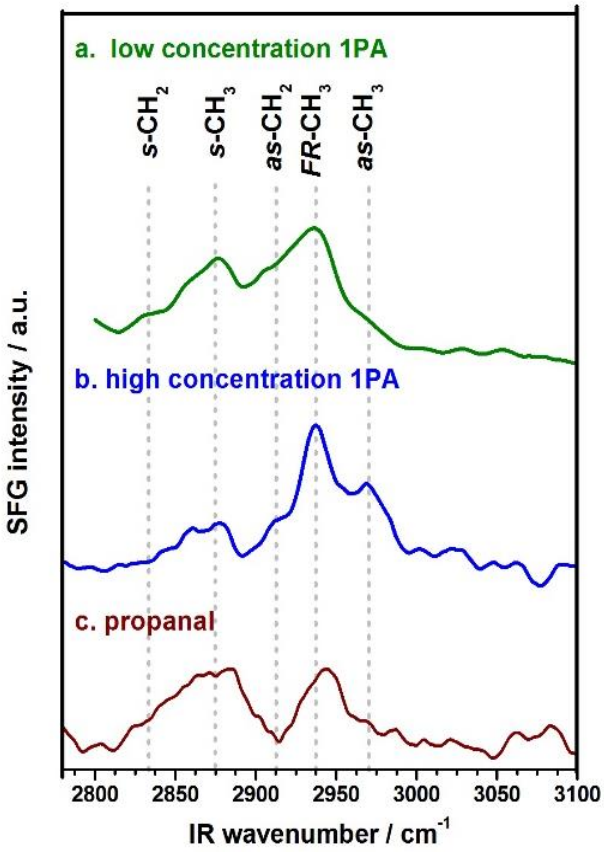

Figure 4 – SFG spectra of gas phase 1-propanol on Pt film under reaction conditions with 760 Torr of O_2 and 60^{o}C. a. 14 Torr of 1-propanol (1PA). b. 68 Torr of 1-propanol (1PA). c. SFG spectra of 230 Torr of propanal on Pt film at 60^{o}C.

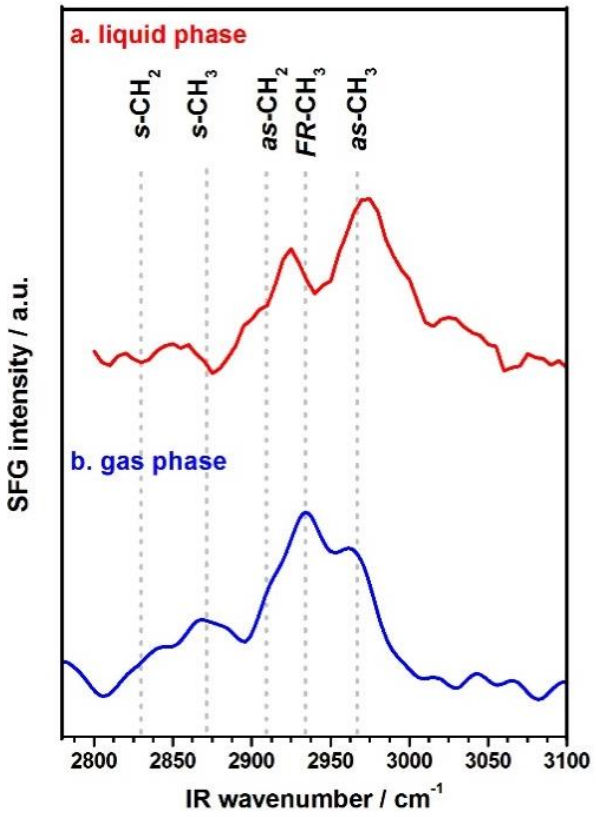

Figure 5 – SFG spectra of 1-propanol on Pt film purged with N_2 inert gas at 60°C in the a. liquid phase and b. gas phase, 80 Torr of 1-propanol.

The surface density effect on molecular structure is further investigated under purging with inert N_2 gas at 60°C as shown in Figure 5. The gas phase spectrum, Figure 5b, is similar to the one taken under O_2 and a higher partial pressure of 1-propanol in Figure 4b. The spectrum shows several vibrational features indicative of a CH_3 group, including a symmetric stretch at ~2870 cm^{-1}, a strong Fermi resonance at ~2935 cm^{-1}, and an asymmetric stretch at ~2960 cm^{-1}. CH_2 stretches appeared at ~2840 cm^{-1} (symmetric) and ~2910 cm^{-1} (asymmetric) as weak shoulders. The liquid phase SFG spectrum, Figure 4a, shows a slight decrease in the CH_2 stretch modes as compared to the gas phase spectrum, as well as a slight increase in the ratio between the asymmetric and symmetric CH_3 stretches. The main spectrum features are the same. It can be assumed that the surface density of 1-propanol is higher at liquid phase, and the molecule structure is more ordered and preferential to a standing up configuration in the liquid phase. Additionally, a decrease in the intensity of the vibrational modes in the liquid phase is observed due to the difference in the refractive index between the gas and the liquid phases of 1-propanol.

In order to provide atomic-level insights into the 1-propanol oxidation on Pt nanoparticles, we used density functional theory (DFT) to model concentration-dependent 1-propanol oxidation on the Pt(111) surface-dominant surface for Pt nanoparticles (see details in Supporting Information).[17] The concentration of 1-propanol molecules on the Pt(111) surface changes their

geometrical configuration. At the 1/16 monolayer configuration, the 1-propanol molecules are almost "lying down" on the surface, a bisectrix connecting hydroxyl-O and methyl-C forms 6^{o} relative to the surface as shown in Figure 6(a). As the 1-propanol concentration increases, the 1-propanol molecules gradually "stand up" on the surface due to the steric intermolecular interaction (Figure S10). At a higher surface coverage, 1/4 monolayer, the 1-propanol molecules are "standing" on the surface with a bisectrix-surface angle of 41^{o} as shown in Figure 6(b). This result agrees well with and explains the change of the relative intensities in the SFG spectra (Figure 5) for the gas-phase and liquid phase adsorptions of 1-propanol molecules. As surface density increases from 1/16 monolayer to 1/4 monolayer, hydrogen atoms from the alcohol group become 0.56 Å closer to the surface and the adsorption energy increases from -0.506 eV to -0.686 eV when the concentration increases.

Moreover, accordingly to the calculations, 1-propanol oxidation to propanal on a Pt(111) surface is endothermic (unfavorable). Oxygen is a natural oxidant that can form stable products, making the overall reaction energetically favorable. Upon this theoretical suggestion, we experimentally confirmed that molecular oxygen promotes the reaction and its shortage suppresses the reaction (Figure 1). Oxygen molecules adsorb and dissociate on the Pt (111) surface and release energy, which decreases when the oxygen concentration increases due to interatomic repulsion (see SI). Atomically adsorbed oxygens oxidize 1-propanol on the Pt(111) surface forming propanal and water (Figure S13). Experimentally, we detect significant amounts of water among the reaction products that confirms this theoretical suggestion. 1-propanol reacts with the decomposed oxygen atoms on the Pt(111) surface, forming water as following:

$$C_2H_5CH_2OH + 2O + Pt(111) \rightarrow C_2H_5CHO + H_2O + O + Pt(111)$$

This reaction is energetically more favorable (by 0.36 eV) than the formation of two hydroxyl groups. As molecular coverage increases, the calculated activation barriers decrease from 3.25 eV at 1/16 monolayer to 1.59 eV at 1/4 monolayer. Calculated heats of formation also increase, supporting the experimental kinetic data. The calculated barriers are larger than experimentally measured, indicating that nanoparticle edges and corners may play an important role in the reaction and/or more complex reaction pathways. Future experimental work will be done on Pt single crystals to prove these theoretical results. Simulation also shows that the molecular orientation of the main product (propanal) is similar to the initial molecular orientation of 1-propanol at both 1/16 monolayer – as shown in Figure 6 (a) and (c) – and 1/4 monolayer as shown Figure 6 (b) and (d). Overall, these theoretical calculations show a distinct difference between low and high surface coverages, correlating with a significant difference between the gas and liquid phases in terms of molecular orientation and activation energy.

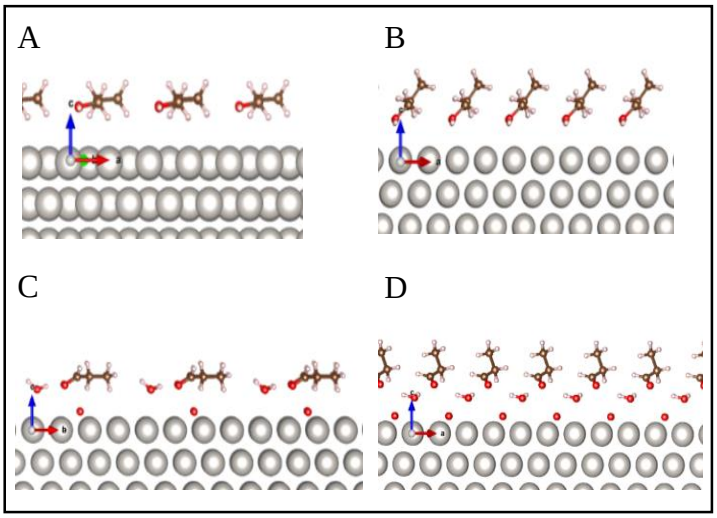

Figure 6 – Minimum energy configurations of 1-propanol molecules on Pt(111) surface for the (A) 1/16 and (B) 1/4 monolayer coverage. Minimum energy configurations of the complex propanal, H_2O and atomic oxygen molecules (red dot) on Pt(111) surface for the (C) 1/16, and (D) 1/4 monolayer coverage.

Conclusion

In summary, we have studied the 1-propanol oxidation reactions catalyzed by Pt nanoparticles with tunable sizes in both the liquid phase and the gas phase. These results broaden our understanding about the differences of alcohol oxidation at solid-gas and solid-liquid interfaces. The liquid-phase reaction differs from the gas-phase reaction in reaction rates, activation energy, dependence of surface concentration of 1-propanol, activation energy on nanoparticle size, and effect of water addition. The results indicate different kinetic processes at the solid-liquid interface vs. the solid-gas interface for the same reaction. Such differences could be partially due to the different orientations of 1-propanol species on the Pt nanoparticle surface. In general, our SFG spectra, combined with reaction kinetics, demonstrate that the concentrations of reactants at the surface in a liquid-phase heterogeneously catalyzed reaction can play a critical role in determining the reaction rate. Further studies will use SFG spectroscopy in the C−O vibrational range to verify the conformations of molecular adsorbates on the catalyst surface. SFG studies will also be carried out on Pt single crystals in order to gain a better insight into the effect of surface sites.

References

(1) Zhao, X.; Yin, M.; Ma, L.; Liang, L.; Liu, C.; Liao, J.; Lu, T.; Xing, W. Recent Advances in Catalysts for Direct Methanol Fuel Cells. *Energy Environ. Sci.* **2011**, *4*, 2736–2753.

(2) Besson, M.; Gallezot, P. Selective Oxidation of Alcohols and Aldehydes on Metal Catalysts. *Catal. Today* **2000**, *57* (1–2), 127–141.

(3) Mallat, T.; Baiker, A. Oxidation of Alcohols with Molecular Oxygen on Solid Catalysts. *Chem. Rev.* **2004**, *104* (6), 3037–3058.

(4) Gomes, J. F.; Bergamaski, K.; Pinto, M. F. S.; Miranda, P. B. Reaction Intermediates of Ethanol Electro-Oxidation on Platinum Investigated by SFG Spectroscopy. *J. Catal.* **2013**, *302*, 67–82.

(5) Gauthier, E.; Benzinger, J. B. Gas Management and Multiphase Flow in Direct Alcohol Fuel Cells. *Electrochim. Acta* **2014**, *13*, 238–247.

(6) Jelemensky, L.; Kuster, B. F. M.; Marin, G. B. Multiple Steady-States for the Oxidation of Aqueous Ethanol with Oxygen on a Carbon Supported Platinum Catalyst. *Catal. Letters* **1995**, *30*, 269–277.

(7) Mallat, T.; Baiker, A. Oxidation of Alcohols with Molecular Oxygen on Platinum Metal Catalysts in Aqueous Solutions. *Catal. Today* **1994**, *19* (93), 247–284.

(8) Wang, H.; An, K.; Sapi, A.; Liu, F.; Somorjai, G. A. Effects of Nanoparticle Size and Metal/support Interactions in Pt-Catalyzed Methanol Oxidation Reactions in Gas and Liquid Phases. *Catal. Letters* **2014**, *144* (11), 1930–1938.

(9) Sapi, A.; Liu, F.; Cai, X.; Thompson, C. M.; Wang, H.; An, K.; Krier, J. M.; Somorjai, G. A. Comparing the Catalytic Oxidation of Ethanol at the Solid-Gas and Solid-Liquid Interfaces over Size-Controlled Pt Nanoparticles: Striking Differences in Kinetics and Mechanism. *Nano Lett.* **2014**, *14* (11), 6727–6730.

(10) Wang, H.; Sapi, A.; Thompson, C. M.; Liu, F.; Zherebetskyy, D.; Krier, J. M.; Carl, L. M.; Cai, X.; Wang, L.-W.; Somorjai, G. A. Dramatically Different Kinetics and Mechanism at Solid/liquid and Solid/gas Interfaces for Catalytic Isopropanol Oxidation over Size-Controlled Platinum Nanoparticles. *J. Am. Chem. Soc.* **2014**, *136* (29).

(11) Mullen, G. M.; Zhang, L.; Evans, E. J.; Yan, T.; Henkelman, G.; Mullins, C. B. Oxygen and Hydroxyl Species Induce Multiple Reaction Pathways for the Partial Oxidation of Allyl Alcohol on Gold. *J. Am. Chem. Soc.* **2014**, *136*, 6489–6498.

(12) Mullen, G. M.; Zhang, L.; Jr, J. E.; Yan, T. Control of Selectivity in Allylic Alcohol Oxidation on Gold Surfaces : The Role of Oxygen Adatoms and Hydroxyl Species †. *Phys. Chem. Chem. Phys.* **2015**, *17*, 4730–4738.

(13) Chibani, S.; Michel, C.; Delbecq, F.; Pinel, C.; Besson, M. On the Key Role of Hydroxyl Groups in Platinum-Catalysed Alcohol Oxidation in Aqueous Medium. *Catal. Sci. Technol.* **2013**, *3* (2), 339–350.

(14) Lambert, A. G.; Davies, P. B.; Neivandt, D. J. Implementing the Theory of Sum Frequency Generation Vibrational Spectroscopy: A Tutorial Review. *Appl. Spectrosc. Rev.* **2005**, *40* (2), 103–145.

(15) Miranda, P. B.; Shen, Y. R. Liquid Interfaces : A Study by Sum-Frequency Vibrational

Spectroscopy. *J. Phys. Chem. B* **1999**, *103*, 3292–3307.

(16) Baldelli, S.; Markovic, N.; Ross, P.; Shen, Y.; Somorjai, G. Sum Frequency Generation of CO on (111) and Polycrystalline Platinum Electrode Surfaces: Evidence for SFG Invisible Surface CO. *J. Phys. Chem. B* **1999**, *103*, 8920–8925.

(17) Richmond, G. L. Molecular Bonding and Interactions at Aqueous Surfaces as Probed by Vibrational Sum Frequency Spectroscopy. *Chem. Rev.* **2002**, *102*, 2693–2724.

(18) Norskov, J. K.; Bligaard, T.; Rossmeisl, J.; Christensen, C. H. Towards the Computational Design of Solid Catalysts. *Nat. Chem.* **2009**, *1*, 37–46.

Chapter 4 Supplemental Information

Experimental Details

Pt Nanoparticle Synthesis

For 2 nm Pt nanoparticles, 50 mg of $H_2PtCl_6 \cdot 6H_2O$ and 50 mg of NaOH was dissolved in two separate portion of 2.5 ml of ethylene glycol. The solutions were mixed and heated to 160^{o}C and kept at that temperature for 3.5 hours under Ar atmosphere. After cooling down, 2.5 ml 1 M HCl solution was added to the black suspension and the nanoparticles were collected by centrifugation. The as-obtained nanoparticles were redispersed in 10 ml of 2.1 mg/ml PVP (Mw = 29,000) in ethanol with sonication. The nanoparticles were washed with hexane precipitation/ethanol redispersion cycles. Finally, the product was dispersed in 10 ml of ethanol.

In order to synthesize 4.5 nm Pt nanoparticles, 50 mg of $H_2PtCl_6 \cdot 6H_2O$ and 220 mg of PVP (Mw = 29,000) were dissolved in 10 ml of ethylene glycol and the solution was placed into a 160^{o}C oil bath for 1 hour under Ar atmosphere. The product was collected by acetone assisted centrifugation. The Pt nanoparticles were washed with hexane precipitation/ethanol redispersion cycles and finally sonicated into 10 ml of ethanol.

For 6 or 7 nm Pt nanoparticles, 80 mg of platinum (II) acetylacetonate and 55 mg of PVP (Mw = 55,000) were dissolved in 5 ml of ethylene glycol. The solution was then heated to 200^{o}C and held at that temperature for 10 or 30 min under Ar atmosphere. After being cooled to room temperature, then the resulting nanoparticles were precipitated with 45 ml of acetone and re-dispersed in 10 ml of ethanol. The nanoparticles were repeatedly washed by precipitating with hexane, centrifuging, and re-dispersing in ethanol before use.

Preparation of the Catalysts

The as-synthesized Pt nanoparticles were loaded on MCF-17 mesoporous silica with 20-30 nm pore size. The Pt nanoparticles and the MCF-17 support were mixed together in ethanol and sonicated in an ultrasonic bath (40 kHz, 80 W) for 2 hrs. The supported nanoparticles were collected by centrifugation. The products were washed with ethanol three times before they were dried at 80^{o}C overnight. The concentration of the Pt nanoparticles on the supported catalysts was determined by Inductive Coupled Plasma Atomic Emission Spectroscopy (ICP-AES). Known amount of the catalysts were sonicated in ethanol and drop-casted on silica wafers for gas phase reactions. For the liquid phase reaction, the catalysts were used as it is. The calculation of the active sites was based on the ICP-AES results and the size of the particles assuming Pt (111) surfaces and that of every surface Pt atom is active in the reaction.

Catalytic Oxidation of 1-Propanol

The gas phase 1-propanol oxidation reaction was performed in a gold covered batch reactor with a volume of 1 L. The temperature of the silica supported catalysts was adjusted with a boron nitride heater plate (50-80^{o}C). Usually 10 Torr of 1-propanol, 50 Torr of O_2 and 710 Torr of He were leaked into the chamber and the gas was circulated with a metal bellow pump. The gas composition was monitored by a gas chromatograph (GC) integrated with a flame ionization detector (FID). The catalytic conversion of 1-propanol was kept under 10% during the data collection. For the water effect experiments, 1-10 Torr of H_2O vapor was introduced to the reaction chamber.

The liquid phase reactions were carried out in a Teflon-lined stainless steel autoclave (Parr). Typically, 15 mg of catalysts were dispersed in 15 mL of liquid 1-propanol. The headspace of the reactor (85 ml) were purged and pressurized with O_2 (1 bar) before the reaction studies. The system was heated to elevated temperature (50-80^{o}C) and kept there for 3 hours under continuous stirring. After the reaction mixture was cooled down, the headspace gas was leaked to the GC-FID through an evacuated gas chamber. After the disassembly of the autoclave, the catalyst was separated with centrifugation and the liquid phase was analyzed with GC-FID. For water effect experiments the ratio of H_2O in 1-propanol was adjusted to 0-75 V/V% while the total amount of liquid was kept 15 ml. For the low 1-propanol concentration reaction, heptane was used as diluter since it has no effect on catalytic activity and activation energy of the alcohol oxidation reaction. The ratio of 1-propanol to heptane was 1:1000.

Supporting Experimental Results

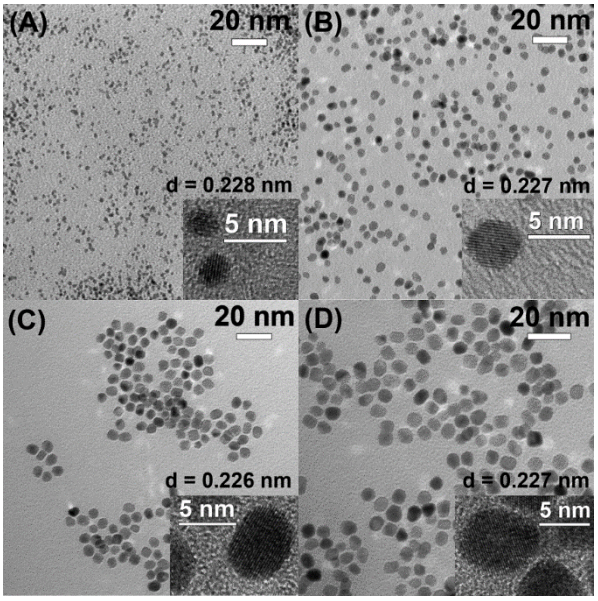

Figure S1 – TEM images of as-synthesized Pt nanoparticles with (A) 2, (B) 4.5, (C) 6, and (D) 7 nm average sizes.

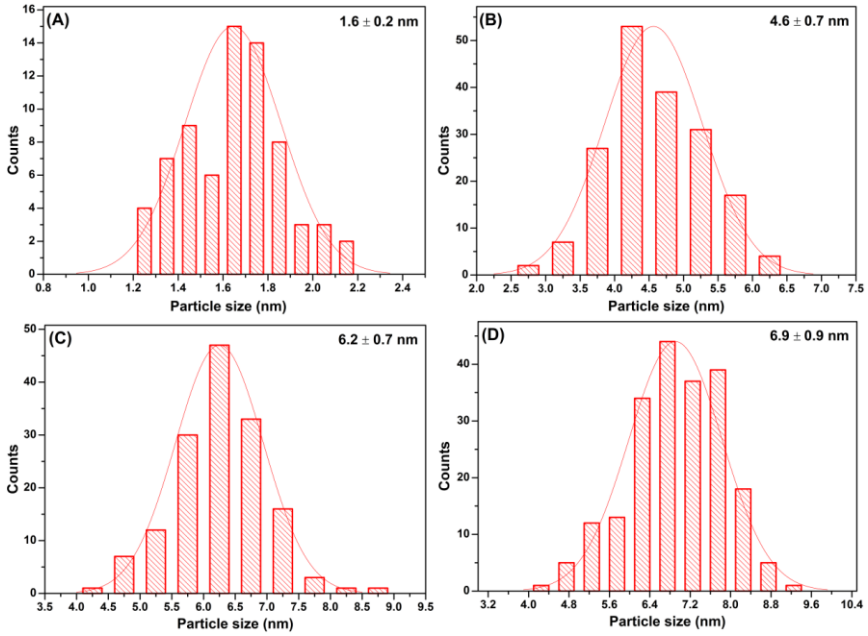

Figure S2 – Size distributions of synthesized Pt nanoparticles: (A) 2 nm Pt NPs, (B) 4.5 nm Pt NPs, (C) 6 nm Pt NPs, (D) 7 nm Pt NPs.

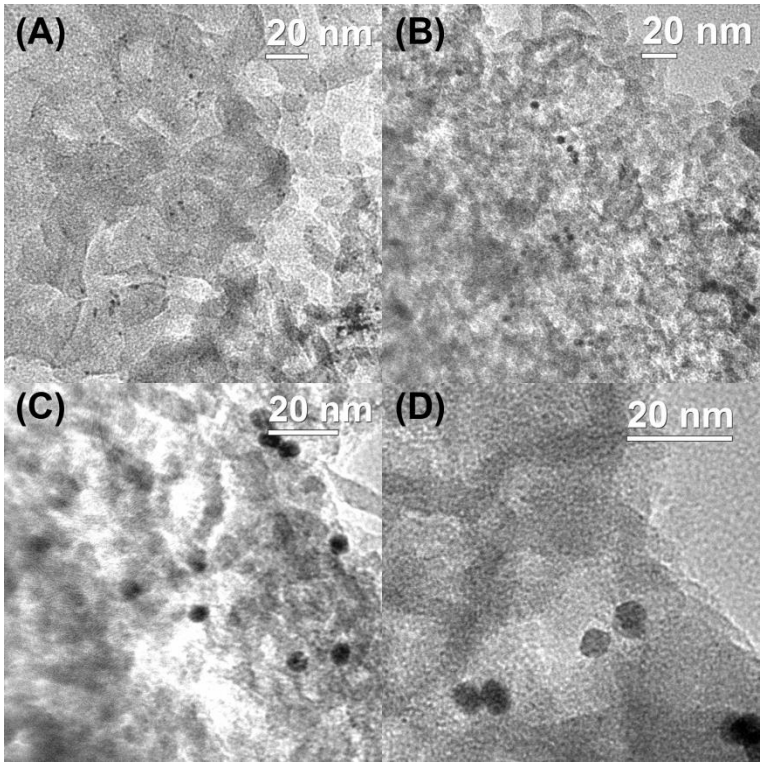

Figure S3 – TEM images of Pt/MCF-17 samples: 2 nm Pt NPs; 4.5 nm Pt NPs; 6 nm Pt NPs; 7 nm Pt NPs.

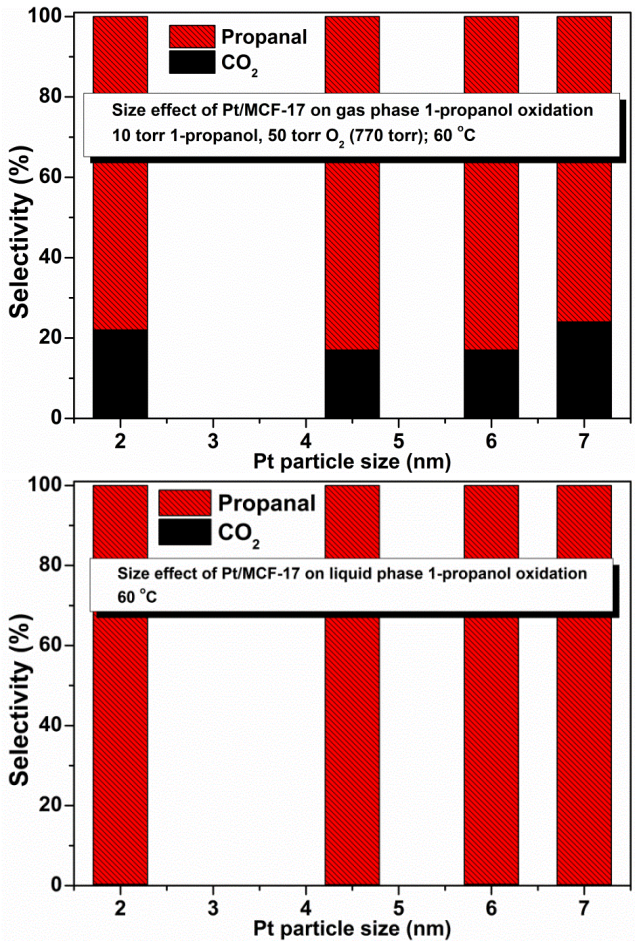

Figure S4 – Selectivity for 1-propanol oxidation at 60°C on Pt/MCF-17 with different Pt NP sizes in (A) gas phase and (B) liquid phase.

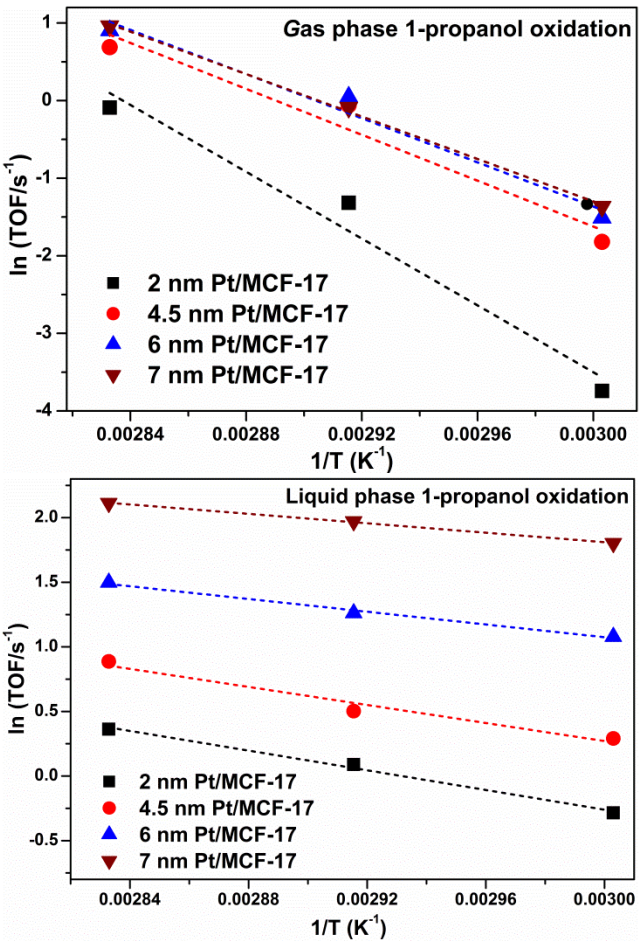

Figure S5 – Temperature dependence of 1-propanol oxidation on Pt/MCF-17 with different Pt NP sizes in (A) gas phase and (B) liquid phase.

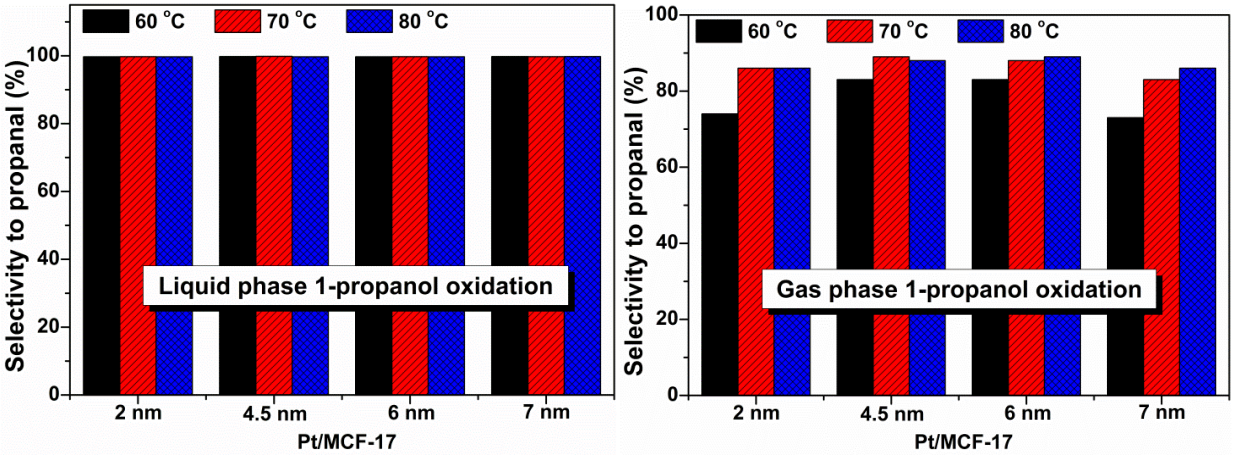

Figure S6 – Selectivity for 1-propanol oxidation at 60-80°C on Pt/MCF-17 with different Pt NP sizes in (A) gas phase and (B) liquid phase.

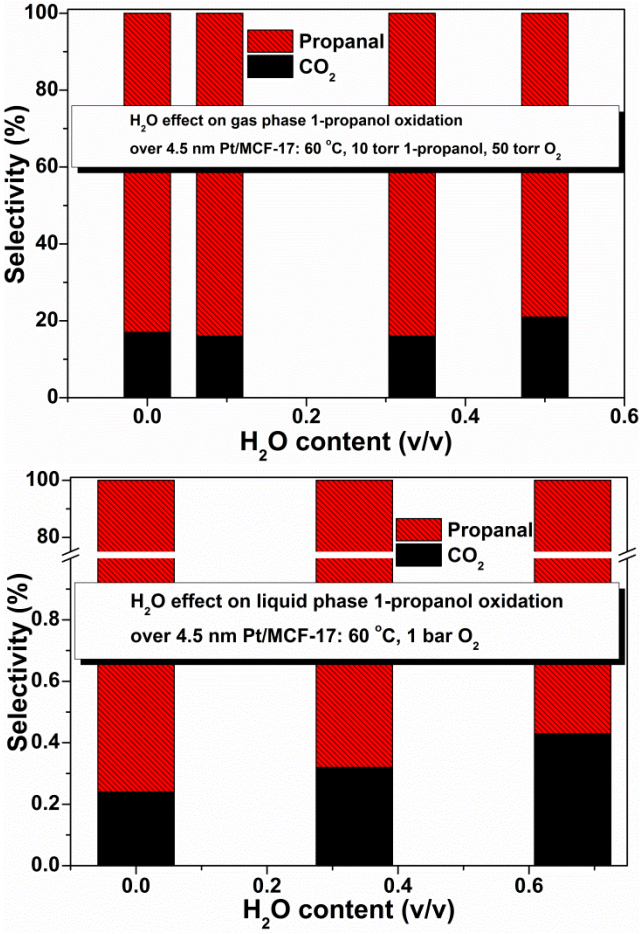

Figure S7 - Selectivity for 1-propanol oxidation at 60°C on 4.5 nm Pt/MCF-17 with different H_2O amounts in (A) gas phase and (B) liquid phase.

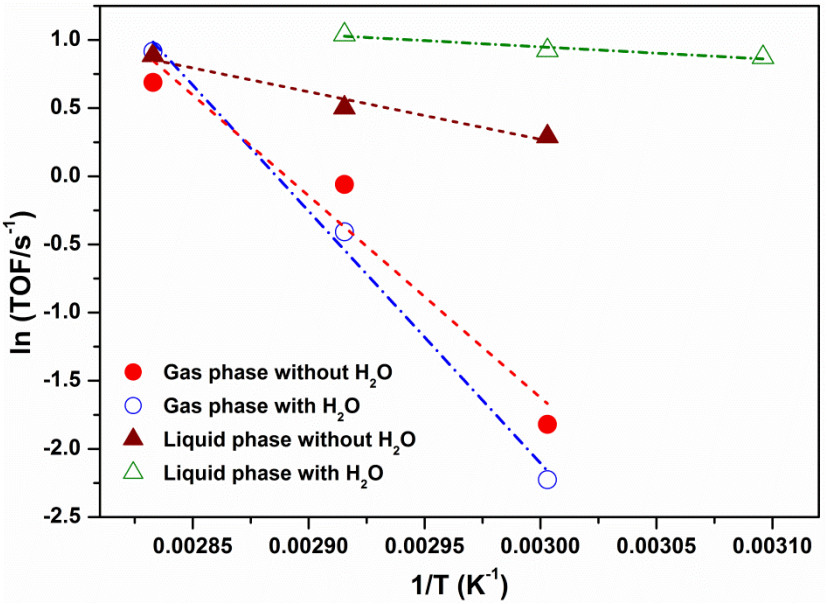

Figure S8 – Temperature dependence of 1-propanol oxidation on 4.5 nm Pt/MCF-17 with and without H_2O in gas and liquid phases.

Computational Information

Computational details

All geometry optimizations within the frame of density functional theory (DFT) are performed with first-principles periodic system calculations using VASP software package.[1] The projector augmented wave (PAW) method is utilized to construct the basis set for the one-electron wave functions with plane-wave basis set limited by cutoff energy of 400 eV.[2] For the constructed slabs, at least 3x3x1 Monkhorst-Pack k-point grid is used (depending on the geometrical dimensions). The Pt(111) slabs used are 4 layers thick and contain a minimum 17 Å vacuum space to exclude surface-surface interaction. The electronic steps are carried out with the energy convergence of 10^{-5} eV while the force convergence of ionic steps is set to be 5×10^{-3} eV/Å. Geometry optimization was performed using the PBE functional including Van der Waals interaction in DF approximation.[3,4] Dimer method has been used to find saddle points for activation energies.[5,6]

Computational Models

Since nanoparticles and nanoparticle-molecule complexes are too large for direct *ab initio* calculations, we simplify our consideration. It is known that Pt(111) surface is the most stable and it is dominant facet in Pt catalyst nanoparticles.[7] Therefore, we consider the IPA adsorption on Pt(111) surface at ab initio level of theory.

The constructed systems correspond to four different concentrations of 1-propanol molecules (**Table ST1).** Next-nearest distance between atoms of different molecules is more than 8 Å for the 1/16 monolayer (ML) coverage. At this separation distance, the molecules are considered to have

extremely small interaction at DFT level of theory. Therefore, we assume that the corresponding molecular configuration represents the adsorption of 1-propanol from low-pressure gas-phase. On the other hand, the determined concentration of the 1-propanol molecules in liquid phase is ~8×10^{24} molecules/m^3 that corresponds to the surface concentration of 3.94 molecules/nm^2. This value is very close to the biggest modeled surface concentration of 3.75 molecules/nm^2 that we call liquid-phase (**Table ST1**).

Computational Results

We considered 28 configurations of 1-propanol on Pt(111) surface for each concentration to find minimum energy configurations. The optimized minimum energy configurations for the liquid phase and gas-phase models are shown on **Figure S9**. In the low-pressure gas-phase configuration, the 1-propanol molecules are almost "lying-flat" on the surface: a bisectrix connecting hydroxyl-O and methyl-C forms 6^o relative to the surface (**Figure S9**). In the liquid-phase, the 1-propanol molecules are "standing" on the surface with bisectrix-surface angle of 41^o. This result agrees and explains the change of the relative intensities in the SFG spectra (**Figure 4**) for the gas-phase and liquid phase adsorption of 1-propanol molecules. Furthermore, while molecular concentration increases, molecular configuration on the surface changes from "lying" to "standing". This configuration change is a result of the steric inter-molecular interaction that forces the molecules to take "standing" position for denser molecular packing on the surface. Also alcohol-H moves closer to the surface and adsorption energy increases when the concentration increases as shown in **Figure S10**.

Experimentally, we observe the catalytic transformation of 1-propanol to propanal as following,

$$C_2H_5CH_2OH + Pt(111) \rightarrow C_2H_5CHO + 2H + Pt(111).$$

Accordingly to the calculations, this reaction on Pt(111) is endothermic (unfavorable) consuming 0.37eV at 1/16 ML coverage. Therefore, the reaction requires additional reactant that should form stable products making the overall reaction energetically favorable. Under reaction conditions, molecular oxygen can serve as the additional reactant, because 1-propanol becomes oxidized. Oxygen molecules adsorb and dissociate on Pt (111) surface providing energy of -1.49eV (negative sign indicating an exothermic reaction) at 1/16 ML coverage. At 1/4 ML coverage, the total energy gains from oxygen adsorption and dissociation decreases to -0.83 eV due to interatomic repulsion.

1-propanol reacts with the decomposed oxygen atoms on Pt(111) surface forming water as following,

$$C_2H_5CH_2OH + 2O+Pt(111) \rightarrow C_2H_5CHO + H_2O + O + Pt(111).$$

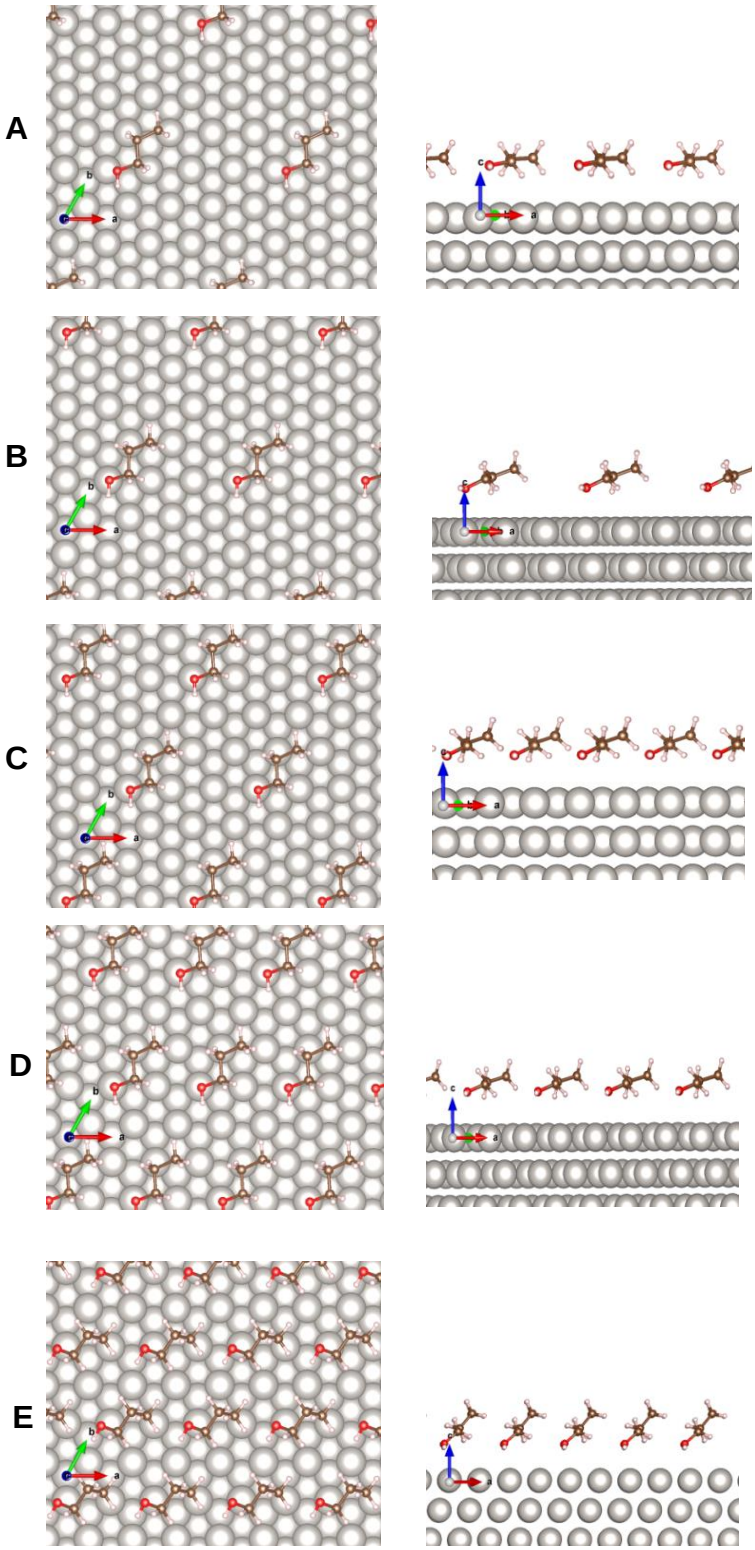

Figure S9 – Minimum energy configurations of 1-propanol molecules on Pt(111) surface for the 1/16 (A), 1/12 (B), 1/9 (C), 1/6 (D) and 1/4 (E) monolayer coverage.

Figure S11 shows the minimum energy configurations of the complex propanal, H2O and atomic oxygen molecules on Pt(111) surface for the 1/16 (A) and 1/4 (B) monolayer coverage. This reaction is energetically more favorable - on 0.36 eV- then the formation of two hydroxyl groups. The exothermic oxidation reaction releases energy of -1.23 eV at 1/16 ML coverage and -1.98 eV at 1/4 ML coverage. The calculated activation barriers are 3.25 eV for 1/16 ML coverage and 1.59 eV for 1/4 ML. The calculated barriers are much bigger than the experimentally measured, thought they are in qualitative agreement. Smaller experimental values may indicate: the gas and liquid coverages are denser than in the models; the reaction may happen on the Pt-NP edges and corners;[8,9] more complex reaction pathway.

Coverage, ML	α	H_{alc}-Pt, Å	E_{ads}, eV
1/16	6°	3.17	-0.506
1/12	16°	2.90	-0.568
1/9	18°	2.88	-0.582
1/6	19°	2.72	-0.674
1/4	41°	2.61	-0.686

Table ST1. 1-propanol molecule orientation as angle of C-C bonds relative to surface normal, adsorption energy and nearest surface-molecule distance for different concentrations of molecules on the Pt(111) surface.

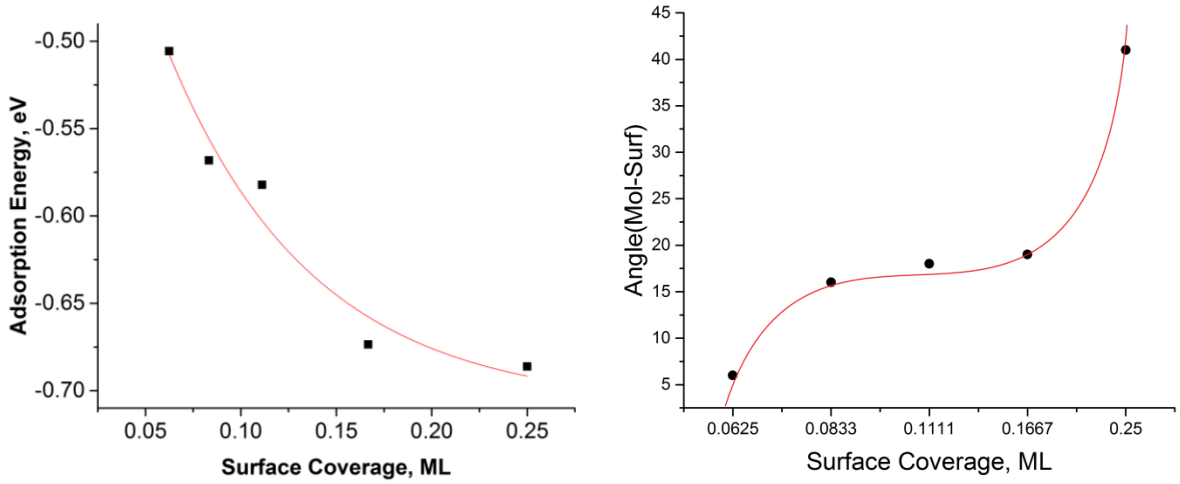

Figure S10 – Dependence of 1-propanol adsorption energy and molecule-surface angle − molecular orientation − on molecular coverage of Pt (111) surface (negative energies are energetically favorable).

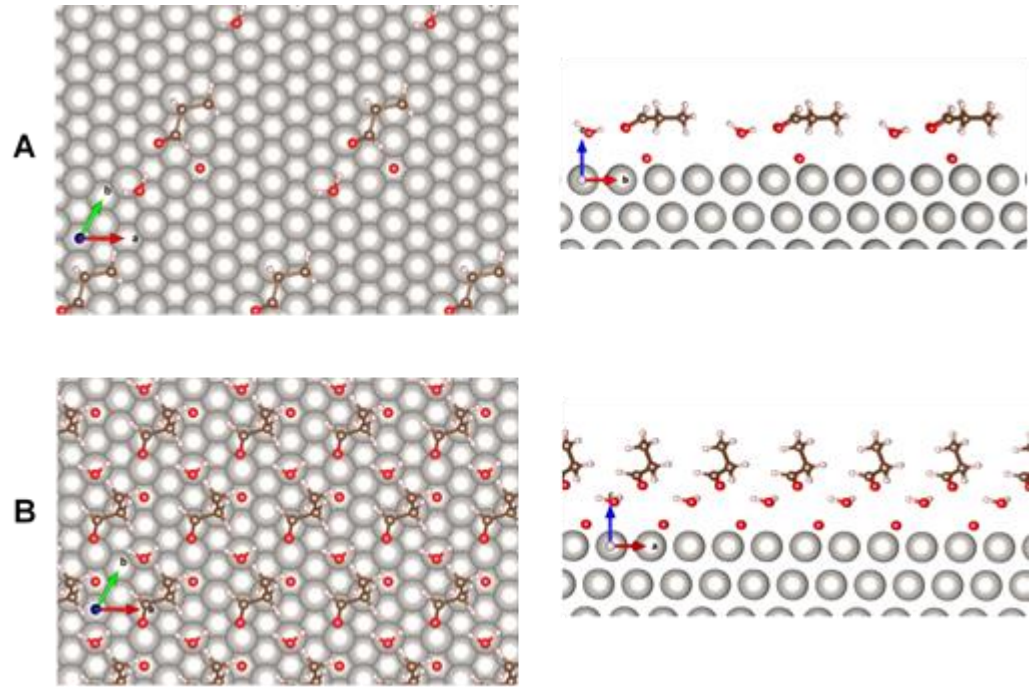

Figure S11 – Minimum energy configurations of the complex propanal, H_2O and atomic oxygen molecules on Pt(111) surface for the 1/16 (A) and 1/4 (B) monolayer coverage.

References

(1) Kresse, G.; Furthmüller, J. Efficient Iterative Schemes for ab initio Total-Energy Calculations Using a Plane-Wave Basis Set. *J. Phys. Rev. B* **1996**, 54, 11169-11186.

(2) Kresse, G.; Joubert, D. From Ultrasoft Pseudopotentials to the Projector Augmented-Wave Method. *J. Phys. Rev. B* **1999**, 59, 1758-1775.

(3) Klimes, J.; Bowler, D.R; Michaelides, A. van der Waals Density Functionals Applied to Solids. *Phys. Rev. B* **2011**, 83, 195131.

(4) Roman-Perez, G.; Soler, J.M. Efficient Implementation of a van der Waals Density Functional: Application to Double-Wall Carbon Nanotubes. *Phys. Rev. Lett*. **2009**, 103, 096102.

(5) Xiao, P.; Sheppard, D.; Rogal, J.; Henkelman, G. Solid-State Dimer Method for Calculating Solid-Solid Phase Transitions. *J. Chem. Phys.* **2014**, 140, 174104.

(6) Henkelman G.; Jónsson, H. A Dimer Method for Finding Saddle Points on High Dimensional Potential Surfaces Using Only First Derivatives. *J. Chem. Phys*. **1999**, 111, 7010-7022.

(7) Nørskov J., Bligaard T., Rossmeisl, J., Christensen C. Towards the Computational Design of Solid Catalysts. *Nat. Chem.* **2009,** 1, 37-46.

Chapter 5 – Nanoparticle Size and Water Effects on Platinum-Catalyzed 2-Butanol Oxidation in the Gas and Liquid Phases

Introduction

Selective oxidation of alcohols to their corresponding aldehydes, ketones, or carboxylic acids is of great importance in chemical production and energy conversion.[1–3] Aldehydes and ketones have been conventionally prepared by oxidizing alcohols using stoichiometric amounts of oxidants such as permanganates and chromates.[4,5] However, due to the waste generated in these reactions, they are being replaced by other catalytic methods. Of special interest is heterogeneous catalysis, as it allows for separation and reuse of the catalyst after the reaction is complete. These heterogeneous catalysts (such as nanoparticles) can possess high efficiency and low waste, making them excellent candidates.

In particular, the 2-butanol oxidation reaction is of note due to its potential as a biofuel and its role in some biological processes.[6,7] 2-butanone, also known as methyl ethyl ketone, is of special interest as well, as it is utilized in devulcanizing rubber and in the production of esters. 2-butanone is also a common solvent, and is used in a wide variety of applications, including as a cleaning agent and a paint remover.[8] Commercially, 2-butanone is generated from the dehydrogenation of 2-butanol using copper or zinc catalysts which require harsh conditions. In contrast, the oxidation of 2-butanol using an oxidant (such as O_2) can be carried out under mild reaction conditions and with less environmental impact.[1] Therefore, understanding the oxidation of 2-butanol to 2-butanone is of great significance.

In addition, the oxidation of 2-butanol is able to be studied in both the gas and liquid phases. This builds upon previous work studying the oxidation of methanol, ethanol, and isopropanol on Pt nanoparticles.[9–11] Turnover frequency was found to increase with particle size for both the gas and liquid phases, but was determined to be significantly higher in the gas phase. Both the gas and the liquid phase reactions heavily favored the production of 2-butanone, with minimal amounts of CO_2 being generated.

Experimental

Size-Controlled Pt Nanoparticle Synthesis

Size-controlled Pt nanoparticles were synthesized using polyvinylpyrrolidone (PVP) as the capping agent. For 2 nm Pt nanoparticles, 80 mg of H_2PtCl_6•6 H_2O, 110 mg PVP (MW=29,000), and 100 mg NaOH were dissolved in 10 mL of ethylene glycol in a three-neck round bottom flask and heated to 160°C for 2 hours under argon atmosphere. The resultant nanoparticles were

then allowed to cool to room temperature and precipitated with acetone, then redispersed in 10 mL ethanol. The nanoparticles were then washed by precipitating with hexane, centrifuging, and redispersing in ethanol prior to use. When measured using transmission electron microscopy (TEM), these nanoparticles were found to actually measure 1.8±0.2 nm in diameter.

To synthesize the 4 nm particles, 50 mg of H_2PtCl_6•6 H_2O and 220 mg PVP (MW=29,000) were dissolved in 10 mL ethylene glycol in a three-neck round bottom flask and heated to 180°C for 30 minutes under argon atmosphere. After cooling to room temperature, the resultant nanoparticles were precipitated with acetone and redispersed in 10 mL of ethanol. The nanoparticles were washed before use by precipitating with hexane, centrifuging, and redispersing in ethanol. When measured using transmission electron microscopy (TEM), these nanoparticles were found to actually measure 4.1±0.4 nm in diameter.

In order to synthesize the 6 nm particles (determined using TEM data to actually be 5.9 nm in diameter), 80 mg of $Pt(acac)_2$ (~0.2 mmol) and 55 mg of PVP (MW=55,000) were dissolved in 5 mL of ethylene glycol in a three-neck round bottom flask. The solution was heated to 200°C for 10 minutes under argon atmosphere. Once cooled to room temperature, the resultant nanoparticles were precipitated with acetone and redispersed in ethanol. Prior to use, the nanoparticles were repeated washed by precipitating with hexane, centrifuging, and redispersing in ethanol. When measured using transmission electron microscopy (TEM), these nanoparticles were found to actually measure 5.8±1.0 nm in diameter.

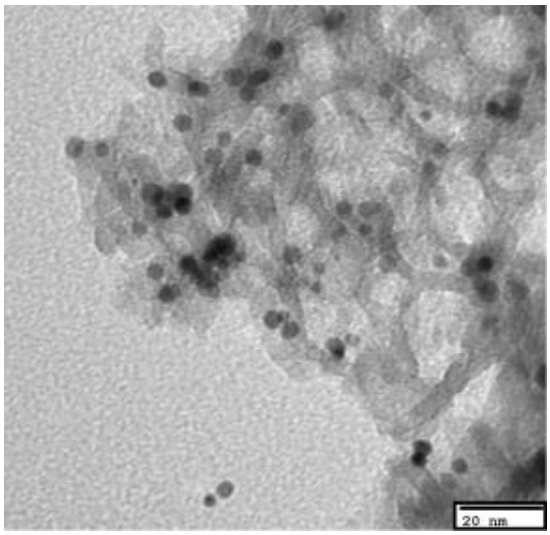

Figure 1 – TEM image of Pt-PVP nanoparticles loaded onto MCF-17 supports. Scale bar shows 20 nm.

The Pt nanoparticles were then loaded into mesoporous silica MCF-17 supports for the study of the 2-butanol oxidation reaction in the both gas and liquid phases. MCF-17 was synthesized according to the literature.[12] The gained MCF-17 had 18.5 nm pore width and 599 m^2/g surface area. The amount of Pt loaded into the supports was measured by inductively coupled plasma atomic emission spectroscopy (ICP-AES).

Thin-Film Pt Catalysts

Thin-film platinum catalyst samples were deposited onto quartz using electron beam evaporation on top of a 2 nm titanium adhesion layer. The base pressure for evaporation was less than 10^{-5} Torr. The thickness of platinum was measured to be 6 nm by a quartz crystal microbalance calibrated to the platinum density and the distance of the sample from the crucible.

Catalytic Measurements

The 2-butanol oxidation reaction was investigated in the gas and liquid phases using Pt nanoparticles loaded into MCF-17 with pure anhydrous 2-butanol from Aldrich. The gas-phase reactions were carried out in a gold-coated batch-reactor equipped with a heater and a metal bellows circulation pump for gas mixing. Each catalyst was dispersed in ethanol and drop-casted on SiO_2 chips, and then set on a boron nitride substrate heater. The reactor was typically filled with 10 Torr of 2-butanol, 50 Torr of oxygen and 710 Torr of helium at 80°C. The products were detected by a gas chromatographer (GC) with a frame ionization detector and a methanizer.

The liquid-phase reactions were carried out in a 100 ml stirred Parr reactor covered by heating tape. The reactor was filled with 10–30 mg of Pt/MCF-17 dispersed in 15 ml of liquid alcohol. The mixture was sealed under 3 bar of oxygen atmosphere. Magnetic stirring was set at a certain speed and the mixture was kept at 80°C. After allowing to react for three hours, the reactor was cooled to 45°C. The gas in the reactor was then transferred into the evacuated gas-phase reactor connected to the GC in order to analyze the reactants and products in the gas phase. The liquid in the reactor was centrifuged to remove the solid catalyst. The supernatant was then injected into the GC to analyze the reactants and products in the liquid phase.

For the gas-phase reaction, the product selectivity and turnover frequency (TOF) were typically calculated at 2-butanol conversion under 30 %. For the liquid-phase reaction, the product selectivity and TOF were typically calculated at oxygen conversion between 20–40 % (corresponding alcohol conversion between 1–4 %). The number of active sites for each catalyst was calculated based on the TEM (particle size) and ICP-AES (Pt loading) data, assuming spherical nanoparticles and the same atomic density on the Pt nanoparticle surface as Pt (111).

SFG Measurements

SFG experiments were carried out using a Ekspla PL2230 picosecond laser. This laser produces a 1064 nm beam with a 50 Hz repetition rate and a 28 ps pulse duration, which is then split (using a LaserVision OPG/OPA) into a 532 nm visible beam (130 μJ) and a tunable infrared beam capable of scanning 2700-3500 cm^{-1} (300 μJ).

The visible and IR beams then pass through a polarizer and waveplate to achieve ppp polarization and directed to the sample surface, with the visible beam incident on the surface at a

40° angle and the IR beam incident at a 50° angle relative to the surface normal. These beams pass through a CaF_2 prism and the catalyst sample deposited on a quartz window. In order to maximize the light transmission between the CaF_2 prism and the quartz window, an IR-transparent index matching gel was utilized consisting of a mixture of d_8-polystyrene and d_{18}-decahydronapthalene.

The SFG signal generated from the surface was then detected by a photomultiplier tube (PMT) detector. A gated integrator system with a 100 ns gate time was used to improve the signal-to-noise ratio.

Results and Discussion

Pt Size Effect on Reaction Rate and Product Selectivity

Catalytic activity of the varying Pt nanoparticle sizes in both the gas and the liquid phase reactions was analyzed to determine selectivity and turnover frequency (TOF) values. The TOF values were calculated by normalizing the overall conversion rate to the number of Pt active sites. The number of active sites were determined based on the nanoparticle size calculated from TEM data. Figure 2 shows the TOF values for the nanoparticles in both the gas and liquid phases. Overall, the gas phase TOF values were found to be roughly an order of magnitude larger than the TOF values in the liquid phase. The TOF values for the liquid phase were found to be 0.16 s^{-1} for the 1.8 nm particles, 2.69 s^{-1} for the 4.5 nm particles, and 3.05 s^{-1} for the 5.9 nm particles. In the gas phase, the TOF values were determined to be 2.58 s^{-1} for the 1.8 nm particles, 9.00 s^{-1} for the 4.5 nm particles, and 11.40 s^{-1} for the 5.9 nm particles. Both the gas and liquid phase reactions showed an increase in turnover frequency with increasing particle size, but the gas phase exhibited a larger size dependence than the liquid phase.

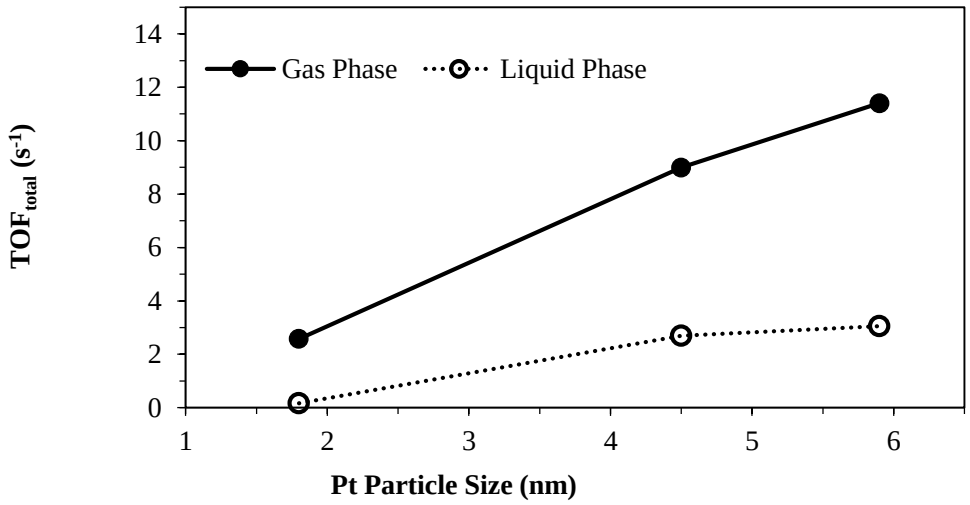

Figure 2 – Size effect on TOF of 2-butanol oxidation reaction in the gas (10 Torr alcohol, 50 Torr O2, He as balance, in total 770 Torr, 80°C) and liquid phase (15 ml pure alcohol, dissolved oxygen under 3 bar, 80°C)

As shown in Figure 3, the gas and the liquid phase reactions were found to be very selective towards 2-butanone (>90% selectivity), with minimal amounts of CO_2 produced. In addition, selectivity increased towards 2-butanone with increasing particle size for both phases, with the liquid phase showing a lower production of 2-butanone at smaller sizes than the gas phase, but approximately the same selectivity at higher nanoparticle sizes.

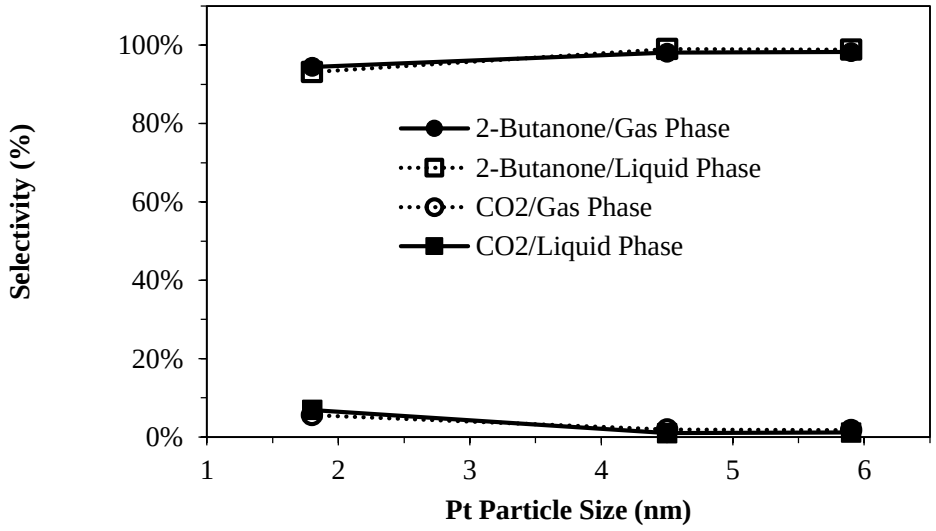

Figure 3 – Size effect on product selectivity of 2-butanol oxidation reaction in the gas (10 Torr alcohol, 50 Torr O_2, He as balance, in total 770 Torr, 80°C) and liquid phase (15 ml pure alcohol, dissolved oxygen under 3 bar, 80°C)

The activation energy for 4 nm Pt nanoparticles was determined to be 119 kJ/mol in the gas phase, but decreased to 64 kJ/mol. This decrease in activation energy despite a decrease in turnover frequency is likely due to a lower oxygen diffusion efficiency in the higher density liquid phase, and may also be due to a difference in the molecular orientation of the 2-butanol on the surface of the Pt.

Water Effect on Reaction Rate and Product Selectivity

As water is one of the products in the oxidation of alcohols, it has the potential to change the reaction circumstances and affect the reaction progress. However, water has also been previously found to have a promoting effect on the liquid phase isopropanol oxidation.[11] Therefore, the effect of water addition on the oxidation reaction of 2-butanol was studied in both the gas and liquid phases. For the gas phase, 1−10 Torr water vapor was introduced with 10 Torr of alcohol and 50 Torr of oxygen over 2 and 6 nm Pt NPs loaded in MCF-17.

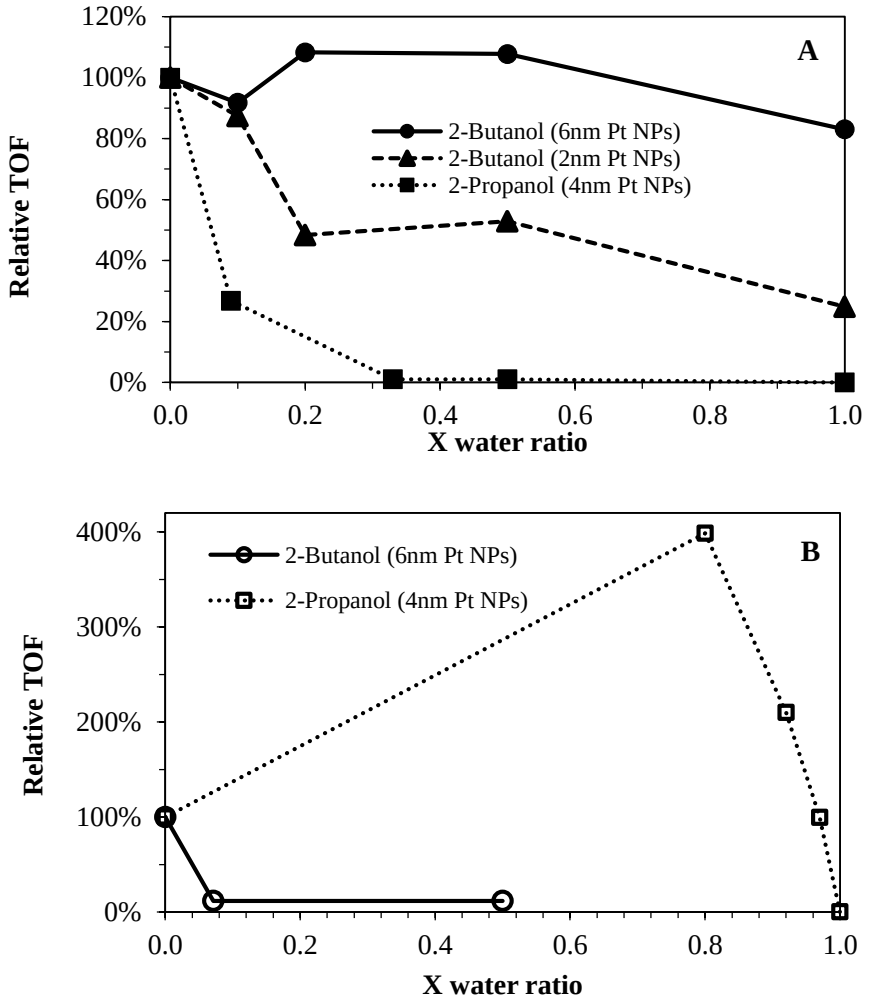

Figure 4 – Water effect on the TOF of alcohol oxidation reactions in the (A) gas and (B) liquid phases. (A) Gas Phase: 10 Torr alcohol, 1-10 Torr water vapor, 50 Torr O_2, He as balance, in total 770 Torr. 2-Propanol oxidation: using 4 nm Pt/MCF-17 at 60°C. 2-Butanol oxidation: using 2 and 6 nm Pt/MCF-17 at 80°C. (B) Liquid Phase: 7.5-15 ml pure alcohol, 0-7.5 ml distilled water, in total 15 ml volume. 2-Propanol oxidation: dissolved oxygen under 1 bar, 60°C over 4 nm Pt/MCF-17. 2-Butanol oxidation: dissolved oxygen under 3 bar, 80°C over 6 nm Pt/MCF-17

When the 2-butanol reaction was catalyzed by 6 nm Pt nanoparticles loaded onto MCF-17, a unique tendency was shown in the gas phase. Water was found to not poison the reaction, and the relative TOF remained at 84% of the water-free reaction activity. This result is drastically different from other alcohols previously studied, such as methanol and isopropanol, in which the coadsorption of water was found to drastically slow the reaction rate. However, when 2 nm Pt nanoparticles were used as the reaction catalyst, the TOF gradually decreased to 25% of the water-free reaction activity. This result may be due to smaller nanoparticles having more defects on their surface, which could possibly hold water on the reaction active sites.

In the liquid phase, the addition of water to the 2-butanol reaction was also found to be significantly different than other, previously studied alcohols. In the isopropanol reaction, water was found to have a large promoting effect, nearly quadrupling the TOF value of the reaction without water. For the 2-butanol reaction, however, water was shown to have a strong inhibiting effect – even the introduction of 10% water (1 mL) to the solution cause a decrease in the TOF value of nearly 90%. Previous studies indicate this result may be correlated with the hydrophobicity of alcohols. Isopropanol is miscible in water, but the longer hydrocarbon chain of 2-butanol makes it less soluble. In the high-density liquid phase, water may preferentially gather around the amphiphilic PVP capping agent, preventing the 2-butanol access toward Pt surface.[13]

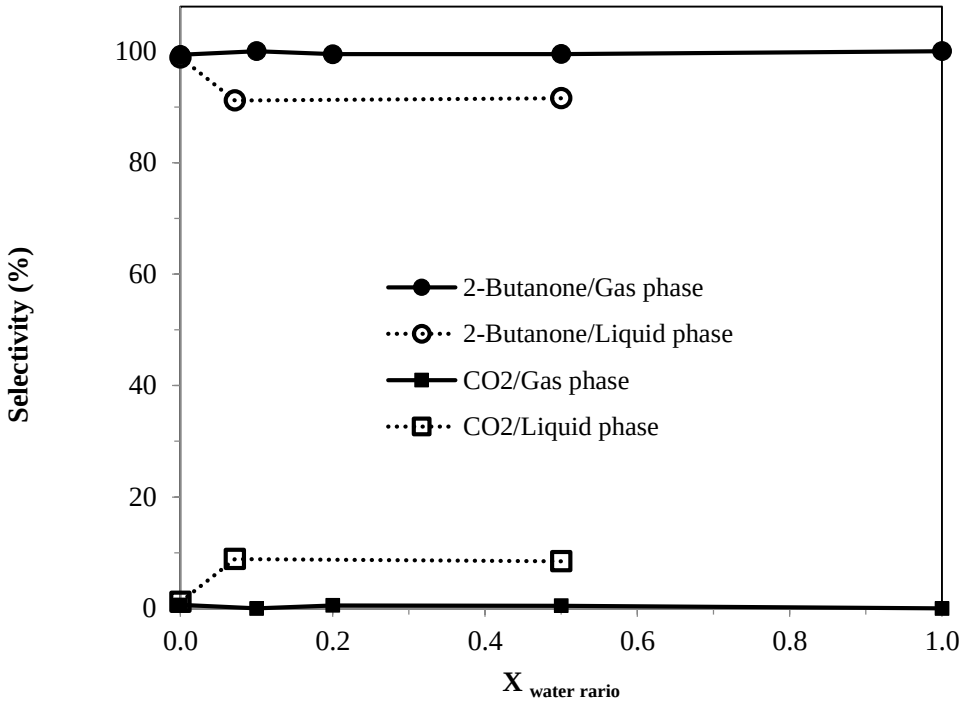

Figure 5 – Water effect on the TOF of alcohol oxidation reactions in the gas and liquid phases. Gas Phase: 10 2-butanol, 1-10 Torr water vapor, 50 Torr O_2, He as balance, in total 770 Torr, using 2 and 6 nm Pt/MCF-17 at 80°C.Liquid phase: 7.5-15 ml pure 2-butanol, 0-7.5 ml distilled water, in total 15 ml volume. dissolved oxygen under 3 bar, 80°C over 6 nm Pt/MCF-17.

Figure 5 shows the water coadsorption effect on product selectivity in both the gas and the liquid phases. In the gas phase, the 2-butanol oxidation showed an insensitivity to the water quantity, producing nearly 100% 2-butanone at all levels of the water to alcohol ratio, and little CO_2 was produced. This result correlates with the TOF data, suggesting that water does not affect the

overall reaction. However, in the liquid phase, the addition of water resulted in a tenfold increase in the CO_2 production and nearly a 10% decrease in the selectivity towards 2-butanone.

Results of SFG Studies

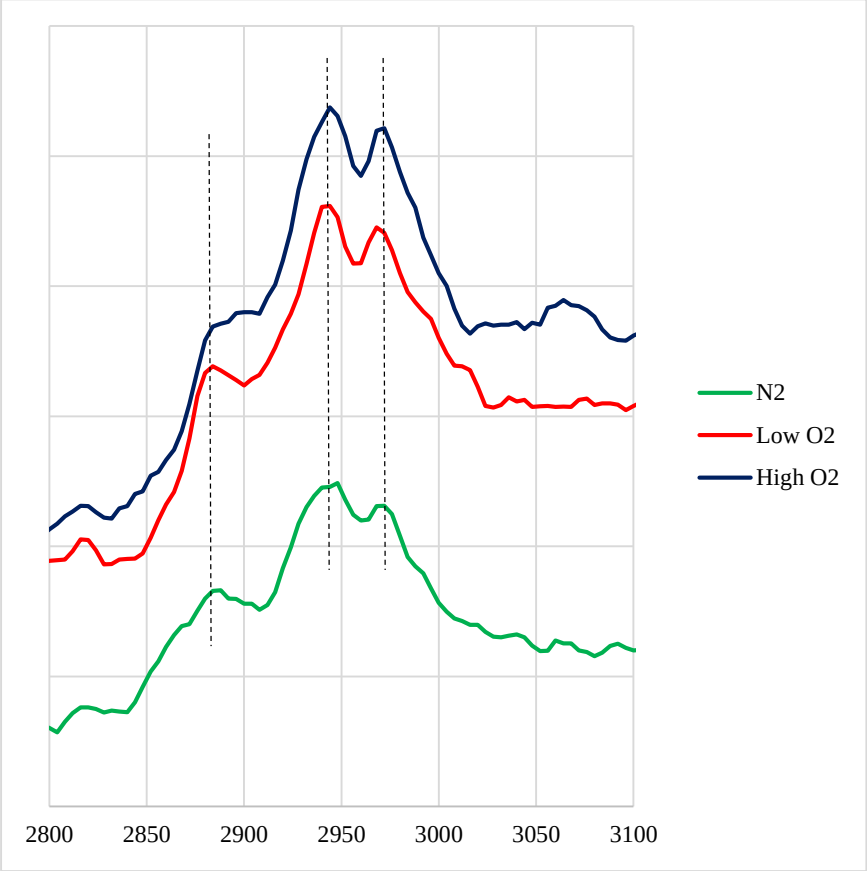

Figure 6 – SFG spectra of 2-butanol with varying ratios of oxygen to alcohol. Notable peaks are at 2880 cm^{-1} (CH_3 symmetric), 2945 cm^{-1} (CH_3 Fermi resonance), and 2975 cm^{-1} (CH_3 asymmetric).

SFG spectra were taken to analyze the effect of oxygen on the surface of the gas-phase oxidation of 2-butanol. 10 torr of 2-butanol was introduced along with in the presence of N_2, at a low oxygen:alcohol ratio (3:1), and a high oxygen:alcohol ratio (10:1). Peaks were found for each of the conditions at 2880 cm^{-1} (determined to be a CH_3 symmetric stretch), 2945 cm^{-1} (CH_3 Fermi resonance), and 2975 cm^{-1} (CH_3 asymmetric stretch). Other peaks were not considered in analysis. Analysis of the data shows that in the presence of oxygen, a higher signal was measured than in the presence of inert nitrogen. Increasing the ratio of oxygen to 2-butanol also yielded a larger signal. This is likely due to a more ordered surface species in the presence of oxygen. The increase in signal could also be attributed to a higher surface molecular density. The CH_3 asymmetric to symmetric peak intensity ratio also decreases with increasing oxygen ratio, suggesting that there is a change in the 2-butanol orientation on the platinum surface.

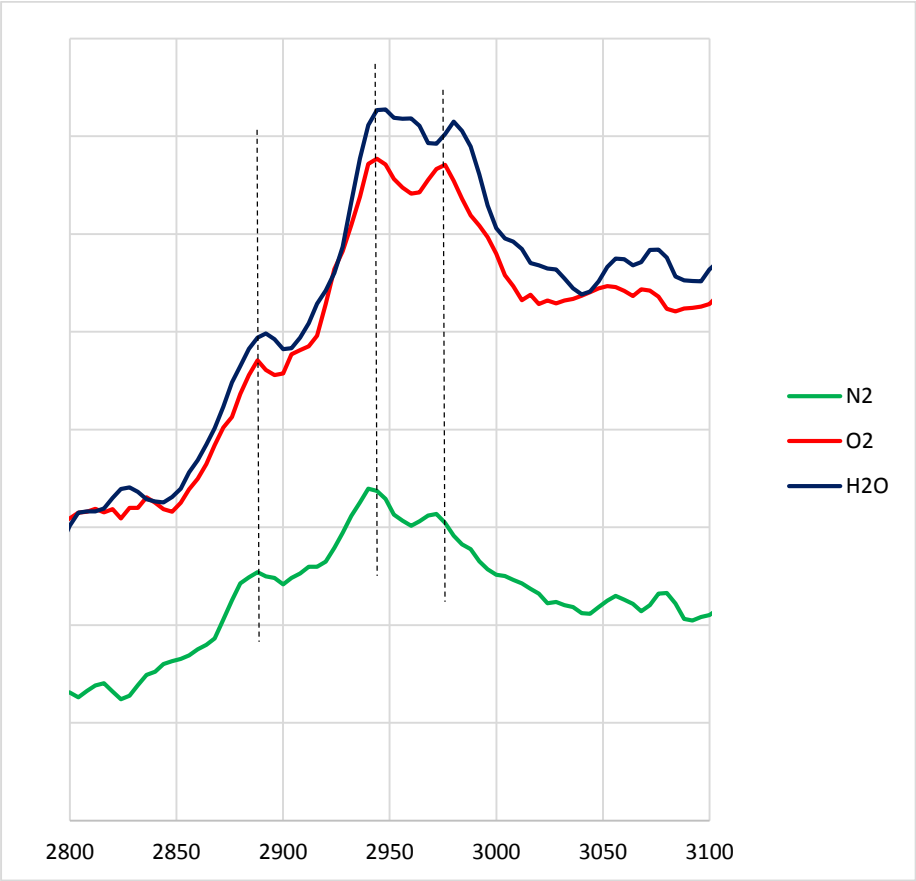

Figure 7 – SFG temperature studies of 2-butanol in the presence of oxygen and water. Notable peaks are at 2895 cm^{-1} (CH_3 symmetric), 2950 cm^{-1} (CH_3 Fermi resonance), and 2985 cm^{-1} (CH_3 asymmetric).

In order to provide insight into the presence of water on the platinum surface during the 2-butanol oxidation reaction, SFG spectra were taken using 10 torr of 2-butanol with N_2, O_2 (100 torr), and both O_2 and H_2O (100 torr and 5 torr, respectively). There was found to be a sharp increase in signal between the N_2 and O_2 peaks, but the addition of water seemed to have very little effect. This supports the catalytic data for the gas-phase 2-butanol reaction, in which the addition of water had little effect on the reaction turnover frequency.

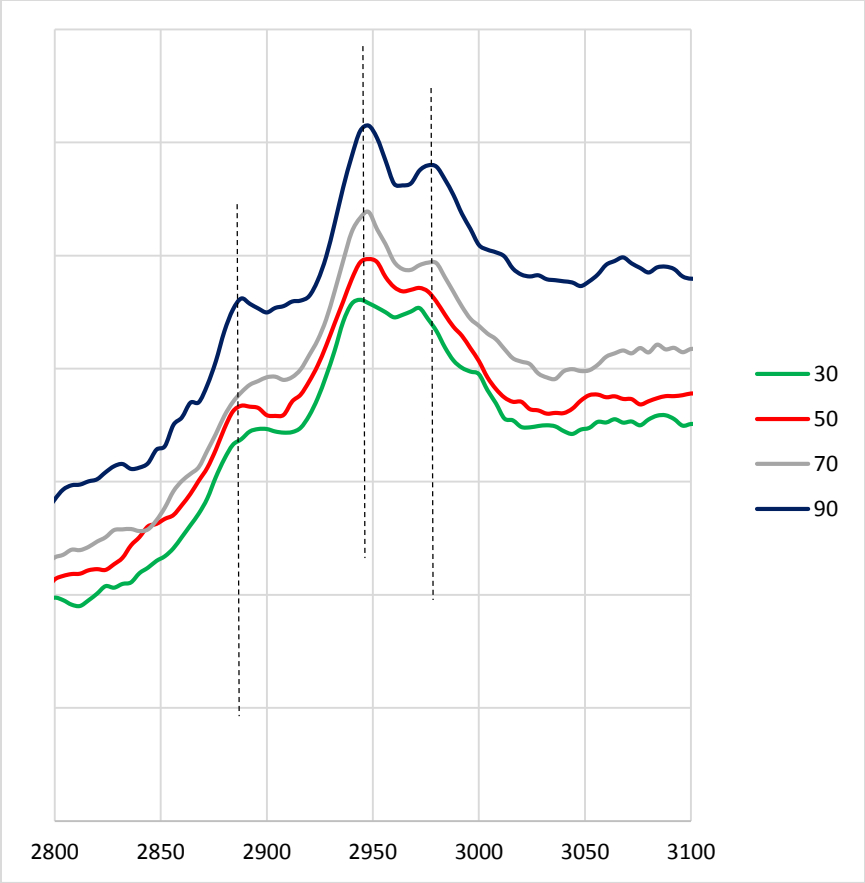

Figure 8 – SFG spectra of 2-butanol in the presence of O_2 at 30, 50, 70, and 90°C. Notable peaks are at 2890 cm^{-1} (CH_3 symmetric), 2945 cm^{-1} (CH_3 Fermi resonance), and 2980 cm^{-1} (CH_3 asymmetric).

In order to examine the temperature effects on the gas-phase 2-butanol oxidation reaction, SFG spectra were taken at 30, 50, 70, and 90°C with 10 torr of 2-butanol and 50 torr O_2. Significant peaks are a CH_3 symmetric stretch at 2890 cm^{-1}, a CH_3 Fermi resonance at 2945 cm^{-1}, and a CH_3 asymmetric stretch at 2980 cm^{-1}. The SFG signal was found to increase with increasing temperature, and the peaks became significantly more defined. This is an indication of either more ordering of the 2-butanol on the Pt surface or a higher surface density of the 2-butanol on the surface at higher temperatures.

Conclusions

Overall, significant differences were found between the gas and the liquid phase 2-butanol oxidation reactions. The gas phase reaction was found to have a higher sensitivity to the Pt nanoparticle size than the liquid phase reaction. The addition of water yielded drastically different results between the gas and the liquid phase reactions. TOF values, product selectivity, and SFG data all suggest that the gas phase 2-butanol oxidation is not affected by the presence of

water. However, in the liquid phase, the addition of water poisons the reaction, which is significantly different than the water effect on the oxidation of other alcohols.

References

(1) Prabu, K.; Prabu, M.; Venugopal, A. K.; Venugopalan, A. T.; Sandilya, W. V. Y. S.; Gopinath, C. S.; Raja, T. Effective and Selective Oxidation of 2-Butanol over Mn Supported Catalyst Systems. *Appl. Catal. A Gen.* **2016**, *525*, 237–246.

(2) Mallat, T.; Baiker, A. Oxidation of Alcohols with Molecular Oxygen on Solid Catalysts. *Chem. Rev.* **2004**, *104* (6), 3037–3058.

(3) Besson, M.; Gallezot, P. Selective Oxidation of Alcohols and Aldehydes on Metal Catalysts. *Catal. Today* **2000**, *57* (1–2), 127–141.

(4) Menger, F. M.; Lee, C. Synthetically Useful Oxidations at Solid Sodium Permanganate Surfaces. *Tetrahedron Lett.* **1981**, *22* (18), 1655–1656.

(5) Lee, D. G.; Spitzer, U. A. The Aqueous Dichromate Oxidation of Primary Alcohols. *J. Org. Chem.* **1970**, *35*, 3589–3590.

(6) Puthiyapura, V. K.; Brett, D. J.; Russel, A. E.; Lin, W. F.; Hardacre, C. Preliminary Investigation on the Electrochemical Activity of Butanol Isomers as Potential Fuel for Direct Alcohol Fuel Cell. *ECT Trans.* **2015**, *69* (17), 809–816.

(7) Carlson, G. P. Effect of Ethanol , Carbon Tetrachloride , and Methyl Ethyl Ketone on Butanol Oxidase Activity in Rat Lung and Liver. *J. Toxicol. Environ. Health* **1989**, *27*, 255–261.

(8) Saha, D.; Ghosh, A.; Saha, B. Combination of the Most Efficient Promoter and Micellar Catalyst for Rate Enhancement of Chromic Acid Oxidation on 2-Butanol to 2-Butanone Conversion in Aqueous Media at Room Temperature. *Res. Chem. Intermed.* **2015**, *41* (11), 8527–8544.

(9) Wang, H.; An, K.; Sapi, A.; Liu, F.; Somorjai, G. A. Effects of Nanoparticle Size and Metal/support Interactions in Pt-Catalyzed Methanol Oxidation Reactions in Gas and Liquid Phases. *Catal. Letters* **2014**, *144* (11), 1930–1938.

(10) Sapi, A.; Liu, F.; Cai, X.; Thompson, C. M.; Wang, H.; An, K.; Krier, J. M.; Somorjai, G. A. Comparing the Catalytic Oxidation of Ethanol at the Solid-Gas and Solid-Liquid Interfaces over Size-Controlled Pt Nanoparticles: Striking Differences in Kinetics and Mechanism. *Nano Lett.* **2014**, *14* (11), 6727–6730.

(11) Wang, H.; Sapi, A.; Thompson, C. M.; Liu, F.; Zherebetskyy, D.; Krier, J. M.; Carl, L. M.; Cai, X.; Wang, L.-W.; Somorjai, G. A. Dramatically Different Kinetics and Mechanism at Solid/liquid and Solid/gas Interfaces for Catalytic Isopropanol Oxidation over Size-Controlled Platinum Nanoparticles. *J. Am. Chem. Soc.* **2014**, *136* (29).

(12) Schmidt-Winkel, P.; Lukens, W. W.; Zhao, D.; Yang, P.; Chmelka, B. F.; Stucky, G. D.; Uni, V.; Barbara, S. Mesocellular Siliceous Foams with Uniformly Sized Cells and Windows and Department of Chemical Engineering Recei V Ed September 9 , 1998 Molecular Sieves with Uniform Large Pores Are Desirable for Chemical Reactions and for Use in Separations Involving La. *J. Am. Chem. Soc.* **1999**, No. 121, 254–255.

(13) Tatsumi, H.; Liu, F.; Han, H.-L.; Carl, L. M.; Sapi, A.; Somorjai, G. A. Alcohol Oxidation at Platinum-Gas and Platinum-Liquid Interfaces: The Effect of Platinum Nanoparticle Size, Water Coadsorption, and Alcohol Concentration. *J. Phys. Chem. C* **2017**, *121* (13).

Chapter 6

Sum Frequency Generation Studies of 1-Butanol on Platinum at the Solid-Gas Interface Under Reaction Conditions

Introduction

As previously examined throughout this work, the oxidation reactions of various alcohols are useful reactions to study for a variety of reasons.[1] Smaller organic molecules (C_1-C_3) have been studied extensively and show significant prospects for applications in fuel cells and electrosynthesis.[2–4] Increasing the number of carbon atoms in an organic molecule increases the number of possible intermediates and may require a more complex oxidation pathway, making the oxidation of 1-butanol an interesting reaction to study. 1-butanol has been determined to be one of the more active isomers of butanol, but has also shown significant self-poisoning effects. The electrooxidation of 1-butanol has been studied utilizing cyclic voltammetry and FTIR spectroscopy, and 1-butanol has also shown potential as a biofuel.[5,6]

Sum frequency generation (SFG) vibrational spectroscopy has been utilized, both previously in this work and elsewhere, to study the oxidation of alcohols on platinum.[7–9] Its surface specificity allows for an examination of the Pt-alcohol interface, providing molecular-level information about the reaction.[10,11] This study utilizes SFG spectroscopy to examine 1-butanol on the surface of Pt thin films under reaction conditions.

Experimental

Sum Frequency Generation

SFG experiments were carried out using a Ekspla PL2230 picosecond laser. This laser produces a 1064 nm beam with a 50 Hz repetition rate and a 28 ps pulse duration, which is then split (using a LaserVision OPG/OPA) into a 532 nm visible beam and a tunable infrared beam capable of scanning 2700-3500 cm^{-1}.

The visible and IR beams then passed through a polarizer and waveplate to achieve the desired polarization (ppp) and were directed to the sample surface, with the visible beam incident on the surface at a 40° angle and the IR beam incident at a 50° angle relative to the surface normal. These beams pass through a CaF_2 prism and the catalyst sample deposited on a quartz window. In order to maximize the light transmission between the CaF_2 prism and the quartz window, an

IR-transparent index matching gel was utilized consisting of a mixture of d_8-polystyrene and d_{18}-decahydronapthalene.

The SFG signal generated from the surface was then detected by a photomultiplier tube (PMT) detector. A gated integrator system with a 100 ns gate time was used to improve the signal-to-noise ratio.

Thin-Film Pt Catalysts

Thin-film platinum catalyst samples were deposited onto quartz using electron beam evaporation on top of a 2 nm titanium adhesion layer. The base pressure for evaporation was less than 10^{-5} Torr. The thickness of platinum was measured to be 6 nm by a quartz crystal microbalance calibrated to the platinum density and the distance of the sample from the crucible.

Reaction Setup

An aluminum reactor was utilized for the SFG studies. A quartz window is pressed against the aluminum with a small hollow in the aluminum underneath to allow reaction gases to come into contact with the catalyst surface. The cell is connected through stainless steel tubing to a gas reservoir and recirculation pump, as well as a gas manifold to allow various reaction gases to be introduced to the system. A mechanical pump and turbomolecular pump are connected to the SFG reactor, allowing the system to be pumped down to 10^{-5} Torr.

Results and Discussion

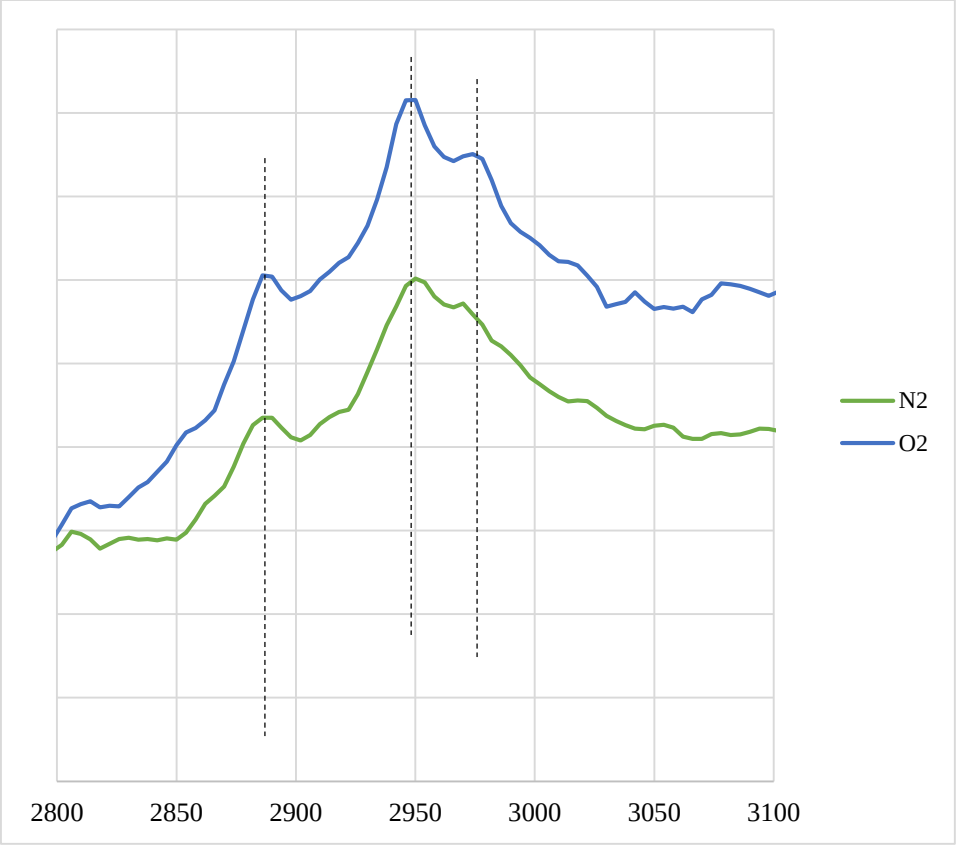

Figure 1 – SFG spectra of gas phase 1-butanol on Pt thin films in the presence of both nitrogen (inert) and oxygen (reactive). Notable peaks are located at 2890 cm^{-1}, 2945 cm^{-1}, and 2975 cm^{-1}.

SFG spectra were taken to analyze the surface structure of 1-butanol on the surface of Pt both in the presence of a non-reactive gas (N_2) and a reactant gas (O_2). Each gaseous mixture included 7 Torr of 1-butanol and 70 Torr of the studied gas in order to provide a 10:1 gas to 1-butanol ratio and was balanced with helium to atmospheric pressure. As previously seen with other gas-phase alcohols, the two spectra share similar peaks – a CH_3 symmetric stretch at 2890 cm^{-1}, a Fermi resonance CH_3 peak at 2945 cm^{-1}, and a CH_3 asymmetric stretch 2975 cm^{-1}. As also previously noted, the oxygen peak is higher intensity than the nitrogen peak. This indicates that under reaction conditions, the 1-butanol molecules are likely more ordered on the surface of the Pt thin film than under inert conditions.

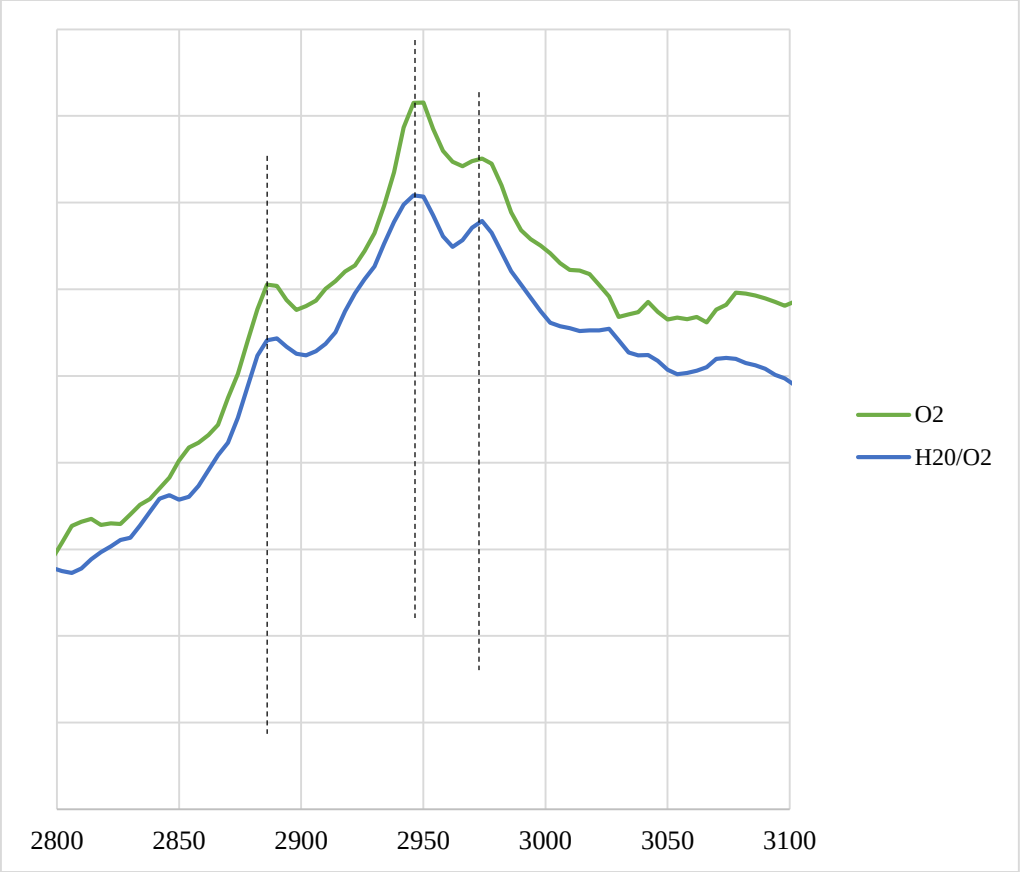

Figure 2 – SFG spectra of 1-butanol on Pt thin films in the presence of oxygen and water/oxygen. Peaks are observed at 2890 cm^{-1}, 2945 cm^{-1}, and 2975 cm^{-1}.

In order to study the effects of water on the 1-butanol oxidation, SFG spectra of 1-butanol (7 Torr) were taken both in the presence of oxygen (70 Torr) and water (5 Torr)/oxygen (70 Torr). Peaks are again observed at 2890 cm^{-1} (CH_3 symmetric stretch), 2945 cm^{-1} (Fermi resonance CH_3), and 2975 cm^{-1} (CH_3 asymmetric stretch). Unlike the previous work on 2-butanol, the 1-butanol spectrum shows a lower intensity with the addition of water. This may be due to competitive adsorption between the water and the alcohol on the platinum surface. Further kinetic work will be performed to determine any unique catalytic effects of water addition to the 1-butanol oxidation reaction.

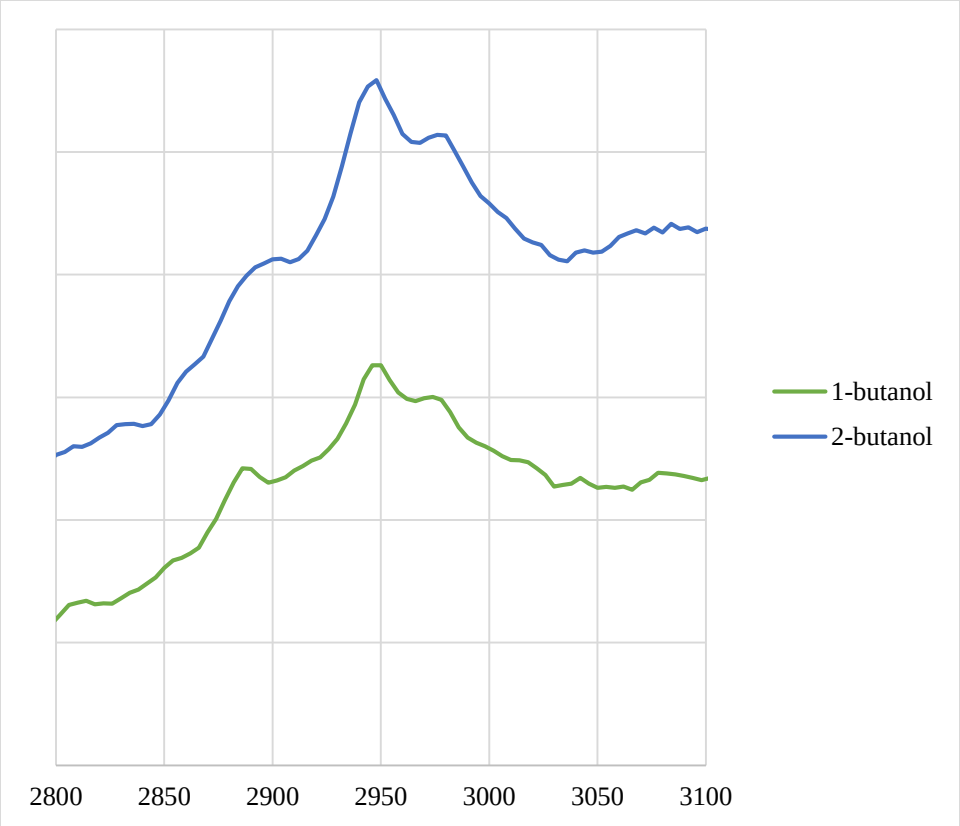

Figure 3 – SFG spectra of 1-butanol and 2-butanol in the presence of oxygen. Both spectra show notable peaks at ~2890 cm^{-1}, ~2945 cm^{-1} and ~2975 cm^{-1}.

As seen in Figure 3, the SFG spectra of 1-butanol and 2-butanol are very similar. The ratio between the peaks at ~2945 cm^{-1} (Fermi resonance CH_3), and 2975 cm^{-1} (CH_3 asymmetric stretch) are nearly exactly the same in the two molecules (1.06:1). However, the 1-butanol spectrum shows a significantly stronger CH_3 symmetric stretch than the 2-butanol. This is especially of note as 1-butanol contains only one CH_3 group, whereas 2-butanol contains two CH_3 groups. This indicates that the shorter CH_3 chain of the 2-butanol is likely isotropically oriented with respect to the surface, yielding no net orientation and therefore no significant SFG signal.

Conclusions

Overall, it was determined that the oxidation of 1-butanol on Pt thin films was observable with SFG spectroscopy. Under oxygen, a reactive gas, the signal of the 1-butanol was higher than under a non-reactive gas, nitrogen. The effects of water addition to the reaction were different than noted on 2-butanol – the presence of water resulted in a less strong SFG spectrum for 1-butanol rather than the increase in signal previously observed on 2-butanol. In comparing the spectra of 1-butanol and 2-butanol (both in the presence of oxygen), the two were noted to be

similar, with a significantly smaller CH_3 symmetric peak observed in the 2-butanol, which is likely indicative of a change in molecular orientation between the two alcohols.

Future work will be carried out to examine 1-butanol oxidation on Pt thin films in the liquid phase. Kinetic studies will also be performed to gather catalytic data and gain further insight into the reaction.

References

(1) Mallat, T.; Baiker, A. Oxidation of Alcohols with Molecular Oxygen on Platinum Metal Catalysts in Aqueous Solutions. *Catal. Today* **1994**, *19* (93), 247–284.

(2) Srinivasan, S. Fuel Cells for Electric Utility and Transportation Applications. *J. Electroanal. Chem.* **1981**, *118*, 51–69.

(3) McNicol, B. Electrocatalytic Problems Associated with the Development of Direct Methanol-Air Fuel Cells. *J. Electroanal. Chem.* **1981**, *118*, 71–87.

(4) Belgsir, E. M.; Bouhier, E.; Essis Yei, H.; Kokoh, K. B.; Beden, B.; Huser, H.; Leger, J. M.; Lamy, C. Electrosynthesis in Aqueous Medium: A Kinetic Study of the Electrocatalytic Oxidation of Oxygenated Organic Molecules. *Electrochim. Acta* **1991**, *36* (7), 1157–1164.

(5) Puthiyapura, V. K.; Brett, D. J.; Russel, A. E.; Lin, W. F.; Hardacre, C. Preliminary Investigation on the Electrochemical Activity of Butanol Isomers as Potential Fuel for Direct Alcohol Fuel Cell. *ECT Trans.* **2015**, *69* (17), 809–816.

(6) Nan-Hai Li; Shi-Gang Sun. In Situ FTIR Spectroscopic Studies of the Electrooxidation of C4 Alcohol on a Platinum Electrode in Acid Solutions Part I. Reaction Mechanism of 1-Butanol Oxidation. *J. Electroanal. Chem.* **1997**, *436* (1–2), 65–72.

(7) Wang, H.; Sapi, A.; Thompson, C. M.; Liu, F.; Zherebetskyy, D.; Krier, J. M.; Carl, L. M.; Cai, X.; Wang, L.-W.; Somorjai, G. A. Dramatically Different Kinetics and Mechanism at Solid/liquid and Solid/gas Interfaces for Catalytic Isopropanol Oxidation over Size-Controlled Platinum Nanoparticles. *J. Am. Chem. Soc.* **2014**, *136* (29).

(8) Sapi, A.; Liu, F.; Cai, X.; Thompson, C. M.; Wang, H.; An, K.; Krier, J. M.; Somorjai, G. A. Comparing the Catalytic Oxidation of Ethanol at the Solid-Gas and Solid-Liquid Interfaces over Size-Controlled Pt Nanoparticles: Striking Differences in Kinetics and Mechanism. *Nano Lett.* **2014**, *14* (11), 6727–6730.

(9) Thompson, C. M.; Carl, L. M.; Somorjai, G. A. Sum Frequency Generation Study of the Interfacial Layer in Liquid-Phase Heterogeneously Catalyzed Oxidation of 2-Propanol on Platinum: Effect of the Concentrations of Water and 2-Propanol at the Interface. *J. Phys. Chem. C* **2013**, *117* (49), 26077–26083.

(10) Baldelli, S.; Markovic, N.; Ross, P.; Shen, Y.; Somorjai, G. Sum Frequency Generation of CO on (111) and Polycrystalline Platinum Electrode Surfaces: Evidence for SFG Invisible

Surface CO. *J. Phys. Chem. B* **1999**, *103*, 8920–8925.

(11) Shen, Y. R. Surface Properties Probed by Second-Harmonic and Sum-Frequency Generation. *Nature* **1989**, *337*, 519–525.

Chapter 7

Sum Frequency Generation Vibrational Spectroscopy of 1,3-Butadiene Hydrogenation on 4 nm $Pt@SiO_2$, $Pd@SiO_2$, and $Rh@SiO_2$ Core-Shell Catalysts

Introduction

The work in this chapter focuses on synthesis and sum frequency generation (SFG) spectroscopy of core-shell nanoparticles, including platinum nanoparticles. The core-shell synthesis and creation of Langmuir-Blodgett films allow for these nanoparticles to be studied with SFG spectroscopy. This technique has the potential to be applied to studying alcohol oxidation reactions, as mentioned in Chapter 8.

Selective hydrogenation of dienes and unsaturated aldehydes, ketones and alcohols on noble metals is a focus for drug and fuel development.[1–3] 1,3-butadiene, the simplest diene, is ideally suited for investigations of partial hydrogenation on nanoparticle catalysts with composition and size control. 1,3-butadiene adsorbs and then is hydrogenated to 1-buten-4-yl radical (1B4R) or 2-buten-1-yl radical (2B1R) intermediates (Figure 1).[2,4] These species are further hydrogenated to 1-butene, 2-butene (*cis*/*trans*) or the butan-1,3-diyl radical (B13R) which makes butane (butan-1,4-diyl radical is excluded because of instability). 1,3-butadiene hydrogenation on Pt has four products: butane, 1-butene and *cis*/*trans*-2-butene. In contrast, Pd induces partial hydrogenation (1-butene and *cis*/*trans*-2-butene) with selectivity >90%.[1,5–8] A challenge of vibrational spectroscopy studies of catalytic surfaces is that the reactants, intermediates and poison species may produce overlapping vibrational features.[9] Since 1,3-butadiene has only four carbon atoms, there are limited reaction intermediates – all of which have adsorption energies studied for Pt(111) and Pd(111) single crystals in density functional theory (DFT) calculations.[10] Because 1,3-butadiene has discrete adsorption modes and makes several products during hydrogenation, it is suitable for SFG studies of reaction selectivity.[11]

SFG vibrational spectroscopy has been applied to a variety of catalytic systems to understand adsorption and reaction processes on Pt single crystals and nanoparticles. Cremer *et al.* characterized ethylene hydrogenation on Pt(111) under ultra-high vacuum and this became the first of many investigations on single crystals.[12–15] While atomically pristine single crystals are well defined, they do not resemble industrial catalysts dispersed on mesoporous supports.[16,17] Current research is aimed at providing insight into selectivity on colloidal nanoparticles.[17–19] Because colloidal nanoparticles demonstrate size and shape control, they provide a route towards

fundamental investigations of industrially relevant materials. SFG experiments on nanoparticles (including Pt nanoparticles with disordered PVP, Pt nanoparticles with removed capping and Pt films on different oxide supports) have developed but are also more challenging than experiments on single crystals.[9,11,20–22] On colloidal nanoparticles, organic capping may interfere with the SFG signal of reaction intermediates of interests. Removing the cap is appealing, however, some physical barrier is necessary to maintain size and shape in compact 2-D films. [9,21] When nanoparticles are surrounded by a SiO_2 shell, capping can be safely removed and SFG can be applied in 2-D.[23]

The high adsorption energy (>140 kJ/mol) and vibrational frequencies (>2990 cm^{-1}) of the 1,3-butadiene molecule make it possible to study hydrogenation intermediates using vibrational spectroscopy with limited ambiguity in SFG spectra. DFT suggests 1,3-butadiene most favorably adsorbs as 1,2,3,4-tetra-σ on Pt(111) and Pd(111).[24] Flat-lying 1,3-butadiene does not have a strong contribution to the SFG spectrum because C-H bonds do not appreciably extend outward from the surface to produce SFG signal in the ppp polarization configuration (dipole selection rule).[25–27] High pressure of 1,3-butadiene (20 Torr) leads to saturation coverage and prevents secondary product formation through the re-adsorption of butenes on vacant sites.[28] The adsorption energies of 1,3-butadiene, 1B4R, 2B1R and B13R suggest products (butane, 1-butene and 2-butenes) become displaced from the surface and do not undergo secondary reactions.[2] Therefore, SFG spectra during reaction show intermediates because products are displaced and the reactant, molecular 1,3-butadiene, does not produce strong SFG peaks in the range 2800-2990 cm^{-1}.[24]

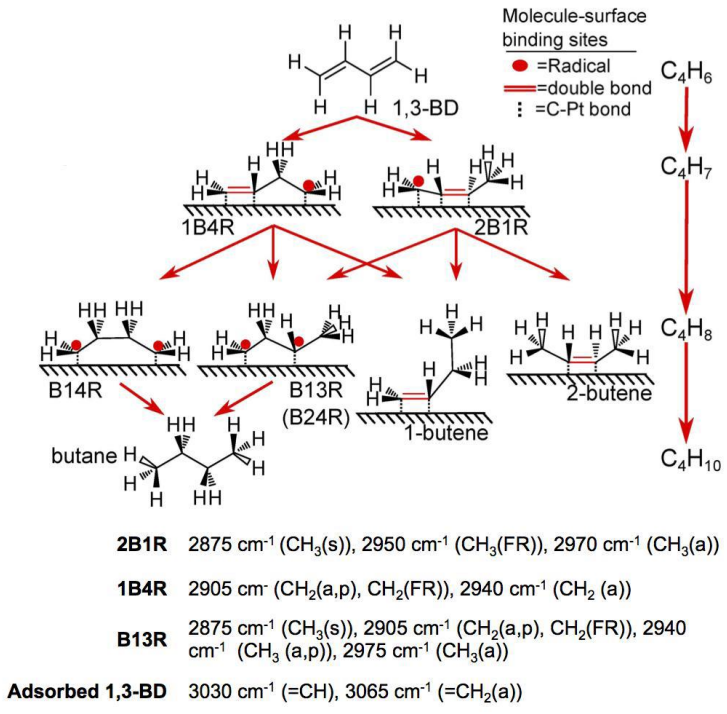

Figure 1 – Schematic of reaction pathways for 1,3-butadiene hydrogenation. Addition of the first H atom leads to 1-buten-4-yl radical (1B4R) or 2-buten-1-yl radical (2B1R) (each "R" is a radical); addition of a second H atom leads to butan-1,4-diyl radical (B14R), butan-1,3-diyl radical (B13R), or 1-butene (1B) and 2-butene (2B) products. B13R can be further hydrogenated

with two H atoms to make butane. The reaction intermediates shown are based on DFT predictions (B14R is not included in analysis because of instability).[2] Peak assignments used for SFG are based on previous experimental works.[15,26,27]

Experimental

Nanoparticle Synthesis and Core-shell Encapsulation.

All synthesis was performed under Ar atmosphere with 29 K polyvinylpyrrolidone (PVP, Sigma-Aldrich) and ethylene glycol (EG, Sigma-Aldrich) solvent. 3.7 ± 0.7 nm Pt-PVP nanoparticles were prepared by combining 20 mL of EG, 100 mg of $H_2PtCl_6 \cdot 6H_2O$ (1.9×10^{-4} mol, Sigma-Aldrich) and 440 mg of PVP (4×10^{-3} mol) in a 50 mL three-neck round bottom flask.[29] The flask was sealed and residual air was evacuated by three cycles of vacuum pumping followed by an Ar purge. 3.8±0.8 nm Pd-PVP were prepared by combining 10 mL of EG, 70 mg of PdCl3 (1.0×10^{-4} mol, Sigma-Aldrich) and 220 mg of PVP (2×10^{-3} mol) in a 25 mL round bottom flask. The synthesis of Pt and Pd was carried out at 165°C with vigorous stirring in Ar flow for 25 min. Continuing for longer times did not increase the size of the nanoparticles. 4.1±1.2 nm Rh-PVP nanoparticles were synthesized with 0.657 g (1×10^{-4} mol) rhodium(II)trifluoroacetatedimer [Rh2(TFA)4] (i.e., 2×10^{-4} mol per Rh atom, Sigma-Aldrich), 220 mg of PVP (2×10^{-3} mol) in 10 mL EG heated to 110°C for 10 min and then 165°C for 1.5 hours.[30]

When the solution returned to room temperature after synthesis, 100 mL of acetone was added to the solution and the nanoparticles were precipitated by centrifugation (VWR Clinical 50, 4000 rpm) for ~10 min. The nanoparticles (black precipitate) were then redispersed in ethanol (10-20 mL) and precipitated with hexane (40-80 mL) at least three times to wash away excess PVP.

Core-shell nanoparticles were synthesized by dissolving 100-300 μL Pt-PVP, Pd-PVP or Rh-PVP and 5-10 μL tetraethyl orthosilicate (TEOS) with 15 mL ethanol in a 20 mL glass scintillation vial.40,41 Subsequently, 2.25 mL of ammonium hydroxide was added dropwise while the mixture was stirred for 5 minutes. After all the ammonium hydroxide was added, the mixture was left in the sonicator for 2 hours. To achieve the thinnest shell while ensuring complete encapsulation of all nanoparticles, the ratio of nanoparticle to TEOS was adjusted. To separate the Pt@SiO_2 nanoparticles from the synthesis mixture, ~6 mL acetone and ~22 mL hexane were combined and centrifuged (4000 rpm) for 10 min. Pt-PVP@SiO_2 were washed two additional times by dissolution in ~2 mL ethanol, precipitation in ~12 mL hexane, and centrifugation. Before Langmuir-Blodgett (LB) film deposition, Pt-PVP@SiO_2 nanoparticles were dissolved in 300 μL ethanol and 300 μL $CHCl_3$ and sonicated for ~1 hour or until dissolved.

Langmuir-Blodgett Film Deposition

LB films were deposited on silica surfaces by submersion in water followed by addition of the nanoparticle solution dropwise to the surface.[9] After the surface pressure increased to 10-20 mN/m, the film was allowed to relax for 30 min for solvents to evaporate. The film was then

compressed at a rate of 5 mm/min to the maximum compression (> 30 mN/m) such that any additional compression would create multilayers. To increase signal for SFG experiments, two LB monolayers were deposited onto the fused SiO_2 prism by resubmersing the prism and repeating compression.

Calcination

To remove PVP from the nanoparticle samples, the silica-supported nanoparticles were placed into a tube furnace (Lindberg Blue M) at 350°C for 10 min. SFG experiments in the aliphatic and aromatic stretching range confirmed the removal of PVP (Figure 3), resulting in a flat baseline in H_2 before introducing the reaction mixture.

1,3-Butadiene Hydrogenation Reactions

1,3-butadiene hydrogenation was performed in a batch reactor equipped with a capacitance manometer pressure gauge (MKS Baratron), a recirculating pump (Senior Aerospace MB-21), a turbomolecular pump (Pfeiffer) and a rotary oil pump. $Pt@SiO_2$, $Pd@SiO_2$ or $Rh@SiO_2$ catalysts were loaded with 10x sand dilution into 1/4 in stainless steel tubing with glass wool. The conversion was monitored using a gas chromatograph (Agilent 6890) equipped with a flame ionization detector and Supelco I-2809-U 23% SP-1700 packed column. Prior to each reaction, the chamber was evacuated down to 10^{-4} Torr by a turbomolecular pump. Selectivity was calculated with total conversion <20%. Blank experiments indicated negligible background activity. To test the background SFG spectra in 20 Torr 1,3-butadiene, blank experiments were performed with a clean SiO_2 prism. These experiments show a C-H stretch at 2995 cm^{-1} but no other features. This peak is noted as a spectator in Figures 6, 7, and 8. Kinetic and SFG experiments were performed in 760 Torr total pressure using Ar background with the 20 Torr 1,3-butadiene and 100 Torr H_2 unless otherwise indicated.

Sum Frequency Generation Vibrational Spectroscopy.

SFG experiments were performed with a mode-locked Nd:YAG dye laser (Continuum Leopard D-20) with 1064 nm fundamental output, 20 Hz repetition rate and 20 ps pulse width. A frequency doubling crystal was used to generate a 532 nm visible (VIS) beam from the fundamental beam. An optical parametric generator/amplifier produced tunable infrared (IR) in the range 2680–3180 cm^{-1}, corresponding to the stretching modes of aliphatic and aromatic groups. Visible and infrared beams of ~220 μJ power were spatially and temporally overlapped at the base of a polished fused silica equilateral (60°) prism (ISP Optics) at angles of 63° and 48°, respectively, from the surface normal to achieve total internal reflection. All of the experiments were performed in ppp polarization combination. SFG photons were detected by a photomultiplier tube with a gated boxcar integrator.

Transmission Electron Microscopy

Nanoparticles were supported on Cu grids (Electron Microscopy Sciences) and imaged using a JEOL 2100 microscope operated at 200 kV.

Results and Discussion

Core-shell oxide encapsulation allows morphological characteristics of size-controlled nanoparticles to be maintained while capping is eliminated by calcination. During synthesis in solution phase, all colloidal nanoparticles become enveloped in organic ligands to prevent aggregation.[31] However, capping blocks active sites and can obscure surface characterization methods. In SFG, the CH_2 stretches of PVP can cover major parts of the spectrum, blocking vibrational features of reaction intermediates of interest.[32] For this study, 4 nm Pt@SiO_2, Pd@SiO_2 and Rh@SiO_2 were synthesized using a modified Stöber synthesis (Figure 2). Adjusting the ratio of nanoparticles to the SiO_2 precursor (tetraethyl orthosilicate, TEOS) ensures complete encapsulation of all nanoparticles with the thinnest possible shell. Langmuir-Blodgett film deposition was used to create 2-D monolayers of Pt-PVP@SiO_2 (Figure 2(D)) of comparable in density to Pt-PVP (Figure 2(B)) at max packing. Because of the space occupied by the SiO_2 shell and evanescent wave attenuation, the intensity of the SFG signal from core-shell Pt is less than a Pt-PVP film. Because PVP dynamically restructure in H2 on Pt@SiO_2 (such as on Pt-PVP shown previously) and the unique red-shifted peak of chemisorbed 1,4-cyclohexadiene (1,4-CHD) is observed (after PVP is removed by calcination), it is clear SFG can probe the Pt surface within the shell.9 (If molecular 1,4-CHD or PVP adsorbed onto the SiO_2 shell or prism, a peak would not appear at 2770 cm^{-1} and the spectrum of PVP would not change in H2.) After the 2-D Pt-PVP@SiO_2 is calcined to removed PVP, a flat SFG background is achieved in H2/Ar background and the nanoparticles are referred to as "Pt@SiO_2."

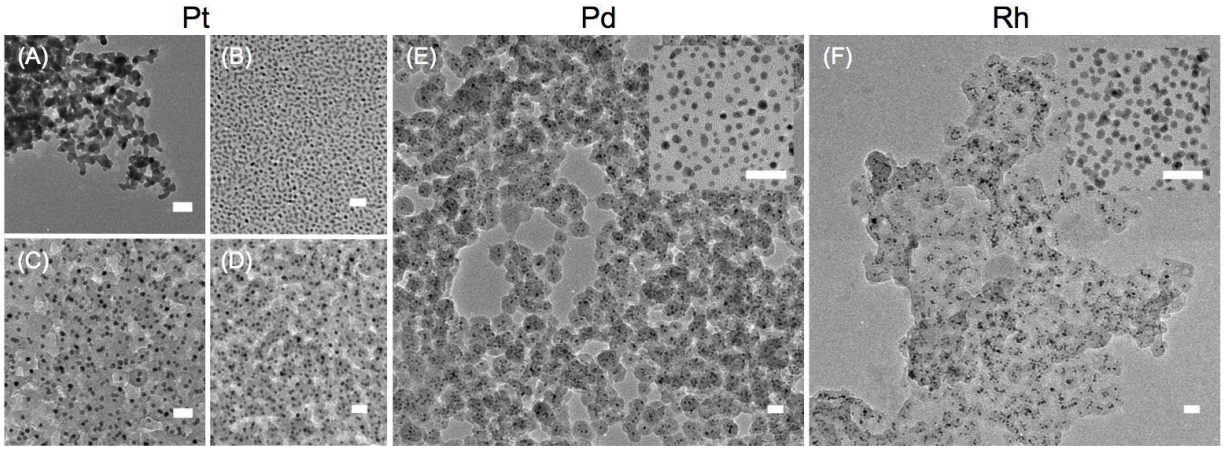

Figure 2 – (A) calcined Pt-PVP, (B) Pt-PVP LB, (C) calcined Pt-PVP@SiO_2, (D) Pt-PVP@SiO_2 LB, (E) Pd@SiO_2 (calcined), initial Pd-PVP (inset), and (F) Rh@SiO_2 (calcined), initial Rh@SiO_2 (inset). Scale bar is 20 nm.

Following calcination, core-shell nanoparticles maintained their original size distribution and the removal of PVP enhanced the diffusion of reactants to the metal surface (Figure 2(C)). In the absence of a SiO_2 shell Pt-PVP nanoparticles irreversibly aggregated during calcination (Figure 2(A)). Kinetic tests using ethylene hydrogenation to count active sites showed a ~4X increase in turnover rate following calcination, suggesting that PVP was successfully removed (Figure S1). In contrast, when no shell is present, a lower ~1.3X increase is achieved because PVP loss

occurs in unison with aggregation. Despite intensive efforts to synthesize core-shell silica structures and encapsulate metals, vibrational spectroscopy studies of surface intermediates produced under reaction conditions have not been performed on these materials.31 Recent work shows that disordering under H_2 allows the reaction on intermediates on Pt-PVP to be identified by SFG without aggressive PVP removal.[9] However, in our experience, the degree of disordering (i.e., decrease of the SFG signal of PVP) is usually less effective with metals other than Pt and capping agents other than PVP. With core-shell catalysts, SFG may be applied to a larger number of catalytic surfaces.

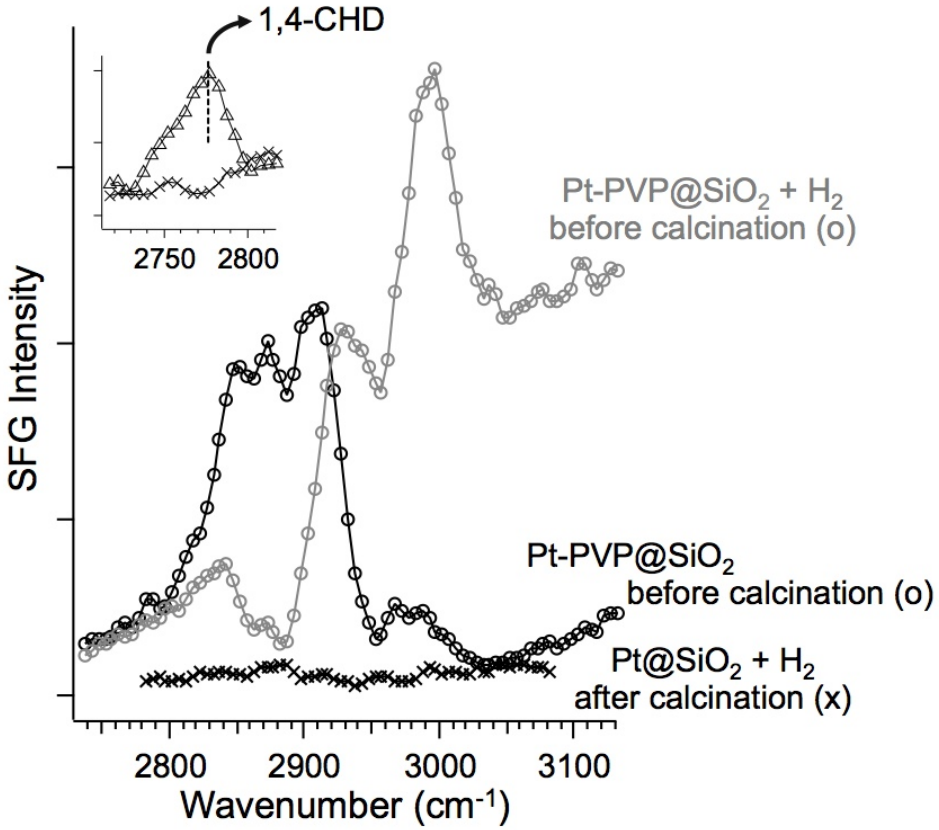

Figure 3 – SFG spectra of 4 nm Pt-PVP@SiO_2 before and after calcination. Ar ("o", 760 Ar) and H_2/Ar ("o", 200 Torr H2, 560 Torr Ar) atmospheres were tested before calcination. Following calcination of Pt-PVP@SiO_2, the nanoparticles are referred to as "Pt@SiO_2." 1,4-Cyclohexadiene (1,4-CHD) hydrogenation was performed on Pt@SiO_2 (inset) first using 200 Torr H_2 and 558 Torr Ar background ("x"), followed by 2 Torr 1,4-CHD, 200 Torr H_2 and 558 Torr Ar reaction conditions ("Δ").

1,3-butadiene hydrogenation is a composition dependent reaction. Pd is known to favor partial hydrogenation, while Pt and Rh catalysts make all products. Selectivity >97% for partial hydrogenation are reported for Pd(111) and Pd nanoparticles grown on Al_2O_3 under ultrahigh vacuum.[1,33] Figure 4 shows the product distribution of 4 nm Pt@SiO_2, Pd@SiO_2 and Rh@SiO_2 at 20, 60 and 100°C. In the view of the reaction pathways in Figure 1, with B14R excluded, an

"unselective" catalyst would produce 41.6% butane, 41.6% 1-butene, and 16.6% 2-butene. This is similar to the observed distribution for $Pt@SiO_2$ (40.0, 44.6 and 15.3%) at 20°C. In contrast, $Pd@SiO_2$ produces exclusively butenes (>94%) at all temperatures. The preference for partial hydrogenation on Pd(111) occurs because B13R is destabilized by 39 kJ/mol compared to 1B4R and 2B1R.[2] At higher temperatures, all three catalysts produce more butenes and less butane. $Pd@SiO_2$ produces the least butane at 20°C, and its product distribution is nearly constant for all temperatures. Butane formation does not increase with temperature proportionately to other products for all catalysts; therefore, it has the least activated hydrogenation route.

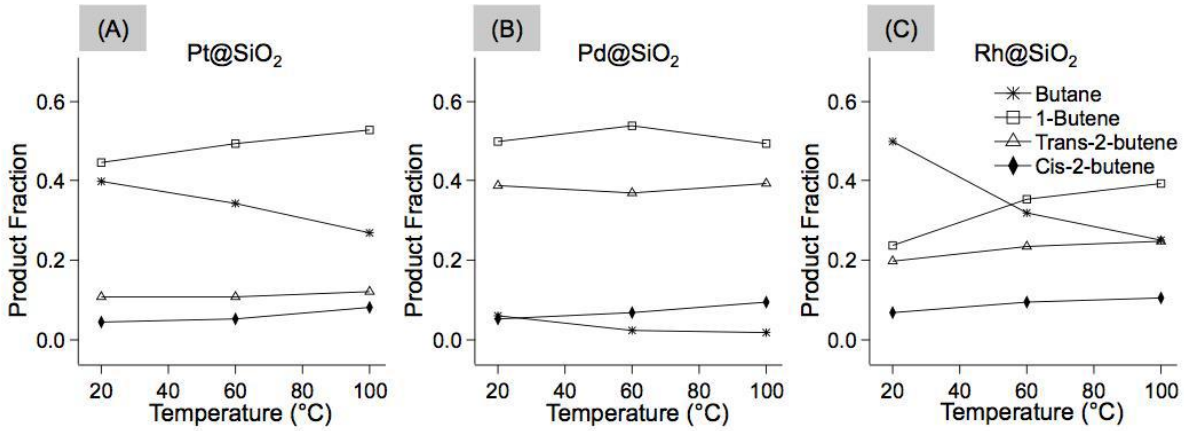

Figure 4 – 1,3-butadiene hydrogenation product distribution at 20, 60 and 100 °C for $Pt@SiO_2$ (A), $Pd@SiO_2$ (B) and $Rh@SiO_2$ (C).

Butane and 1-butene can be obtained through multiple reaction pathways but 2B1R is the only intermediate to produce *cis*/*trans*-2-butene (Figure 1). Figure 5 shows that all butenes/all products ratio increases with temperature for $Pt@SiO_2$ and $Rh@SiO_2$ and remains constant for $Pd@SiO_2$. The 2-butene / 1-butene ratio remains constant at all temperatures for all catalysts. Similar to the product distribution at 20°C, the level of 2-butenes in all butenes (25.6%) is close to an unselective catalyst for $Pt@SiO_2$ (28.5%). In contrast, $Pd@SiO_2$ and $Rh@SiO_2$ favor higher levels of 2-butene (46.7 and 52.9%, respectively). Because $Pd@SiO_2$ prefers 2-butenes does not form B13R, it can be inferred that 2B1R is the most prevalent intermediate (i.e., 7 times higher preference for 2B1R over 1B4R based on 2-butene to 1-butene ratio). These results show that SFG can be used to differentiate between a reaction that has multiple paths (e.g., $Pt@SiO_2$) and one that favors one path (e.g., $Pd@SiO_2$).

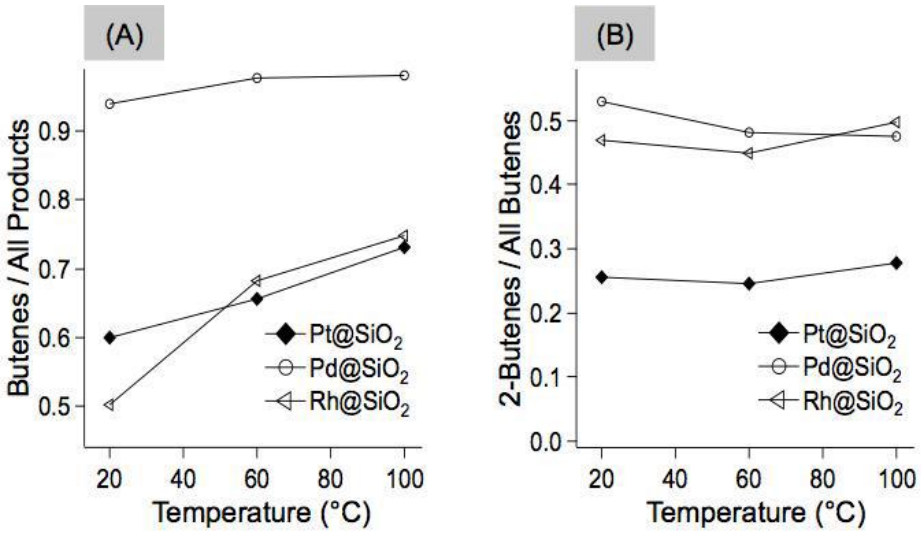

Figure 5 – Partial hydrogenation fraction (butenes / all products) (A) and preference for cis/trans-2-butenes (2-butenes / all butenes) (B) calculated from data in Figure 4.

SFG experiments were performed following calcination to identify reaction intermediates on Pt, Pd and Rh surfaces. Figure 6 shows SFG spectra on $Pt@SiO_2$ collected before, during and after reaction. Major features during reaction at 20 °C include 2875 cm^{-1} (CH_3(s)), 2905 cm^{-1} (CH_2(a,p), CH_2 (FR)), 2940 cm^{-1} (CH_3(a,p), CH_2(a)), 2970 cm^{-1} (CH_3(a))) and a C-H stretch from molecular 1,3-butadiene at 2995 cm^{-1} (not used for reaction interpretation).15,26,27,33-35 As temperature is increased, the overall intensity of all peaks is reduced, however, the most prominent feature at 2905 cm^{-1} remains. Particularly at 20°C, where SFG intensity is high and the catalysts has an unselective product distribution, the SFG spectrum likely reflects some combination of 1B4R, 2B1R and B13R because among these intermediates, CH_2 and CH_3 vibrations are active.

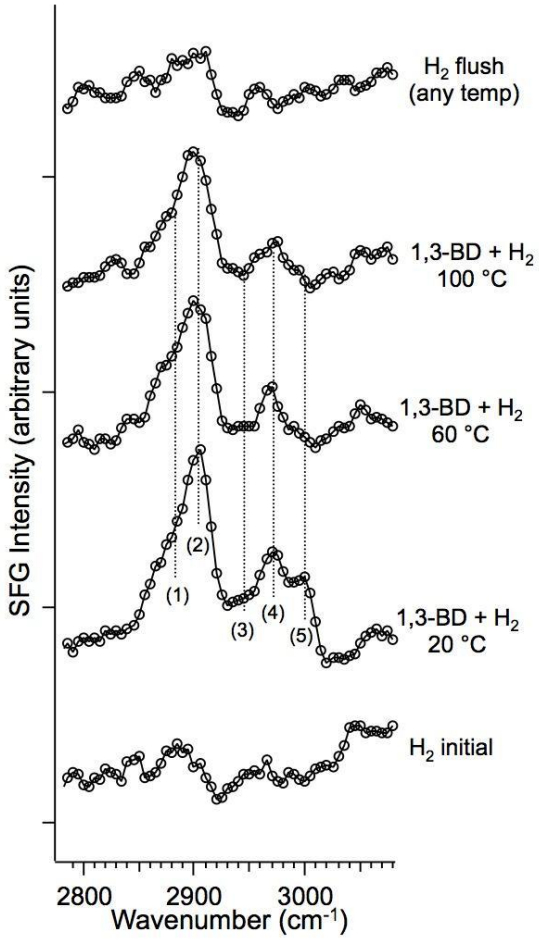

Figure 6 – SFG spectra of 1,3-butadiene hydrogenation on 4 nm Pt@SiO_2. The calcined LB film is first treated with 100 Torr H2 and 660 Torr Ar (H2 initial) and then reaction conditions (20 Torr 1,3-butadiene, 100 Torr H2 and 640 Torr Ar) at 20, 60 and 100 ° C. At any temperature, the peaks observed during reaction disappear when flushed with only H2, suggesting that the peaks originate from reactive intermediates. Five peaks appear under reaction conditions: (1) 2875 cm^{-1} (CH_3(s)), (2) 2905 cm^{-1} (CH_2(a,p), CH_2 (FR)), (3) 2940 cm^{-1} (CH_3(a,p), CH_2(a)), (4) 2970 cm^{-1} (CH_3(a))) and (5) C-H stretch from molecular 1,3-butadiene at 2995 cm^{-1} (not used in analysis).

The SFG spectra of Pd@SiO_2 are shown in Figure 7. Seven peaks appear under reaction conditions including 2875 cm^{-1} (CH_3(s)), 2905 cm^{-1} (CH_2(a,p), CH_2 (FR)) and 2940 cm^{-1} (CH_3(a,p), CH_2(a)), 2975 cm^{-1} (CH_3(a)), 3030 cm^{-1} (=CH), 3065 cm^{-1} (=CH_2(a)) and a C-H stretch from molecular 1,3-butadiene at 2995 cm^{-1} (not used for reaction interpretation). Although vibrational features become diminished at temperatures above 20°C, the product distribution remains constant (Figure 5(E)), so the reaction pathway is not expected to shift dramatically. Compared to Pt@SiO_2, the strong feature at 2905 cm^{-1} is reduced and peaks corresponding with CH_3 resonances are relatively more intense. The increase in CH_3 to CH_2 stretch ratio is expected because the preference for 2B1R is shown by kinetic results. The ratio of *trans*-2-butene over *cis*-2-butene is most pronounced for Pd@SiO_2 and originates from the

original (*trans*) 1,2,3,4-tetra-σ adsorption mode of 1,3-butadiene. (The ratio of *trans*-2-butene to *cis*-2-butene is 7.5, 2.9 and 2.5 for Pd@SiO_2, Rh@SiO_2 and Pt@SiO_2 at 20°C, respectively). The adsorption energy of 1,2,3,4-tetra-σ is calculated to be 38 kJ/mol more stable on Pd(111) than Pt(111).24 Therefore, 1,2,3,4-tetra-σ and *trans* complexes are more predominant on Pd@SiO_2. Only Pd@SiO_2 SFG spectra contain peaks assigned to 1,3-butadiene (peaks (6) and (7) in Figure 7). 1,3-butadiene has ordered adsorption on Pd resulting in resolved SFG peaks and a preference for *trans*-2-butene.

The SFG spectra during reaction of Rh@SiO_2 (Figure 8) indicate poison species not reaction intermediates. Calcination eliminates PVP from the spectrum, providing a flat background in H_2. As the 1,3-butadiene hydrogenation reaction mixture is introduced, new peaks appear across the entire aliphatic stretch range including the peak at 2875 cm^{-1} possibly indicating butylidyne,36 a species known to be unreactive. When H_2 is reintroduced in the absence of 1,3-butadiene at any temperature (20-100°C), all major peaks remain except the C-H stretch from molecular 1,3-butadiene at 2995 cm^{-1} on the glass prism. Although the SFG spectra shown in Figure 8 cannot be used to identify reaction pathways, they indicate that the surface becomes covered by persistent C hetero species, which produce many aliphatic stretches and cannot be eluted even by ramping with H2 up to 200 °C.

In contrast, both Pt@SiO_2 and Pd@SiO_2 revert back to the baseline spectra at any temperature when H2 is reintroduced without 1,3-butadiene. Previous experiments of pyrrole hydrogenation comparing Rh(111) to Pt(111) showed Rh(111) was capable of cracking the hydrocarbon chain into fragments at 25°C.37 Because the 4 nm Rh nanoparticles have more high energy edge sites, there may be stronger affinity to crack 1,3-butadiene.[17,31]

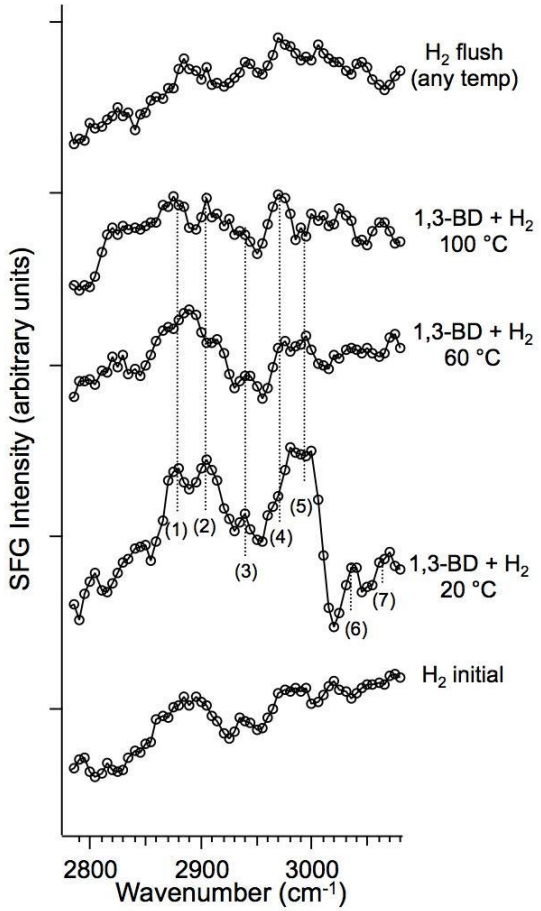

Figure 7 – SFG spectra of 1,3-butadiene hydrogenation on 4 nm Pd@SiO_2. The calcined LB film is first treated with 100 Torr H2 and 660 Torr Ar (H2 initial) followed by reaction conditions (20 Torr 1,3-butadiene, 100 Torr H_2 and 640 Torr Ar) at 20, 60 and 100°C. At any temperature, the peaks observed during reaction disappear when flushed with only H2, suggesting that the peaks originate from reactive species. Seven peaks appear under reaction conditions at 20°C: (1) 2875 cm-1 (CH3(s)), (2) 2905 cm-1 (CH2(a,p), CH2 (FR)), (3) 2940 cm-1 (CH3(a,p), CH2(a)), (4) 2975 cm-1 (CH3(a))), (5) C-H stretch from molecular 1,3-butadiene at 2995 cm-1 (not used in analysis), (6) 3020 cm-1 (=CH) and 3060 cm-1 (=CH2(a)).

Poisoning of the Rh@SiO_2 catalyst was is observed in kinetic experiments where 79% deactivation following reactions at 20, 60 and 100°C occurs compared to 37 and 39% deactivation for the Pt@SiO_2 and Pd@SiO_2 catalysts over a ~12 h period (Figure S1). The product distributions also changed most strongly for Rh@SiO_2. For Rh@SiO_2, butane production increased from 49.7 to 59.4%, while for Pt@SiO_2 and Pd@SiO_2, each product fraction was reproduced by 3% or better at 20°C following 20, 60 and 100°C. The Arrhenius plots of Pt@SiO_2 and Pd@SiO_2 show linear behavior at 20, 60 and 100°C, while Rh@SiO_2 is less linear (Figure S1). In summary, 1,3-butadiene hydrogenation on Rh@SiO_2 is characterized by

irreversible accumulation of organic material, which blocks sites, impacts the SFG spectrum and shifts product selectivity.

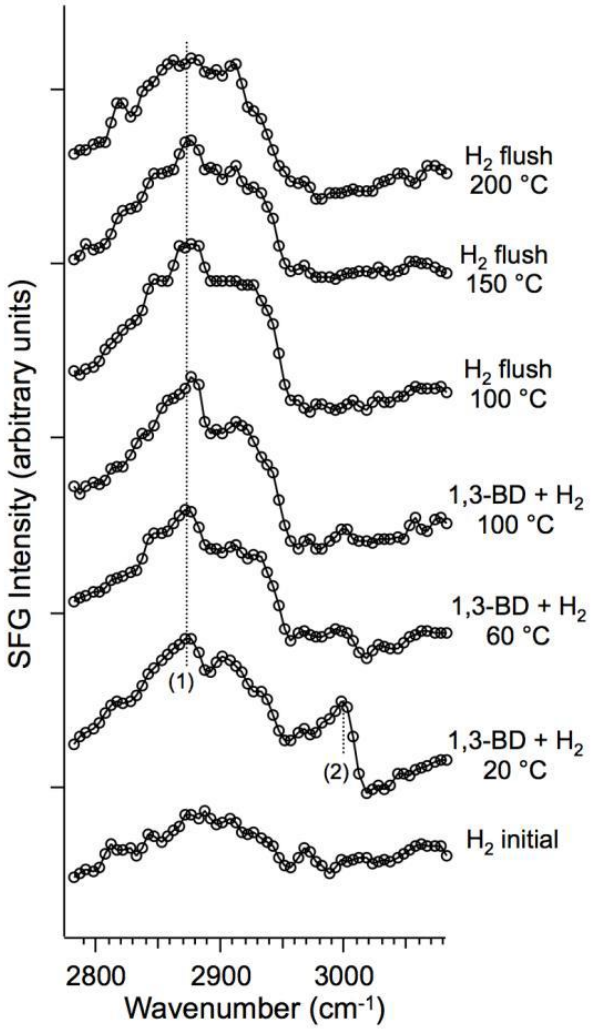

Figure 8 – SFG spectra of 1,3-butadiene hydrogenation on 4 nm Rh@SiO_2. The calcined LB film is first treated with 100 Torr H_2 and 660 Torr Ar (H_2 initial) and then reaction conditions (20 Torr 1,3-butadiene, 100 Torr H_2 and 640 Torr Ar) at 20, 60 and 100°C. After the reaction the sample is flushed with 100 Torr H_2 at 100, 150 and 200°C. Labeled peaks are (1) 2875 cm^{-1} (CH_3(s) possibly of butylidyne) and (2) C-H stretch from molecular 1,3-butadiene at 2995 cm^{-1} (not used in analysis).

Conclusions

In this study, SFG vibrational spectroscopy was used to monitor catalytic processes on noble metal nanoparticles in SiO_2 during 1,3-butadiene hydrogenation. Core-shell catalysts allow the capping agent to be removed through calcination while still maintaining nanoparticle size

monodispersity. Three compositions (4 nm Pt, Pd and Rh) were compared based on product distribution and SFG spectra. At 20 °C, Pt@SiO_2 is unselective and does not discriminate along 1B4R, 2B1R and B13R, producing butane, 1-butane and *cis*/*trans*-2-butene like an unselective catalyst. In contrast, Pd@SiO_2 prefers one pathway through ordered *trans* 1,3-butadiene adsorption and 2B1R to make exclusively 1-butene and *cis*/*trans*-2-butene, with a preference for *trans*-2-butene. Reaction selectivity correlates to vibrational features observed during reaction.

The lack of reversibility of the Rh@SiO_2 catalysts compared to Pt@SiO_2 and Pd@SiO_2 catalysts suggests surface poisoning and reveals the importance of comparing SFG spectra before, during and after reaction conditions to identify intermediates and not spectators. Further efforts may use core-shell 2-D systems to develop fundamental *in situ* techniques for examining reactions on industrial catalysts in 3-D. These core-shell systems also provide a potential way to use SFG spectroscopy to study nanoparticle-catalyzed reactions in the liquid phase.

References

(1) Silvestre-Albero, J.; Rupprechter, G.; Freund, H. Atmospheric Pressure Studies of Selective 1 , 3-Butadiene Hydrogenation on Well-Defined Pd / Al 2 O 3 / NiAl (110) Model Catalysts : Effect of Pd Particle Size. *J. Catal.* **2006**, *240*, 58–65.

(2) Valcarcel, A.; Clotet, A.; Ricart, J. M.; Delbecq, F.; Sautet, P. Selectivity Control for the Catalytic 1 , 3-Butadiene Hydrogenation on Pt (111) and Pd (111) Surfaces : Radical versus Closed-Shell Intermediates. *J. Phys. Chem. B* **2005**, *109*, 14175–14182.

(3) Alves, J. A.; Bressa, S. P.; Mart, O. M.; Barreto, G. F. Selective Hydrogenation of 1 , 3-Butadiene : Improvement of Selectivity by Using Additives. *Chem. Eng. J.* **2004**, *99*, 45–51.

(4) Horiuti, J.; Polanyi, M. Outlines of a Theory of Proton Transfer. *J. Mol. Catal. A* **2003**, *199*, 185–197.

(5) Hugon, A.; Delannoy, L.; Krafft, J.; Louis, C. Selective Hydrogenation of 1 , 3-Butadiene in the Presence of an Excess of Alkenes over Supported Bimetallic Gold - Palladium Catalysts. **2010**, *4* (i), 10823–10835.

(6) Furlong, B. K.; Hightower, J. W.; Chan, T. Y.; Sarkany, A.; Guczi, L. 1 , 3-Butadiene Selective Hydrogenation over Pd / Alumina and CuPd / Alumina Catalysts. **1994**, *117*, 41–51.

(7) Sarkany, A.; Zsoldos, Z.; Furlong, B.; Hightower, J. W.; Guczi, L. Hydrogenation of 1-Butene and 1,3-Butadiene Mixtures over Pd/ZnO Catalysts. *J. Catal.* **1993**, *141*, 566–582.

(8) Lee, D. C.; Kim, J. H.; Kim, W. J.; Kang, J. H.; Moon, S. H. Selective Hydrogenation of 1 , 3-Butadiene on TiO 2 -Modified Pd / SiO 2 Catalysts. *Appl. Catal. A Gen.* **2003**, *244*, 83–91.

(9) Krier, J. M.; Michalak, W. D.; Baker, L. R.; An, K.; Komvopoulos, K.; Somorjai, G. A. Sum Frequency Generation Vibrational Spectroscopy of Colloidal Platinum Nanoparticle

Catalysts: Disordering versus Removal of Organic Capping. *J. Phys. Chem. C* **2012**, *116* (33), 17540–17546.

(10) Morin, C.; Simon, D.; Sautet, P. Intermediates in the Hydrogenation of Benzene to Cyclohexene on Pt (1 1 1) and Pd (1 1 1): A Comparison from DFT Calculations. *Surf. Sci.* **2006**, *600*, 1339–1350.

(11) Michalak, W. D.; Krier, J. M.; Komvopoulos, K.; Somorjai, G. A. Structure Sensitivity in Pt Nanoparticle Catalysts for Hydrogenation of 1,3-Butadiene: In Situ Study of Reaction Intermediates Using SFG Vibrational Spectroscopy. *J. Phys. Chem. C* **2013**, *117* (4), 1809–1817.

(12) Cremer, P.; Stanners, C.; Niemantsverdriet, J. W.; Shen, Y. R. The Conversion of Di-O-Bonded Ethylene to Ethylidyne on Pt(111) Monitored with Sum Frequency Generation : Evidence for an Ethylidene (or Ethyl) Intermediate. *Surf. Sci.* **1995**, *328*, 111–118.

(13) Yang, M.; Chou, K. C.; Somorjai, G. A. In-Situ Observation of π -Allyl c -C 6 H 9 Intermediate during High-Pressure Cyclohexene Catalytic Reactions on Pt (111) Using Sum Frequency Generation Vibrational Spectroscopy. **2003**, *2* (111), 5267–5272.

(14) Yang, M.; Chou, K. C.; Somorjai, G. A. The Structures and Reactions of Linear and Cyclic C6 Hydrocarbons Adsorbed on the Pt(111) Crystal Surface Studied by Sum Frequency Generation Vibrational Spectroscopy: Pressure, Temperature, and H2 Coadsorption Effects. *J. Phys. Chem. B* **2004**, *108*, 14766–14779.

(15) Kliewer, C. J.; Bieri, M.; Somorjai, G. A. Hydrogenation of the A,b-Unsaturated Aldehydes Acrolein, Crotonaldehyde, and Prenal over Pt Single Crystals: A Kinetic and Sum Frequency Generation Vibrational Spectroscopy Study. *J. Am. Chem. Soc.* **2009**, *131*, 9958–9966.

(16) Somorjai, G. A.; Park, J. Y. Molecular Factors of Catalytic Selectivity. *Angew. Chemie Int. Ed.* **2008**, *47*, 9212–9228.

(17) Roduner, E. Size Matters : Why Nanomaterials Are Different. *Chem. Soc. Rev.* **2006**, *35*, 583–592.

(18) Sautet, P. Theoretical Chemistry as a Tool for Interpreting Catalysts Selectivities. *Top. Catal.* **2000**, *13*, 213–219.

(19) Somorjai, G. A.; Frei, H.; Park, J. Y. Advancing the Frontiers in Nanocatalysis , Biointerfaces , and Renewable Energy Conversion by Innovations of Surface Techniques. *J. Am. Chem. Soc.* **2009**, *131*, 16589–16605.

(20) Baker, L. R.; Kennedy, G.; Van Spronsen, M.; Hervier, A.; Cai, X.; Chen, S.; Wang, L. W.; Somorjai, G. A. Furfuraldehyde Hydrogenation on Titanium Oxide-Supported Platinum Nanoparticles Studied by Sum Frequency Generation Vibrational Spectroscopy: Acid-Base Catalysis Explains the Molecular Origin of Strong Metal-Support Interactions. *J. Am. Chem. Soc.* **2012**, *134* (34), 14208–14216.

(21) Baker, L. R.; Kennedy, G.; Krier, J. M.; Spronsen, M. Van. The Role of an Organic Cap in Nanoparticle Catalysis : Reversible Restructuring of Carbonaceous Material Controls Catalytic Activity of Platinum Nanoparticles for Ethylene Hydrogenation and Methanol Oxidation. *Catal. Letters* **2012**, *142*, 1286–1294.

(22) Bratlie, K. M.; Komvopoulos, K.; Somorjai, G. A. Sum Frequency Generation Vibrational Spectroscopy of Pyridine Hydrogenation on Platinum Nanoparticles. *J. Phys. Chem. C* **2008**, *112*, 11865–11868.

(23) Joo, S. H.; Park, J. Y.; Tsung, C.; Yamada, Y.; Yang, P.; Somorjai, G. A. Thermally Stable Pt/mesoporous Silica Core-Shell Nanocatalysts for High-Temperature Reactions. *Nat. Mater.* **2008**, *8*, 126–131.

(24) Valcarcel, A.; Clotet, A.; Ricart, J. M.; Delbecq, F.; Sautet, P. Comparative DFT Study of the Adsorption of 1,3-Butadiene, 1-Butene and 2-Cis/trans-Butenes on the Pt(111) and Pd(111) Surfaces. *Surf. Sci.* **2004**, *549*, 121–133.

(25) Lambert, A. G.; Davies, P. B.; Neivandt, D. J. Implementing the Theory of Sum Frequency Generation Vibrational Spectroscopy: A Tutorial Review. *Appl. Spectrosc. Rev.* **2005**, *40* (2), 103–145.

(26) Shahidt, G.; Sheppard, N. IR Spectra and the Structures of the Chemisorbed Species Resulting from the Adsorption of the Linear Butenes on a Pt/SiO2 Catalyst. *J. Chem. Soc. Faraday Trans.* **1994**, *90*, 513–516.

(27) Shahidt, G.; Sheppard, N. IR Spectra and the Structures of the Chemisorbed Species Resulting from the Adsorption of the Linear Butenes on a Pt/SiO2 Catalyst. *J. Chem. Soc. Faraday Trans.* **1994**, *90*, 507–511.

(28) Oudar, J.; Pinol, S.; Pradier, C.-M.; Berthier, Y. 1,3-Butadiene Hydrogenation on Single Crystals of Platinum. *J. Catal.* **1987**, *107*, 445–450.

(29) Somorjai, G. A.; Li, Y. Selective Nanocatalysis of Organic Transformation by Metals : Concepts, Model Systems, and Instruments. *Top. Catal.* **2010**, *53*, 832–847.

(30) Biacchi, A. J.; Schaak, R. E. The Solvent Matters : Kinetic versus Thermodynamic Shape Control in the Polyol Synthesis of Rhodium Nanoparticles. *ACS Nano* **2011**, *5*, 8089–8099.

(31) Tsung, C.; Kuhn, J. N.; Huang, W.; Aliaga, C.; Hung, L.; Somorjai, G. A.; Yang, P. Sub-10 Nm Platinum Nanocrystals with Size and Shape Control : Catalytic Study for Ethylene and Pyrrole. *J. Am. Chem. Soc.* **2009**, *131*, 5816–5822.

(32) Borodko, Y.; Habas, S. E.; Koebel, M.; Yang, P.; Frei, H.; Somorjai, G. A. Probing the Interaction of Poly(vinylpyrrolidone) with Platinum Nanocrystals by UV-Raman and FTIR. *J. Phys. Chem. B* **2006**, *110*, 23052–23059.

(33) Silvestre-Albero, J.; Rupprechter, G.; Freund, H.-J. From Pd Nanoparticles to Single

Crystals: 1,3-Butadiene Hydrogenation on Well-Defined Model Catalysts. *Chem. Commun.* **2006**, *0*, 80–82.

Chapter 8

Investigating Platinum Nanoparticles as Liquid-Phase Catalysts for Isopropanol Oxidation

Introduction

The oxidation of alcohol is a useful reaction with many applications in the fields of chemical production and energy conversion. In particular, liquid phase alcohol oxidation using molecular oxygen on a heterogeneous catalyst (such as platinum) has been determined to be a reaction with both low environmental impact and high efficiency.[1,2]

Previous work has been carried out using sum frequency generation (SFG) spectroscopy to study alcohol oxidation at the solid-liquid interface using platinum thin-film catalysts.[3,4] In an attempt to move from the model thin-film catalysts to a more real-world catalyst, Pt nanoparticles were synthesized and utilized for both catalytic reactions and sum frequency generation (SFG) studies. Nanoparticles continue to be a growing field, especially in the liquid phase, as they are highly controllable and have the potential for reaction selectivity. In certain structure-sensitive reactions, the size of Pt nanoparticles can have a significant effect on their catalytic performances.[5–7] SFG delivers a useful tool for examining the surface and providing molecular information that can provide an insight into catalytic behavior.[8–10]

Multiple challenges were faced in undertaking this experiment. First, it was necessary to ensure that the nanoparticle film would stay intact throughout the cleaning and reaction – this work shows that bare nanoparticles will not remain attached to the solid surface when placed in liquid phase environments. It was also necessary to be able to distinguish between the nanoparticles and the reactants or intermediates in the obtained SFG spectra. The capping agent (in this case, PVP) often contains C-H bonds that will show up in the same IR range as the C-H bonds studied during alcohol oxidation, obstructing the results. Previous work has used hydrogen gas to cause disordering and remove interference from the capping agent, but this is clearly not a viable option in a liquid-phase reaction.[11] In addition, as with any catalytic reaction, a reasonable product yield was needed. Therefore, the Pt nanoparticles must be bound to the surface in such a way that left the active sites accessible by the reactants.

Experimental

Nanoparticle Synthesis

Platinum nanoparticles were synthesized under argon atmosphere using a previously established method.[6] Polyvinylpyrrolidone (molecular weight = 29,000) was utilized as a capping agent. 4.0 ± 0.3 nm Pt-PVP nanoparticles were prepared by combining 20 mL of EG, 100 mg of $H_2PtCl_6 \cdot 6H2O$ (1.9×10^{-4} mol, Sigma-Aldrich), and 440 mg of PVP (4×10^{-3} mol) in a 50 mL three-neck round bottom flask. The flask was sealed and residual air was evacuated by three cycles of vacuum pumping followed by an Ar purge. The synthesis was carried out at 165°C with vigorous stirring in Ar flow for 25 min.

When the solution returned to room temperature after synthesis, 100 mL of acetone was added to the solution and the nanoparticles were precipitated by centrifugation (VWR Clinical 50, 4000 rpm) for ~10 min. The nanoparticles (black precipitate) were then redispersed in ethanol (10-20 mL) and precipitated with hexane (40-80 mL) three times to wash away excess PVP.

Core-shell nanoparticles were synthesized by dissolving 100-300 µL Pt-PVP, Pd-PVP or Rh-PVP and 5-10 µL tetraethyl orthosilicate (TEOS) with 15 mL ethanol in a 20 mL glass scintillation vial.40,41 Subsequently, 2.25 mL of ammonium hydroxide was added dropwise while the mixture was stirred for 5 minutes. After all the ammonium hydroxide was added, the mixture was left in the sonicator for 2 hours. To separate the $Pt@SiO_2$ nanoparticles from the synthesis mixture, ~6 mL acetone and ~22 mL hexane were combined and centrifuged at 4000 rpm for 10 min. $Pt\text{-}PVP@SiO_2$ were washed two additional times by dissolution in ~2 mL ethanol, precipitation in ~12 mL hexane, and centrifugation. Before Langmuir-Blodgett (LB) film deposition, $Pt\text{-}PVP@SiO_2$ nanoparticles were dissolved in 300 µL ethanol and 300 µL $CHCl_3$ and sonicated for approximately one hour or until dissolved.

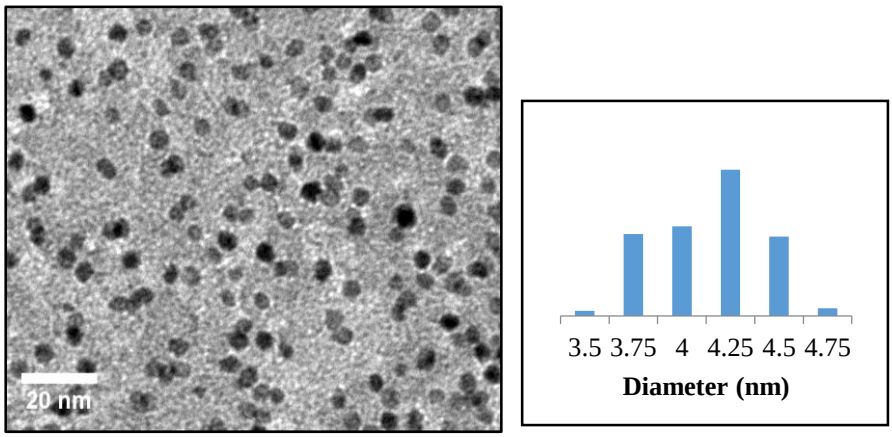

Figure 1 – TEM image of synthesized 4 nm Pt-PVP nanoparticles along with a bar graph showing the corresponding measured size distribution.

Langmuir-Blodgett Film Deposition

Silica-encapsulated, PVP-capped Pt nanoparticles were dissolved in a 50/50 ethanol/chloroform solution, then added dropwise to the surface of a water-filled trough. The solvent was then left to evaporate for approximately 30 minutes, creating a layer of nanoparticles on the surface of the water. The film was then compressed at a rate of 5 mm/min using Teflon barriers while monitoring the surface tension using a probe. Once the surface tension leveled off – indicating a monolayer of nanoparticles – the quartz substrate was raised from the water, allowing the silica-encapsulated nanoparticle film to be deposited on the quartz surface.

The silica-encapsulated Pt-PVP nanoparticles were then calcined on the quartz surface at temperatures ranging from 350°C to 550°C for 3 hours to remove the PVP capping agent.

Ethylene Hydrogenation

Ethylene hydrogenation is a useful catalytic reaction, as it is a structure-insensitive reaction. By using an experimentally determined rate, it is possible to use the known turnover for platinum to back calculate and determine the number of active sites, as a single Pt atom will convert approximately 10 molecules of ethylene to ethane per second, regardless of the coordination environment.[12] This allows for the study of the activity and accessibility of the nanoparticles. Ethylene hydrogenation also has a known vibrational spectrum of its surface species, making it particularly useful in this study.[13]

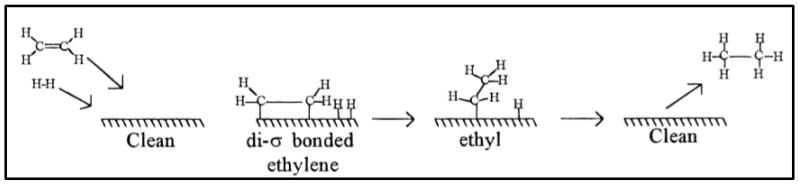

Figure 2 – A schematic showing the hydrogenation of ethylene on a surface.[12]

Ethylene hydrogenations were carried out in a batch mode reactor system consisting of a 1 L reaction chamber, a recirculation pump, a gas manifold for controlled introduction of gases, and a boron nitride sample heater. Mechanical and turbomolecular pumps were attached to allow for evacuation of the chamber to approximately 10^{-5} Torr. A gas chromatograph with a flame ionization detector (FID) was attached to the reactor for identification of products and determination of yield. The GC detector was calibrated for each molecule, allowing rates of production to be calculated from peak areas.

Alcohol Oxidation Reactor

In order to study liquid phase reactions with SFG spectroscopy, a specific flow cell and setup were utilized. A Teflon cell with a volume of 770 µL was used for the reaction flow cell. Teflon was chosen for the cell material, as its chemical inertness prevents it from interfering with any possible alcohol oxidation reactions. However, Teflon is a fairly soft material and has low thermal conductivity, which prevents it from being used above 80°C. The flow of the cell was

controlled by a peristaltic pump (Watson-Marlow 120U) which was run at 40-80 µL/min. Prior to passing through the Teflon cell, the reactant liquid was bubbled with a mixture of nitrogen and air controlled by mass flow controllers. After passing through the reactor, the liquid was pumped to a liquid-vapor exchange column in which the vapors from the product were mixed with nitrogen gas which was then able to be sampled by a gas chomatograph.

Sum Frequency Generation

For all SFG experiments in this study, a picosecond neodymium:yttrium aluminum garnet (Nd:YAG) laser was used. This laser produces a 1064 nm beam with 20 ps pulses of 15-20 mJ. This 1064 nm beam then is split into a 532 nm visible beam and a tunable infrared beam capable of scanning 2700-3500 cm^{-1}. The visible and IR beams then pass through a polarizer and waveplate to achieve the desired polarization and are directed to the sample surface. The visible beam strikes the surface at an incident angle of 62° and the IR beam at an angle of 45°. These beams pass through a CaF_2 prism and the catalyst sample deposited on a quartz window. CaF_2 is utilized due to its high IR wavelength transmission, but the sample itself is deposited on quartz for greater ease in sample preparation and to allow use in aqueous phase reactions.

In order to maximize the light transmission between the CaF_2 prism and the quartz window, an IR-transparent index matching gel was utilized consisting of a mixture of d_8-polystyrene and d_{18}-decahydronapthalene.

The SFG signal generated from the surface was then detected by a photomultiplier tube (PMT) detector, and a gated integrator system with a 100 ns gate time was used to improve the signal-to-noise ratio.

Transmission Electron Microscopy

Transmission electron microscopy (TEM) was used to characterize nanoparticles. All images were collected using a JEOL 2100-F 200 kV Field-Emission TEM and analyzed using ImageJ software.

Results

TEM images

TEM images of the synthesized core-shell Pt nanoparticles found that the SiO_2 did not surround the Pt-PVP nanoparticles in a true “core-shell” structure, but rather formed a looser, less defined encapsulation around the nanoparticles. It is therefore more appropriate to refer to them as “silica-encapsulated Pt nanoparticles” rather than “core-shell” nanoparticles. Regardless of the structure, the silica does surround the nanoparticles and prevent aggregation, achieving the goal of using the silica.

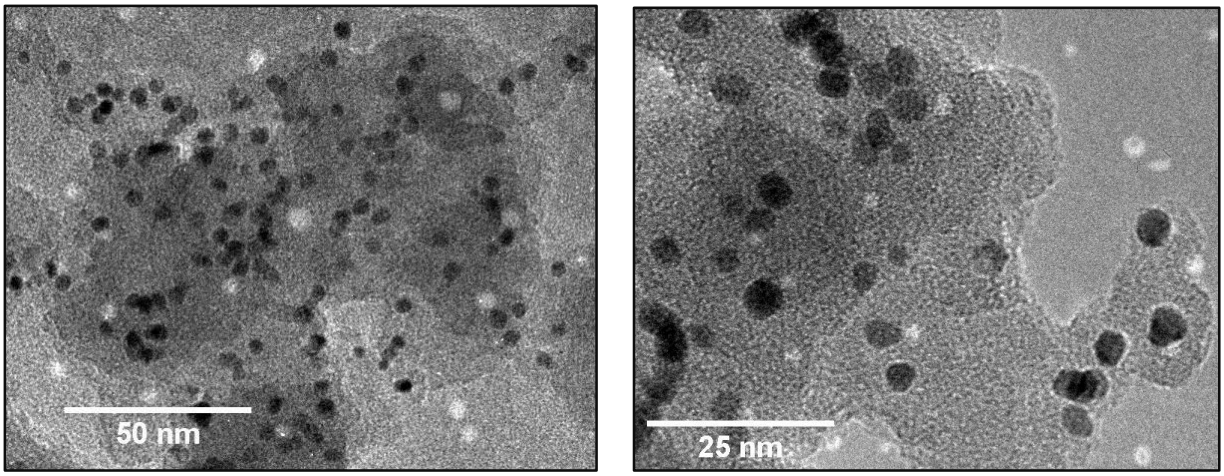

Figure 3 – TEM images of Pt-silica nanoparticles show silica-encapsulated platinum nanoparticles rather than true "core-shell" nanoparticles.

Scanning electron microscopy (SEM) images were also taken both before and after washing the silica-encapsulated Pt nanoparticles in isopropanol for 12 hours. No measurable difference was recorded in the amount of post-washing Pt nanoparticles as compared to prior to the washing, indicating that the silica-encapsulated Pt nanoparticles are stable enough on the surface to use as a liquid-phase catalyst for extended periods of alcohol oxidation. In contrast, Pt nanoparticles without the silica encapsulation were drop-casted onto quartz substrates and washed with isopropanol. SEM images determined that after just one hour, 32% of the nanoparticles were lost. This indicates that the PVP-encapsulated Pt nanoparticles were not a viable catalyst option without the presence of the silica encapsulation.

Nanoparticle Calcination

As previously discussed, ethylene hydrogenation is a useful reaction, as it is a structure-insensitive reaction that can be used to determine the number of active sites of Pt available for catalysis. In this study, ethylene hydrogenation was carried out on drop casted samples at 350, 450, and 550°C in order to find the optimum temperature for calcination. This is an important step, as too low of a temperature may not remove enough of the PVP, blocking active sites and slowing the reaction. On the other hand, too high of a temperature may potentially cause a deactivation of the catalyst.

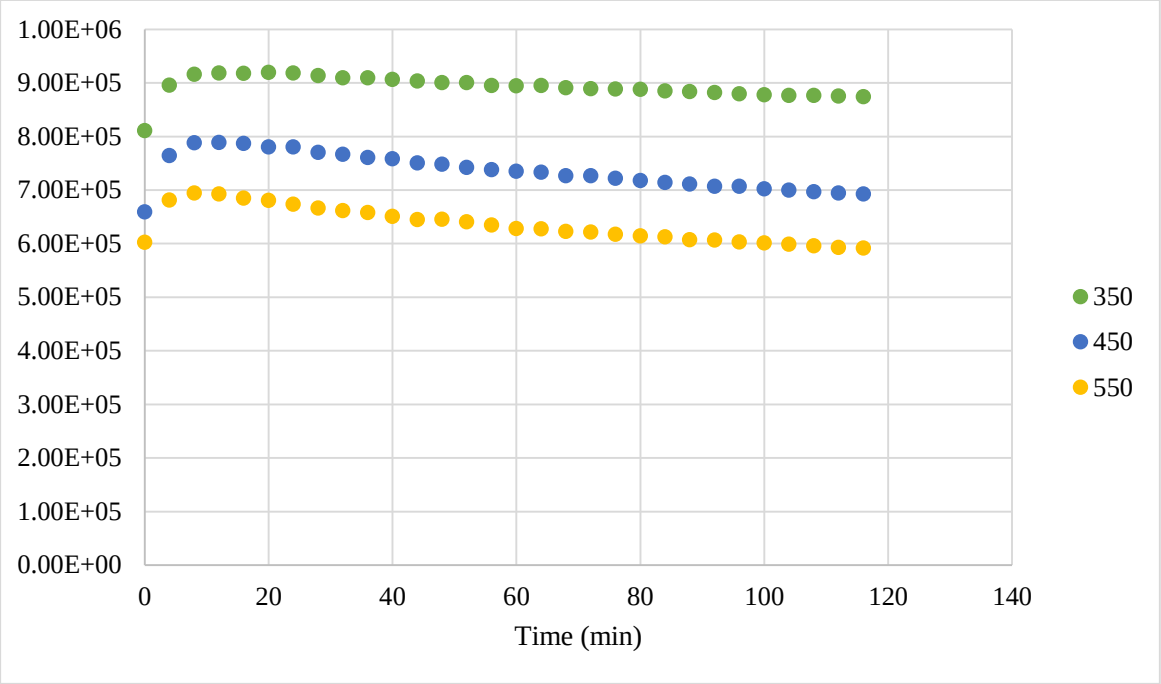

Figure 4 – Catalytic data from ethylene hydrogenation on silica-encapsulated platinum nanoparticles calcined at 350, 450, and 550 degrees Celsius.

Temperature (°C)	Rate (min^{-1})
350	456.2
450	949.5
550	941.5

Table 1 – Calculated reaction rates of ethylene hydrogenation on platinum nanoparticles calcined at various temperatures.

In examining the catalytic data from the ethylene hydrogenations, it was determined that 450°C yielded the highest overall reaction rate for the reaction, making it the best temperature to calcine the silica-encapsulated Pt nanoparticles samples at for the remainder of the studies.

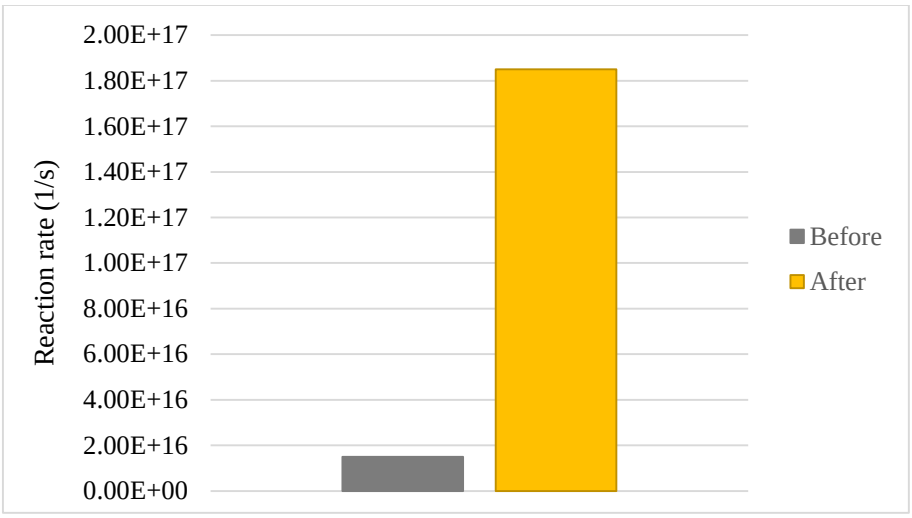

Figure 5 – Effects of calcination on the overall reaction rate of ethylene hydrogenation.

In addition to determining the ideal calcination temperature, the overall effects of calcination on the reaction rate were studied. In order to determine the general effectiveness and necessity of calcining the silica-encapsulated Pt nanoparticles, ethylene hydrogenation reactions were carried out using the nanoparticle catalysts both before and after calcination at 450°C. Prior to calcination, a reaction rate of 1.49×10^{16} s^{-1} was observed. After calcination, the reaction rate was found to be 1.85×10^{17} s^{-1}. Therefore, calcination lead to a 15 times faster reaction than without calcination. Based on the reaction rate data, it was determined that after calcination, approximately 2.86×10^{15} active sites/cm^2 were available for the reaction.

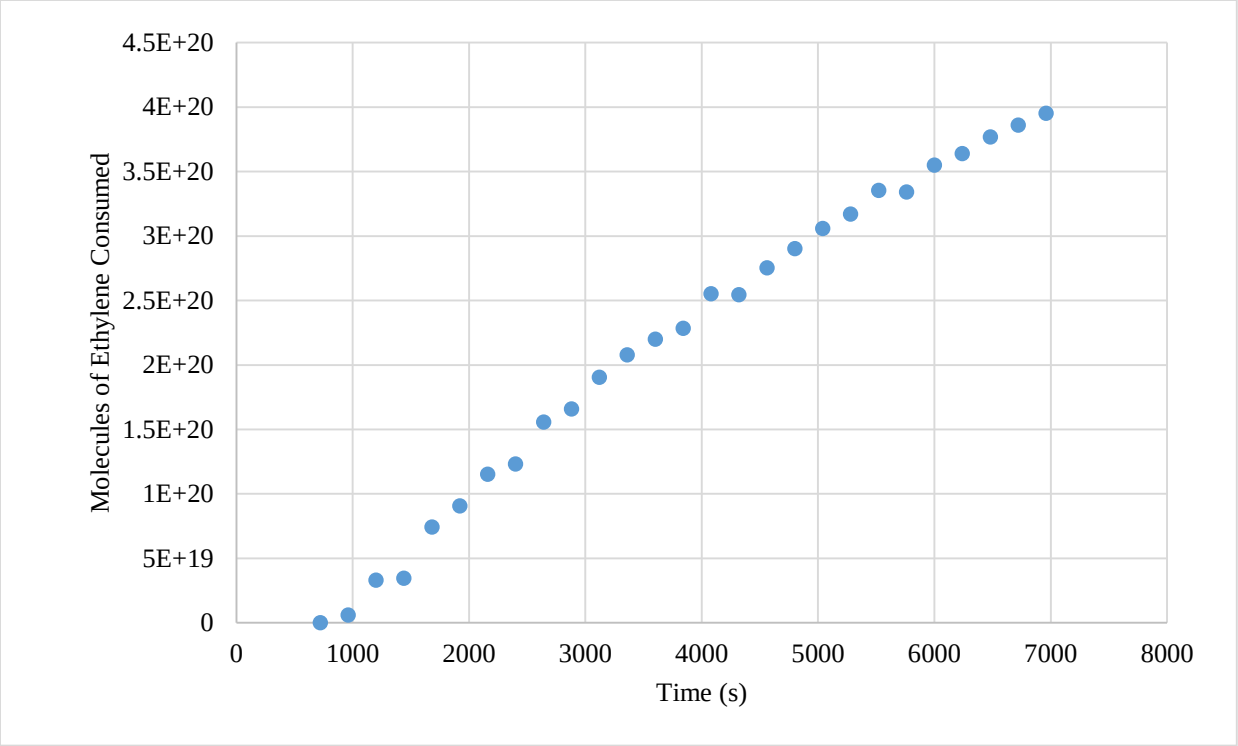

Figure 6 – Consumption of ethylene over the course of the hydrogenation reaction on silica-encapsulated Pt nanoparticles, as monitored using gas chromatography.

SFG Data

As liquid phase spectra are significantly more difficult to obtain than gas phase spectra, SFG was utilized first in the gas phase, since it is easier to obtain and has been studied more. Once again, ethylene hydrogenation provided an ideal option, especially since it has already been studied using SFG spectroscopy.[12]

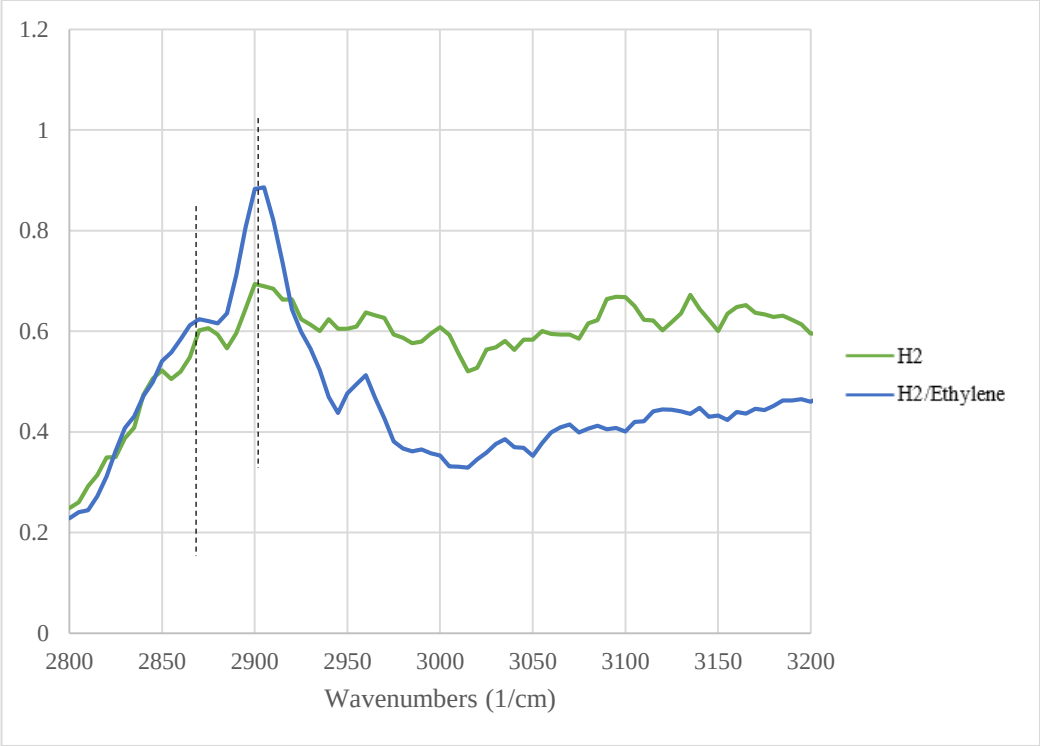

Figure 7 – SFG spectra of Pt-PVP nanoparticles in H_2 and under reaction conditions with H_2 and ethylene. Intermediates of ethylene hydrogenation can be observed on the surface. The peak at ~2870 cm^{-1} indicates the presence of ethylidyne, and the peak at ~2900 cm^{-1} is indicative of di-σ bonded ethylene.

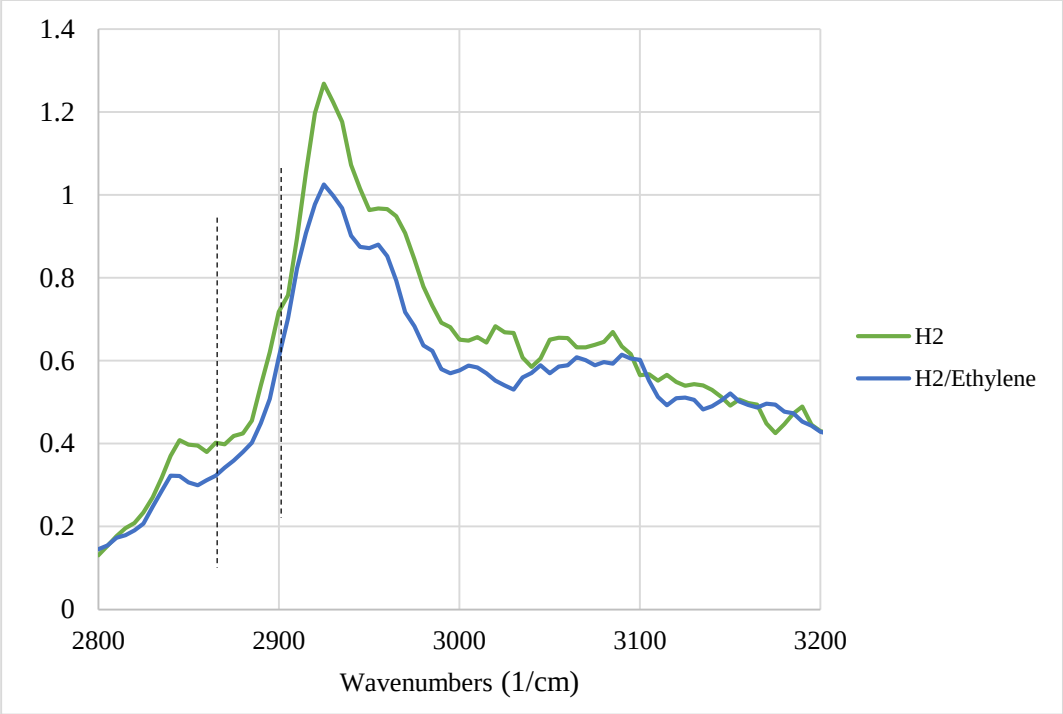

Figure 8 – SFG spectra of silica-encapsulated Pt nanoparticles in H_2 and under reaction conditions with H_2 and ethylene. Lines at 2870 cm^{-1} and 2900 cm^{-1} indicate the approximate location of where ethylene hydrogenation reaction intermediates should be located.

As shown in Figure 7, SFG spectra were first taken on Pt-PVP nanoparticles (without silica encapsulation). A spectrum of the nanoparticles was first taken in the presence of hydrogen. No noticeable peaks were seen, which aligned with the previously established concept of hydrogen disordering. A spectrum was then taken on the same catalyst using a 3:1 ratio of hydrogen to ethylene.

Ethylene hydrogenation yields three potential intermediates on the surface – π-bonded ethylene, di-σ bonded ethylene, and ethylidyne. In this case, peaks were seen at ~2870 cm^{-1} and ~2900 cm^{-1}, aligning with the previously established ethylidyne and di-σ bonded ethylene peaks.[13] These peaks indicate that the Pt-PVP nanoparticles are active catalysts for the hydrogenation of ethylene.

The same scans were then repeated on the silica-encapsulated Pt nanoparticles as seen in Figure 8. Unlike with the Pt-PVP nanoparticles, the scans with and without ethylene appeared nearly identical. The ethylidyne peak previously noted at 2870 cm^{-1} was not able to be seen at all, and the di-σ bonded ethylene peak at ~2900cm^{-1} appeared only as a slight shoulder on a larger peak generated from the silica-encapsulated Pt nanoparticle. The peaks visible at ~2925 cm^{-1} and ~2955 cm^{-1} are likely from the catalyst, and may be from residual carbon fragments left over

from the calcination of the PVP capping agent. The lack of ethylene peaks may also be due to a scattering of light by the silica shell.

Isopropanol Oxidation

The liquid phase oxidation of isopropanol to acetone was previously studied on Pt thin films, making it an excellent candidate to study using silica-encapsulated Pt nanoparticles.[3,4] The overall stoichiometry of the reaction is as follows:

$$(CH_3)_2CHOH + ½\ O_2 \rightarrow (CH_3)CO + H_2O.$$

It is generally accepted that the reaction occurs through the dehydrogenation of the alcohol and a buildup of hydrogen on the surface of the catalyst. Oxygen then reacts with the adsorbed hydrogen to form water. While oxygen is needed for the reaction to proceed, too much oxygen has been found to reversibly poison the reaction, likely through the blocking of active surface sites and preventing the adsorption of alcohol.[3]

Kinetic data shows a dramatic difference in the alcohol oxidation reaction rate between Pt thin film catalysts and silica-encapsulated Pt nanoparticles. Previous studies utilizing Pt thin films as alcohol oxidation catalysts found that an induction period exists in which there is a slow buildup of oxygen on the surface, after which there is a sharp rise in the reaction rate.[3]

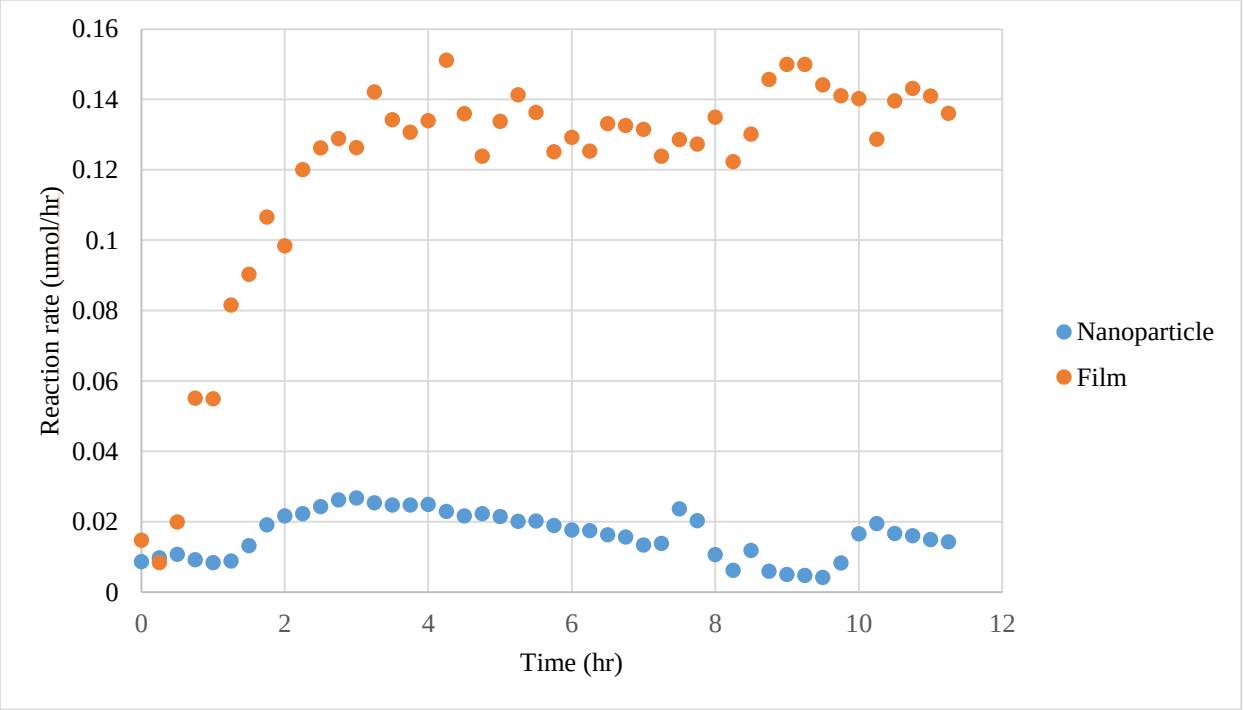

Figure 9 – Liquid-phase isopropanol oxidation utilizing both platinum nanoparticles and a platinum thin film as catalysts.

The isopropanol oxidation reaction rate over time was measured using both the Pt thin film and the silica-encapsulated Pt nanoparticles as catalysts. A 15% isopropanol concentration and a 32 μM oxygen concentration were used for both catalysts. Both catalysts noted an induction period of approximately one hour. On the thin film catalyst, no deactivation was noted, and the rate leveled off after the induction period. However, the silica-encapsulated nanoparticles yielded a significant deactivation after approximately 4 hours of reaction. This may be due to a difference in permeability of the silica to the smaller oxygen molecules as compared to the larger isopropanol molecules.

It was determined that the platinum nanoparticles had a peak reaction rate one order of magnitude lower than the platinum thin film catalyst. The peak turnover frequency for the thin films was found to be 60 hr^{-1}. In contrast, the peak turnover frequency for the silica-encapsulated Pt nanoparticles was determined to be 2.57 hr^{-1}, over 20 times lower than the reaction on the Pt thin films. This is likely a diffusion limitation, occurring as a result of oxygen and isopropanol needing to diffuse through the pores of the silica encapsulation.

Conclusion

It was determined that silica-encapsulated nanoparticles calcined at 450°C did not wash off the surface of the quartz substrate – unlike Pt-PVP nanoparticles – and did produce a higher turnover than non-calcined Pt nanoparticles. The silica-encapsulated Pt nanoparticles were able to generate turnover in both the gas phase (ethylene hydrogenation) and the liquid phase (IPA oxidation). This kinetic data – combined with microscopy data – proves that these catalysts are both accessible and stable after synthesis/cleaning. However, despite several attempts in both the gas and liquid phases, it was not possible to see surface species on silica-encapsulated platinum nanoparticles using SFG spectroscopy.

References

(1) Mallat, T.; Baiker, A. Oxidation of Alcohols with Molecular Oxygen on Platinum Metal Catalysts in Aqueous Solutions. *Catal. Today* **1994**, *19* (93), 247–284.

(2) Besson, M.; Gallezot, P. Selective Oxidation of Alcohols and Aldehydes on Metal Catalysts. *Catal. Today* **2000**, *57* (1–2), 127–141.

(3) Thompson, C. M.; Carl, L. M.; Somorjai, G. A. Sum Frequency Generation Study of the Interfacial Layer in Liquid-Phase Heterogeneously Catalyzed Oxidation of 2-Propanol on Platinum: Effect of the Concentrations of Water and 2-Propanol at the Interface. *J. Phys. Chem. C* **2013**, *117* (49), 26077–26083.

(4) Wang, H.; Sapi, A.; Thompson, C. M.; Liu, F.; Zherebetskyy, D.; Krier, J. M.; Carl, L. M.; Cai, X.; Wang, L.-W.; Somorjai, G. A. Dramatically Different Kinetics and Mechanism at Solid/liquid and Solid/gas Interfaces for Catalytic Isopropanol Oxidation over Size-Controlled Platinum Nanoparticles. *J. Am. Chem. Soc.* **2014**, *136* (29).

(5) Rioux, R. M.; Hsu, B. B.; Grass, M. E.; Song, H.; Somorjai, G. A. Influence of Particle Size on Reaction Selectivity in Cyclohexene Hydrogenation and Dehydrogenation over

Silica-Supported Monodisperse Pt Particles. *Catal. Letters* **2008**, *126* (1–2), 10–19.

(6) Tsung, C.; Kuhn, J. N.; Huang, W.; Aliaga, C.; Hung, L.; Somorjai, G. A.; Yang, P. Sub-10 Nm Platinum Nanocrystals with Size and Shape Control : Catalytic Study for Ethylene and Pyrrole. *J. Am. Chem. Soc.* **2009**, *131*, 5816–5822.

(7) Wang, H.; An, K.; Sapi, A.; Liu, F.; Somorjai, G. A. Effects of Nanoparticle Size and Metal/support Interactions in Pt-Catalyzed Methanol Oxidation Reactions in Gas and Liquid Phases. *Catal. Letters* **2014**, *144* (11), 1930–1938.

(8) Miranda, P. B.; Shen, Y. R. Liquid Interfaces : A Study by Sum-Frequency Vibrational Spectroscopy. *J. Phys. Chem. B* **1999**, *103*, 3292–3307.

(9) Baldelli, S.; Markovic, N.; Ross, P.; Shen, Y.; Somorjai, G. Sum Frequency Generation of CO on (111) and Polycrystalline Platinum Electrode Surfaces: Evidence for SFG Invisible Surface CO. *J. Phys. Chem. B* **1999**, *103*, 8920–8925.

(10) Gomes, J. F.; Bergamaski, K.; Pinto, M. F. S.; Miranda, P. B. Reaction Intermediates of Ethanol Electro-Oxidation on Platinum Investigated by SFG Spectroscopy. *J. Catal.* **2013**, *302*, 67–82.

(11) Krier, J. M.; Michalak, W. D.; Baker, L. R.; An, K.; Komvopoulos, K.; Somorjai, G. A. Sum Frequency Generation Vibrational Spectroscopy of Colloidal Platinum Nanoparticle Catalysts: Disordering versus Removal of Organic Capping. *J. Phys. Chem. C* **2012**, *116* (33), 17540–17546.

(12) Cremer, P. S.; Su, X.; Shen, Y. R.; Somorjai, G. A.; August, R. V. Ethylene Hydrogenation on Pt (111) Monitored in Situ at High Pressures Using Sum Frequency Generation. *J. Am. Chem. Soc.* **1996**, *118*, 2942–2949.

(13) Cremer, P.; Stanners, C.; Niemantsverdriet, J. W.; Shen, Y. R. The Conversion of Di-O-Bonded Ethylene to Ethylidyne on Pt(111) Monitored with Sum Frequency Generation : Evidence for an Ethylidene (or Ethyl) Intermediate. *Surf. Sci.* **1995**, *328*, 111–118.